ABSTRACT

FU, YONGWEI. Using Sensors to Determine In Situ Porosity and Pore Size Distribution. (Under the direction of Dr. Joshua Heitman).

Knowledge of soil porosity (ϕ) and pore size distribution (PSD) is important for understanding the movement of water, air and other fluids, as well as the transport and reaction of chemicals. Monitoring spatial and temporal dynamics of ϕ can only be accomplished through destructive measurements and laboratory determination of PSD is tedious and time consuming. A field experiment was conducted to use the thermo-time domain reflectometry (thermo-TDR) technique for measuring *in situ* ϕ while soils were compacted by wheel traffic. The thermo-TDR technique accurately measured change in ϕ when compared to the destructive core method. The thermo-TDR technique also effectively reduced variability between measurements compared to the core method because thermo-TDR can measure *in situ* ϕ changes repeatedly at the same position. We further expanded the thermo-TDR sensor application by using soil electrical conductivity (σ), water content (θ), and thermal conductivity (λ) measurements to determine PSD. The van Genuchten (VG) model is commonly used to characterize the shape of the soil water retention curve (SWRC) and thus PSD. We proposed an approach to estimate the parameters of the VG model from soil porosity, particle size distribution, $\sigma(\theta)$ measurements at saturated and residual soil water contents, as well as $\sigma(\theta)$ values measured at intermediate water contents. The proposed method performs well on newly collected data for three soils and two additional soils from the literature when compared to direct SWRC measurements. Based on the similarity between SWRCs and λ curves presented as a function of θ, we also developed another simple approach to estimate VG parameters using $\lambda(\theta)$ data. The SWRCs of three soils from published data were estimated from measured $\lambda(\theta)$ data and soil properties, and then compared with direct SWRC measurements. In addition, a simple generalized Archie's model for estimating σ from θ was developed and validated. A standard value

for the water phase exponent (w) in the new proposed model was given as 2. Overall, our work provides potential for *in situ* measurement of both porosity and pore size distribution in the field through thermal and electrical sensors.

Using Sensors to Determine In Situ Porosity and Pore Size Distribution

by
Yongwei Fu

A dissertation submitted to the Graduate Faculty of
North Carolina State University
in partial fulfillment of the
requirements for the degree of
Doctor of Philosophy

Soil Science

Raleigh, North Carolina
2020

APPROVED BY:

Joshua Heitman Committee Chair	Aziz Amoozegar
Brina Montoya	Chadi Sayde

DEDICATION

I dedicate this to my advisor and my family who inspired me to pursue the doctoral degree.

BIOGRAPHY

Yongwei Fu was born in Shanxi Province, China. He received the bachelor's degree of Agronomy from Nanjing Agricultural University in 2013. Then he did his master's degree in Soil science at China Agricultural University in 2016.

ACKNOWLEDGMENTS

I would like to firstly thank my advisor Dr. Heitman for his patient and careful guidance to me on research and behavior. Thanks to my girlfriend, Dr. Min Chai. You are not only my love, but also my best partner in research. Thanks to my parents, I can always feel your support and love even if you are thousands of miles away.

TABLE OF CONTENTS

LIST OF TABLES

LIST OF FIGURES

Chapter 1: Using Sensors to Determine In Situ Soil Porosity and Pore Size Distribution

1.1 Introduction

Pore space is the portion of the soil's volume that is not occupied by solid material (Nimmo, 2005). It regulates many critical processes in soil including water retention and infiltration, movement of fluids, soil nutrient dynamics, root penetration, and susceptibility to erosion (Horn and Smucker, 2005; Abu-Hamdeh et al., 2006; Lipiec et al., 2007; Rabot et al., 2018).

Porosity (ϕ) is the parameter most frequently used to characterize the pore space in soil. Soil porosity displays large spatial and temporal variabilities due to both internal factors (e.g., water content and aggregation) and external forces (e.g., raindrop impact and mechanical disturbance) (Fabiola et al, 2003; Zhang et al., 2018). The core method, commonly used for determination of bulk density and thus porosity, cannot be repeated at the same location since it is destructive. Alternatives like the excavation and the clod methods are more labor-intensive since the sampled volume needs to be determined after extraction, and these too are destructive (Blake and Hartge, 1986). Recently the time domain reflectometry (thermo-TDR) technique was developed which produces minimal soil disturbance and is able to make rapid and repeated *in situ* electrical conductivity (σ), thermal conductivity (λ) and water content (θ) measurements. It has been shown as a reliable tool for monitoring the dynamics of ϕ in the vadose zone (Liu et al., 2014; Tian et al., 2018). To the best of our knowledge, such an approach has not been applied to evaluate changes in ϕ associated with soil compaction from traffic.

Under field condition, the changes in total porosity are always related with alterations in pore size distribution (Lipiec et al., 2006). Pore size distribution is another prominent indicator of pore space which is defined as the relative abundance of each pore size in a representative volume of soil. Laboratory techniques like mercury porosimetry, soil water retention curve (SWRC)

measurements, gas adsorption and imaging techniques have been developed to characterize the pore size distribution. However, these methods still have their own limitations. For example, mercury porosimetry does not measure the actual pore size but the largest entrance pressure towards this pore (pore neck) then assumes cylindrical pores when applying the Young-Laplace law to convert potential into pore diameter (Giesche, 2006). The time required for measuring a complete SWRC is usually long because of the long equilibration time at each matric potential. Because of the analogy between electrical and hydraulic flow, there has been considerable interests in relationship between σ and permeability (Katz and Thompson, 1986; Friedman and Seaton, 1998; Skaggs, 2011). As σ is an easily measured soil property, it is beneficial to use soil σ measurements as an aid to the prediction of hydraulic properties of soils (Mualem and Friedman, 1991; Doussan and Ruy, 2009; Niu et al., 2015). This led us to hypothesize that there may be potential to use σ to also estimate the SWRC and thus obtain the pore size distribution.

Among factor affecting soil σ, soil θ is the dominant one (Friedman, 2005). As θ increases from air-dry to saturation, ions adsorbed on the surface of soil particles are released which forms a double electric layer or enters the soil solution thus increasing the mobility of electrical charge. Previous studies have developed linear or nonlinear (polynomial or power law) relationships between θ and σ on different soils (Archie, 1942; Gupta and Hanks, 1972; Rhoades et al., 1976). However, these relationships have several empirical parameters which are dependent on soil type and need be calibrated when applied to different soils.

Both λ(θ) curves and SWRCs are governed by similar factors (i.e. particle geometry, pore size distribution, pore-water arrangement, and interfacial properties) and can be divided into similar regimes (Tarnawski and Gori, 2002; Lu and Khorshidi, 2015). Because of the linkage between λ(θ) variation patterns and SWRC regimes, researchers have focused on empirical relationships

between λ and SWRC (McCumber and Pielke, 1981; Likos, 2014; Kim et al., 2015; Lu and Dong, 2015; Lu et al., 2019). However, these relationships were developed either to estimate λ(θ) from SWRCs or at limited matric potential range. Since λ and θ can be easily measured by sensors, an approach to estimate SWRCs from λ(θ) is needed to extend the application of sensors to determine the pore size distribution.

To use the sensors to characterize the soil pore space, we first investigated changes in soil pore space during compaction using in-situ thermo-TDR measurements (Chapter 2). Then σ(θ)-SWRC and λ(θ)-SWRC approaches were developed to estimate the SWRCs from easily measured properties (σ and λ) by sensors and other soil properties (Chapters 3 and 4, respectively). A simple σ(θ) relationship was also proposed (Chapter 5). These studies expand the application of thermal and electrical sensors and make it possible to further estimate the dynamics of in-situ pore size distribution in the field.

1.2 References

Abu-Hamdeh, N.H., Abo-Qudais, S.A., Othman, A.M., 2006. Effect of soil aggregate size on infiltration and erosion characteristics. Eur. J. Soil Sci. 57, 609–616.

Archie, G.E., 1942. The electrical resistivity log as an aid in determining some reservoir characteristics. Trans. AIME 146, 54–62.

Blake, G.R., Hartge, K.H., 1986. Bulk density. In: Klute, A. (Ed.), Methods of Soil Analysis: Part 1, Physical and Mineralogical Methods. Am. Soc. Agr., Madison, WI, pp. 363–375.

Fabiola, N., Giarola, B., Da Silva, A.P., Imhoff, S., Dexter, A.R., 2003. Contribution of natural soil compaction on hardsetting behavior. Geoderma 113, 95–108.

Friedman, S.P., Seaton, N.A., 1998. Critical path analysis of the relationship between permeability and electrical conductivity of three-dimensional pore networks. Water Resour. Res. 34, 1703–1710.

Friedman, S.P., 2005. Soil properties influencing apparent electrical conductivity: A review. Comput. Electron. Agric. 46, 45–70.

Doussan, C., Ruy, S., 2009. Prediction of unsaturated soil hydraulic conductivity with electrical conductivity. Water Resour. Res. 45, 1–12.

Giesche, H., 2006. Mercury porosimetry: a general (practical) overview. Part. Part. Syst. Charact. 23, 9–19.

Gupta, S.C., Hanks, R.J., 1972. Influence of water content on electrical conductivity of the Soil. Soil Sci. Soc. Am. J. 36, 855–857.

Horn, R., Smucker, A., 2005. Structure formation and its consequences for gas and water transport in unsaturated arable and forest soils. Soil Tillage Res. 82, 5–14.

Katz, A.J., Thompson, A.H., 1986. Quantitative prediction of permeability in porous rock. Phys. Rev. B 34, 8179–8181.

Kim, D., Kim, G., Baek, H., 2015. Relationship between thermal conductivity and soil-water characteristic curve of pure bentonite-based grout. Int. J. Heat Mass Transf. 84, 1049–1055.

Likos, W.J., 2014. Modeling thermal conductivity dryout curves from soil-water characteristic curves. J. Geotech. Geoenviron. Eng. 140, 04013056.

Lipiec, J., Kuś, J., Słowińska-Jurkiewicz, A., Nosalewicz, A., 2006. Soil porosity and water infiltration as influenced by tillage methods. Soil Tillage Res. 89, 210–220.

Lipiec, J., Walczak, R., Witkowska-Walczak, B., Nosalewicz, A., Słowińska-Jurkiewicz, A., Sławiński, C., 2007. The effect of aggregate size on water retention and pore structure of two silt loam soils of different genesis. Soil Tillage Res. 97, 239–246.

Liu, X., Lu, S., Horton, R., Ren, T., 2014. In Situ Monitoring of Soil Bulk Density with a Thermo-TDR Sensor. Soil Sci. Soc. Am. J. 78, 400.

Lu, N., Dong, Y., 2015. Closed-form equation for thermal conductivity of unsaturated soils at room temperature. J. Geotech. Geoenviron. Eng. 141, 04015016.

Lu, N., Khorshidi, M., 2015. Mechanisms for Soil-Water Retention and Hysteresis at High Suction Range. J. Geotech. Geoenviron. Eng. 141, 04015032.

Lu, S., Lu, Y., Peng, W., Ju, Z., Ren, T., 2019. A generalized relationship between thermal conductivity and matric suction of soils. Geoderma 337, 491–497.

McCumber, M.C., Pielke, R.A., 1981. Simulation of the effects of surface fluxes of heat and moisture in a mesoscale numerical model. J. Geophys. Res. 86, 9929–9938.

Mualem, Y., Friedman, S.P., 1991. Theoretical prediction of electrical conductivity in saturated and unsaturated soil. Water Resour. Res. 27, 2771–2777.

Nimmo, J.R., 2005. Porosity and pore size distribution. In: Encyclopedia of Soils in the Environment. Elsevier, London, pp. 295–303.

Niu, Q., Fratta, D., Wang, Y.H., 2015. The use of electrical conductivity measurements in the prediction of hydraulic conductivity of unsaturated soils. J. Hydrol. 522, 475–487.

Rabot, E., Wiesmeier, M., Schlüter, S., Vogel, H.J., 2018. Soil structure as an indicator of soil functions: A review. Geoderma 314, 122–137.

Rhoades, J.D., Raats, P.A.C., Prather, R.J., 1976. Effects of liquid-phase electrical conductivity, water content, and surface conductivity on bulk soil electrical conductivity. Soil Sci. Soc. Am. J. 40, 651–655.

Skaggs, T.H., 2011. Assessment of critical path analyses of the relationship between permeability and electrical conductivity of pore networks. Adv. Water Resour. 34, 1335–1342.

Tarnawski, V.R., Gori, F., 2002. Enhancement of the cubic cell soil thermal conductivity model. Int. J. Energy Res. 26, 143–157.

Tian, Z., Lu, Y., Ren, T., Horton, R., Heitman, J.L., 2018. Improved thermo-time domain reflectometry method for continuous in-situ determination of soil bulk density. Soil Tillage Res. 178, 118–129.

Zhang, M., Lu, Y., Heitman, J., Horton, R., Ren, T., 2018. Temporal changes of soil water retention behavior as affected by wetting and drying following tillage. Soil Sci. Soc. Am. J. 81, 1288–1295.

Chapter 2: Measuring Dynamic Changes of Soil Porosity During Compaction

Abstract

Knowledge of soil porosity and pore-size distribution changes in response to compaction is important for understanding heat, water, and air flow in soils. In this study, we used the thermo-time domain reflectometry (thermo-TDR) technique to investigate the dynamics of in-situ soil porosity and pore-size distribution as affected by number of traffic passes, water content and soil depth. The study was conducted at a field site located near Clayton, NC, USA. A roller was dragged across the length of a 3- by 12-m plot three to five times to repeatedly compact the soil after tillage. Nine thermo-TDR probes, installed at 2.5-, 7.5-, and 12.5-cm depths (representing 0-5, 5-10, and 10-15 cm depth intervals, respectively) at three locations within the plot, were used to determine dynamic changes in soil porosity after each compaction event. Pore-size distribution changes within the top soil layer were determined for a subset of conditions by measuring in-situ infiltration at low tension using a mini disk (also known as tension) infiltrometer. Nine core samples were also collected (considered to be a destructive method) near each thermo-TDR probe for measuring total porosity and water content after each compaction. The results showed that the thermo-TDR technique can accurately monitor the change of soil porosity during soil compaction compared to the destructive core method. Variability of replicated soil porosity measurements by the thermo-TDR technique (with a root mean square error (RMSE) of 0.011 m^3 m^{-3} and mean standard error (MSE) of 0.010 m^3 m^{-3}) was lower than that of the core method (with a RMSE of 0.017 m^3 m^{-3} and MSE of 0.019 m^3 m^{-3}). As expected, total soil porosity decreased with the number of passes with a major portion of compaction (59-89% of the total porosity decrease) occurring during the first pass. The phenomenon, large pores are preferentially reduced due to compaction, has been shown by various studies. The trend of topsoil (0-5 cm) compaction differed from that of

subsoil layers (5-10 and 10-15 cm). Changes in porosity were highly sensitive to soil water content. For the sandy-textured soil in this study, soil porosity decreased as water content increased (during compaction period), and the maximum compaction (associated with the lowest porosity) was reached at an initial water content range between 0.08 and 0.10 g g^{-1}. Above this range, the compaction level decreased with increasing water content. In addition, there was a shift in pore-size distribution for the surface layer. More importantly, pore-size distribution continued to change with additional traffic passes even after soil total porosity became stable.

Keywords: soil compaction, porosity, pore-size distribution, traffic, water content, thermo-TDR.

2.1 Introduction

Soil compaction is a key concern for many agricultural, environmental and engineering professionals throughout the world. Some of the primary causes of soil compaction are heavy machinery traffic, short crop rotations, and animal trampling (Williamson and Neilsen, 2000; Fabiola et al., 2003). Soil compaction is generally accompanied by the removal of the soil air, change in the soil structure, reduction in total volume of pores, alteration in pore-size distribution, and increase in the soil strength (Taylor, 1971). Thus, soil compaction, which can induce substantial changes in soil physical, chemical and biological processes, has significant influences on crop production and many environmental issues, such as soil erosion, soil degradation and pollution of surface water (Gupta et al., 1989).

Soil compaction involves changes in bulk density and porosity. Decrease in soil porosity has been widely reported in mechanically compacted soils (Dickerson, 1976; Silva et al., 2008). In loamy and acidic soils, logging operations have been observed to cause the increase of bulk density and decrease in the total porosity of soils down to 30-cm depth (Herbauts et al., 1996). However, pores of different sizes are not reduced proportionally during the soil compaction process. The fact

that large pores are preferentially reduced due to compaction has been presented in various research (Pagliai et al., 2003; Schäffer et al., 2007; Dörner et al., 2010; Matthews et al., 2010; Lipiec et al., 2012). Large pores in soil even totally disappeared after repeated wheel traffic in some studies (Startsev and McNabb, 2001; Servadio et al., 2005).

Soil water content is one of the major factors that influence compaction. For a specific compaction effort, starting with a dry soil, soil compaction level increases initially with increasing water content. However, when water content is higher than an most sensitive value, soil becomes increasingly plastic and incompressible, and soil compaction level decreases as water content increases (Medvedev and Cybulko, 1995). The number of traffic passes is another important factor that influences soil compaction level. For example, with each wheel pass, soil bulk density may increase. However, after the first pass, the compaction level generally decreases during the second and subsequent passes (Özgöz et al., 2006). The effects of soil compaction are also reduced with depth below the soil surface (Afzalinia and Zabihi, 2014).

Under field conditions, soil porosity varies naturally with time and location. For assessing changes associated with soil compaction, the core method, commonly used for determination of bulk density, cannot be repeated at the same location since it is destructive. The thermo-TDR technique, however, is a promising tool for determining soil bulk density and porosity repeatedly at the same location without disturbing the soil after installation (Ren et al., 1999; Ochsner et al., 2001; Lu et al., 2017; Tian et al., 2018). Soil porosity is estimated from co-located thermo-TDR sensor measurements of soil water content and heat capacity. Despite several field evaluations of thermo-TDR-based bulk density measurements, to-date, such an approach has not been applied to evaluate changes in porosity associated with soil compaction from traffic. Potentially complimentary to total porosity measurements, the tension infiltrometer (also known as disc or

disk infiltrometer), which has been used for in-situ characterization of water-conducting macroporosity and mesoporosity in surface soils (Watson and Luxmoore, 1986; Wilson and Luxmoore, 1988) has not been used to evaluate changes during field traffic and compaction.

Most existing studies on soil compaction have mainly focused on the influence of a single factor on either soil porosity or pore-size distribution relying on destructive measurements. Our aim in this study was to investigate changes in soil pore space during compaction using in-situ thermo-TDR measurements. Our specific objectives were to: i) compare thermo-TDR porosity estimates to destructive core sampling measurements during soil compaction, and ii) examine the effects of water content, soil depth, and number of traffic passes on compaction at a field site using in-situ thermo-TDR measurements along with complementary pore-size distribution estimates in the top soil layer from a tension infiltrometer.

2.2 Material and Methods

2.2.1 Field Experiment

The field experiment was conducted from October 2017 to January 2018 at the Central Crops Research Station, Clayton, NC, USA, in an area mapped as Goldsboro loamy sand (fine-loamy, siliceous, subactive, thermic Aquic Paleudults). The texture of the surface soil horizon at the site is sand (88% sand, 10% silt, 2% clay). An experimental plot, 3-m wide and 12-m long, was tilled to approximately 15-cm depth with a rotary tiller to achieve a loose soil layer. Following tillage, shallow soil pits were dug at three locations and thermo-TDR probes were installed (with plane of the needles oriented horizontally) at 2.5-, 7.5-, and 12.5-cm depths (3 pits × 3 depths = nine sensors) to measure the dynamics of total soil porosity during compaction for the 0- to 5-, 5- to 10-, and 10- to 15-cm depth intervals (Fig. 2.1). The thermo-TDR sensors were custom-fabricated in-house according to the specifications described by Tian et al. (2018). Additionally, we collected nine

core samples (50-mm high and 50-mm in diameter) from the 0-5, 5-10, and 10-15 cm depth intervals at the three locations (three replications) near thermo-TDR sensor positions for measuring the initial total porosities within the same plot. The pits were then backfilled carefully with the same type of soil obtained from an adjacent field area. After measuring the initial volumetric heat capacity and water content at each depth-location with the thermo-TDR probe, the plot was compacted by dragging a 61-cm diameter and 122-cm wide steel roller weighing 756 N (mass ≈ 77 kg) across the length of the plot. Following the roller pass, thermo-TDR heat capacity and water content data were again recorded, and intact core samples were again collected from three positions and three depths near the thermo-TDR probes within the plot. This procedure (compaction followed by thermo-TDR measurement and intact core sample collection) was repeated to produce a series of compaction events (through roller passes).

The experiment was repeated a total of four more times, either after a rainfall event or a dry period, to obtain data at different soil water contents. For each experiment, the plot was re-tilled, sensors were re-installed, and intact core samples were collected as described above. In this study, the plot were compacted three times at water contents of 0.02 and 0.12cm^3 cm^{-3}, and five times at water contents of 0.15, 0.19, and 0.21 cm^3 cm^{-3} (all the water contents herein and following in this paper are the initial water content at 2.5- cm depth before any roller pass).

For pore-size distribution measurement, we used a mini disk infiltrometer (disk diameter: 4.5 cm; Meter, Pullman, WA). After each compaction event, we placed the infiltrometer on a smooth surface near each nest of thermo-TDR probes and determined water infiltration from the infiltrometer into the soil at tensions of 0.5-, 3-, and 6-cm of water. As infiltration measurement began, we recorded the volume of water infiltrating into the soil for a corresponding time interval to calculate the hydraulic conductivity, which we used to determine the pore-size distribution

following the procedure described by Watson and Luxmoore (1986). Details on calculation are presented in the Appendix A.

2.2.2 Theory of the Thermo-TDR Technique for Determining Soil Porosity

The heat capacity of a bulk soil can be calculated as the sum of the heat capacities of its components (Campbell et al., 1991):

$$C = \rho_b c_s + C_w \theta \quad [1]$$

where C and C_w are the volumetric heat capacities of bulk soil and water (4.18 MJ m^{-3} K^{-1}), respectively; c_s is the specific heat of soil solids (0.904 MJ Mg^{-1} K^{-1}); ρ_b is the soil bulk density (Mg m^{-3}); and θ is soil volumetric water content (m^3 m^{-3}).

The thermo-TDR technique is capable of measuring C and θ simultaneously. Details about the theory, equipment, and procedures for measurements are presented in Lu et al. (2017). Using these values, ρ_b is estimated by (Ochsner et al., 2001):

$$\rho_b = \frac{C - C_w \theta}{c_s} \quad [2]$$

The total porosity can be calculated by:

$$\phi = 1 - \frac{\rho_b}{\rho_s} \quad [3]$$

where ρ_s is the density of soil solids (i.e., soil particle density, here assumed to be 2.65 Mg m^{-3}). Combining Eqs. [2] and [3], ϕ (m^3 m^{-3}) can then be obtained by:

$$\phi = 1 - \frac{C - C_w \theta}{\rho_s c_s} \quad [4]$$

Details about the error analysis of sensor measurements are presented in Appendix B.

2.2.3 Pore-Size Distribution Measurement Using Mini Disk Infiltrometer

A mini disk infiltrometer is a small version of tension infiltrometer for measuring the unsaturated hydraulic conductivity of soil at different low tensions (0-20 cm; White et al, 1992). Overall, the hydraulic conductivity of the soil is strongly related to pore geometry, pore-size distribution, connectivity, water content, and matric potential (Brady and Weil, 1999). This in turn makes it possible to obtain the pore-size distribution from hydraulic conductivity using infiltration measurements under tension.

Measurements were conducted at 0.5- to 3-, and 3- to 6-cm tension ranges, corresponding to minimum pore radii of 0.05 and 0.025 cm, respectively. Herein, we use the definition of large pores: those pores that drain at <3 cm of tension (Luxmoore, 1981). Details about the required calculations are provided in Appendix A.

2.3. Results and Discussion

2.3.1 Comparison of Soil Porosity from Thermo-TDR Technique and Core Method

Figure 2.2 presents the thermo-TDR estimated ϕ versus values from the core method from all experimental runs. In general, ϕ data from the two methods showed a high degree of agreement, indicating that the thermo-TDR technique is able to measure ϕ accurately. The root mean square error (RMSE) between thermo-TDR estimated and core method measured ϕ was 0.016 m^3 m^{-3}. The corresponding relative error (RE) values for in-situ thermo-TDR ϕ were within 6% of the ϕ values determined by core method, except for two data points where the REs of thermo-TDR ϕ were larger than 10%. This result may have been caused in part by error associated with collecting intact soil samples for the core method. For our results, inserting the sampling cylinder (also

referred to as ring) may have compacted the soil which inevitably causes underestimation of core method ϕ values.

It is important to note that the thermo-TDR sensors can provide in-situ measurements of ϕ repeatedly at the same location without disturbing the soil. The core method, however, does not have such a capability because it is a destructive method. Therefore, there will be potential for introducing spatial differences in addition to temporal differences associated with compaction among the soil samples collected by core method as they are collected from new locations each time. This adds an additional complicating factor related to soil spatial variability into measurements aimed at evaluating change in ϕ associated with compaction events. Figure 2.3 compares the variability of ϕ from the core method and thermo-TDR approach. The variability of the thermo-TDR values was smaller than that from the core method. When comparing replicates to the mean, the RMSE of core method values and those from the thermo-TDR method were 0.017 and 0.011 $m^3 m^{-3}$, respectively. The larger RMSE associated with the core method may be due, in part, to the addition of spatial variability within this comparison. Additionally, the variability of change in soil porosity [$\Delta\phi$, which is defined as the difference between soil porosity measurement values after compaction and initial porosity (before any roller pass)] from the core method and thermo-TDR method were compared. Figure 2.4 shows that $\Delta\phi$ values by thermo-TDR were more consistently distributed around the 1:1 line than those by the core method. In the case of Fig. 2.4, the thermo-TDR values represents $\Delta\phi$ at a consistent set of positions (i.e., measurement locations) as ϕ changes, whereas the core method values represent a new measurement location for each set of measurements (i.e., $\Delta\phi$ is potentially due to both compaction and change in position). This likely adds to the scatter observed in the data for the core method, and thereby increases mean standard error (MSE) when comparing individual locations to the mean of observations. Overall, results

indicated that the thermo-TDR technique can effectively provide repeated and in-situ measurement of ϕ dynamics.

2.3.2 Effect of Number of Passes on Soil Porosity at Shallow Depth

Repeated traffic passes over an area is one of the most important factors influencing the soil compaction process because soil deformation usually increases with the number of traffic passes (Bakker and Davis, 1995). Soil porosity determined by thermo-TDR technique at the 0-5 cm depth as a function of the number of traffic passes is shown in Fig. 2.5. The most substantial soil deformation (decrease of ϕ) occurred after the first pass of the roller, which accounted for 59%-89% of the total ϕ decrease, depending on the soil water content. The rate of soil deformation was reduced in the subsequent passes of the roller, and there was no substantial change in ϕ after the third pass. This trend may be due to soil consolidation caused by repeated passes on the same track. In their study, Pytka and Dąbrowski (2001) reported that the increase of peak stress between the first and second pass was significantly higher than that between the second and third pass. For subsequent passes, the stress increased slightly after the fourth and fifth passes where the changes were lower than those measured in the second and third passes. It should be noted that in our observations there were some small differences in ϕ between the fourth and fifth passes, which are opposite the expected trend (i.e., ϕ increased). This was most likely due to slight relocation in sensor depth following compaction (i.e., sensor position shifted downward during consolidation). We have limited our primary comparisons about the effect of number of passes on ϕ only to the 2.5- cm depth. There was also considerable variation between depths within the same profile (discussed later) and relationships varied with water content (discussed next). While considering the influence of the number of passes, it is difficult to compare results at different depths directly (Quiroga et al., 1999). Nonetheless, at the 2.5-cm depth, the variability among repetitions of ϕ was

small, indicating that measurements by thermo-TDR method reflected ϕ dynamics accurately as number of passes increased.

2.3.3 Effect of Water Content on Soil Porosity

Soil water content plays an important role in the soil compaction processes (Hamza and Anderson, 2005). Figure 2.6 shows the effect of soil water content on ϕ during compaction across all depths. Here we present water content on a mass basis, because volumetric water contents at the initial condition no longer match the volumetric water contents at corresponding ϕ in the figure (i.e., volume ratios change with changes in porosity and soil volume), whereas mass-based water content should remain mostly unchanged following compaction. When the soil is subjected to a force (e.g., traffic), the soil particles are pushed downward exerting force on neighboring particles. At lower water contents (< 0.05 g g^{-1}), soil pores were mainly occupied by air and friction between particles preventing them from moving too far. Thus, the minimum soil porosity achieved by compaction was as high as 0.43 m^3 m^{-3}, which agrees with the findings of Medvedev and Cybulko (1995), that the compaction level is low under relatively dry conditions. As water content increased up to the most sensitive water content range (0.08-0.10 g g^{-1}), water films (which act as a lubricant) were developed around the soil particles, allowing them to move more easily and reorient themselves into a denser configuration thus resulting in a decrease in ϕ to a minimum of 0.36 m^3 m^{-3}. As shown in Fig. 2.6, above the most sensitive water content range, soil compaction level was reduced because soil particles did not move significantly. Under wet conditions, since water cannot be compressed, in order for soil to become compacted water must be displaced from soil pores. Since water cannot move out of most pores instantaneously, the minimum porosity during compaction process remained large (up to 0.44 m^3 m^{-3} in our study) with increasing water content.

2.3.4 Soil Porosity Changes with Depth Due to Compaction

Figure 2.7 is an example of ϕ dynamics determined by the thermo-TDR method at depths of 2.5-, 7.5-, and 12.5-cm at water content of 0.15 cm^3 cm^{-3} during the compaction process. Compared to the initial values, ϕ values were consistently reduced at all depths during the compaction process. However, the magnitude of ϕ change varied with depth. Values of ϕ decreased by 0.07, 0.05 and 0.04 m^3 m^{-3} at 2.5-, 7.5-, and 12.5-cm depth, respectively, indicating that the greatest change occurred at 2.5 cm and the least changes occurred at 12.5 cm depth. This can be explained by the impact of individual particles on their neighboring particles due to vertical pressure at the soil surface; resulting in the pressure decrease with depth (see Fig. 13.29, Hillel, 1998). In addition, the reduction of porosity due to the first pass accounted for 59%, 52%, and 33% of the total porosity change (following all passes) at 2.5-, 7.5-, and 12.5-cm depths, respectively. This indicates that compaction effects for first pass decreased substantially with increasing soil depth. However, compaction effects for the second pass caused 21%, 43% and 38% of the total porosity change at 2.5-, 7.5-, and 12.5-cm depths, respectively, while the changes for the third pass were 20%, 10%, and 34%, respectively. These differences among different depths for the passes may be related to the different mechanisms between topsoil compaction due to ground pressure and subsoil compaction caused by total axle load that is independent of ground pressure (Håkansson and Reeder, 1994; Botta et al., 2002). As depth increases, the increase in the principal compressive stress gradually diminishes, which becomes increasingly dependent on the load (see Fig. 12.12, Norton, 2009). Overall, dynamics of soil porosity with depth across all water contents follow a similar trend as that at 0.15 cm^3 cm^{-3} although the magnitude of porosity changes is different.

2.3.5 Pore-Size Distribution Due to Compaction

Figure 2.8 shows the change of three pore-size classes (>0.05 cm, 0.025-0.05 cm, and <0.025 cm in radius) as affected by soil compaction at water contents of 0.15 and 0.19 cm^3 cm^{-3}. Since the maximum infiltration depth of infiltrometer measurements in this study was 5.34 cm (calculated from the measurement data), only the pore-size distribution related to soil water content in the 0- to 5-cm layer is considered. There was a shift in soil pore-size distribution: the fraction of pores >0.05 cm decreased while the fraction of other pores increased during the compaction process. This could be explained by the fact that loading mainly influences the larger pore spaces between the soil particles (Monroy et al., 2010). Due to their weaker internal structure, large pores are preferentially compressed during compaction, which results in an increase of smaller pores. In addition, the trend of changes in pores < 0.05 cm was different from the large pores and not the same at both water contents during the compaction process. This may be due to the limitation of measurements of pore sizes with the tension infiltrometer. The infiltrometer measurement should be conducted on a smooth area on the soil surface. Conducting measurement at different locations may cause inevitable impact of spatial variability among the data.

Many studies have shown that soil compaction is a reorganization process of different size pores (Thom et al., 2007; Tarantino and De Col, 2008; Birle, 2012). In our study, as the number of passes increased, the response of pore-size distribution differed considerably from that of ϕ. A major change of ϕ occurred in the first pass, whereas pore-size distribution changed continuously even when ϕ became relatively stable, as shown in Fig. 2.8. This phenomenon occurs because a small reduction in the fraction of larger pores caused by compaction gives a much larger increase in the fraction of smaller pores that are more resistant against mechanical stress than larger pores.

A decrease in connectivity of large pores and an increase in the fraction of spherical pores has also been reported during the soil compaction process (Schäffer et al., 2007).

2.4 Conclusion

In this study, we simultaneously measured the dynamic changes of soil porosity and pore-size distribution at a site with a sandy-textured soil. Based on our findings, we conclude that:

1. The thermo-TDR probes can provide accurate monitoring of the dynamics of soil porosity during compaction.
2. The thermo-TDR technique effectively reduces the variability of measurement results compared to the core method.
3. Both the change in porosity and pore-size distribution are sensitive to water content during compaction.
4. As depth increases, change of porosity is reduced. This difference decreases as the number of traffic passes increases.
5. Different from porosity, pore-size distribution continues to change even after multiple traffic passes.

2.5 Acknowledgements

This research was supported through the China Scholarship Council, US Army Research Laboratory (Grant Number: W911NF-16-1-0287) and US National Science Foundation (Grant Number: 1633806).

2.6 Appendix A

Pore-size distribution measurement using mini disk infiltrometer

According to capillary theory, the maximum pore radius r (cm) at specific water pressure head h (negative tension expressed as -cm H_2O) is

$$r = -\frac{2\sigma \cos\alpha}{\rho g h} \quad [A1]$$

where σ is the surface tension of water (72.86 N m^{-1} at 20 °C), α is the contact angle between the water and the pore wall (assumed to be 0), ρ is the density of water (1 g cm^{-3}), and g is acceleration due to gravity (9.80 m s^{-2}).

According to capillary theory and Poiseuille's law, the flow rate through a single macropore can be given by (Bodhinayake et al., 2004)

$$Q(r) = \frac{\pi \rho g}{8\mu} r^4 \quad [A2]$$

where $Q(r)$ is the flow rate (cm^3 s^{-1}), μ is the viscosity of water (1.002 mPa s at 20°C), and the water flux density I (cm s^{-1}) is given by

$$I(r) = Q(r) N(r) \quad [A3]$$

where $N(r)$ is the maximum number of effective pores at specific radius range per unit area.

Substitution of Eq. [A2] into Eq. [A3] yields

$$I(r) = \frac{\pi \rho g}{8\mu} r^4 N(r) \quad [A4]$$

Since tension infiltration measurements are determined under approximately steady-state conditions, a unit hydraulic gradient is assumed. Then, the steady-state vertical water flux is set to be approximately equal to the measured hydraulic conductivity value corresponding to the same pressure head h (the same pore radius r). The hydraulic conductivity, K (cm s^{-1}), is then simply:

$$K(r) = I(r) \quad [A6]$$

where I is the volumetric flux measured at each tension. Details about obtaining the K from mini disk infiltrometer measurement can be found in Zhang (1997) and Dohnal et al. (2010).

Pore conductivity (K_p) at specific radius range was determined as the difference between two consecutive infiltration rates at corresponding water tensions. Then the maximum number of effective pores at specific radius range per unit area can be obtained by

$$N = 8\mu K_p \Big/ \left[\pi \rho g \left(r_{min} \right)^4 \right] \quad [A7]$$

where r_{min} is the minimum equivalent pore radius (cm), and all other terms are as defined previously. The total water conducting porosity Θ_m at specific radius range per unit area can be calculated from:

$$\Theta_m = N \pi r_{min}^{\ 2} \quad [A8]$$

2.7 Appendix B

Error analysis

Soil porosity values obtained from the thermo-TDR method were compared with core method results. RE, RMSE, and MSE were calculated to evaluate the performance of thermo-TDR measured porosity during soil compaction:

$$\mathrm{RE} = \left| \frac{\phi_t - \phi_c}{\phi_c} \right| \times 100\% \quad [B1]$$

$$\mathrm{RMSE} = \sqrt{\frac{\sum_{j=1}^{n} \left(\phi_t - \phi_c \right)^2}{n}} \quad [B2]$$

$$\mathrm{MSE} = \sum_{j=1}^{n} \sqrt{\frac{\sum_{i=1}^{m} \left(\phi_{ij} - \bar{\phi}_j \right)^2}{m-1}} \Big/ n \quad [B3]$$

where m is the replication time of each measurement, n is the number of measurements, ϕ_t represents the thermo-TDR sensor measured value, ϕ_c is the value determined from the core method, ϕ_{ij} is the i-th replication of soil porosity at j-th measurement and $\bar{\phi}_j$ is the average porosity value from m replications at j-th measurement.

2.8 References

Afzalinia, S., Zabihi, J., 2014. Soil compaction variation during corn growing season under conservation tillage. Soil Till. Res. 137, 1–6.

Bakker, D.M., Davis, R.J., 1995. Soil deformation observations in a vertisol under field traffic. Aust. J. Soil Res. 33, 817–832.

Birle, E., 2012. Effect of initial water content and dry density on the pore structure and the soil-water retention curve of compacted clay, in: Mancuso, C., Jommi, C., D'Onza, F. (Eds.), Unsaturated Soils: research and applications. Springer Berlin Heidelberg, Berlin, Heidelberg, pp, 145–152.

Bodhinayake, W., Si, B.C., Xiao, C., 2004. New method for determining water-conducting macro- and mesoporosity from tension infiltrometer. Soil Sci. Soc. Am. J. 68, 760–769.

Botta, G.F., Jorajuria, D., Draghi, L.M., 2002. Influence of the axle load, tyre size and configuration on the compaction of a freshly tilled clayey soil. J. Terramechanics 39, 47–54.

Brady, N.C., Weil, R.R., 1999. The Nature and Properties of Soils. Prentice Hall, Upper Saddle River, New Jersey.

Campbell, G.S., Calissendorff, C., Williams, J.H., 1991. Probe for measuring soil specific heat using a heat-pulse method. Soil Sci. Soc. Am. J. 55, 291–293.

Dickerson, B.P., 1976. Soil compaction after tree-length skidding in northern Mississippi. Soil Sci. Soc. Am. J. 40, 965–966.

Dohnal, M., Dusek, J., Vogel, T., 2010. Improving hydraulic conductivity estimates from minidisk infiltrometer measurements for soils with wide pore-size distributions. Soil Sci. Soc. Am. J. 74, 804–811.

Dörner, J., Sandoval, P., Dec, D., 2010. The role of soil structure on the pore functionality of an Ultisol. J. Soil Sci. Plant Nutr. 10, 495–508.

Fabiola, N., Giarola, B., Da Silva, A.P., Imhoff, S., Dexter, A.R., 2003. Contribution of natural soil compaction on hardsetting behavior. Geoderma. 113, 95–108.

Gupta, S.C., Hadas, A., Schafer, R.L., 1989. Modeling soil mechanical behaviors during compaction. In: Larson, W.E., Blake, G.R., Allmaras, R.R., Voorhees, W.B., Gupta, S.C., (Eds), Mechanics and Related Processes in Structured Agricultural Soils. NATION ASI Series E, Appl. Sci. 172. Kluwer Academic Publishers, Dordrechant, pp, 137-152.

Håkansson, I., Reeder, R.C., 1994. Subsoil compaction by vehicles with high axle load-extent, persistence and crop response. Soil Till. Res. 29, 277–304.

Hamza, M.A., Anderson, W.K., 2005. Soil compaction in cropping systems: A review of the nature, causes and possible solutions. Soil Till. Res. 82, 121–145.

Herbauts, J., El Bayad, J., Gruber, W., 1996. Influence of logging traffic on the hydromorphic degradation of acid forest soils developed on loessic loam in middle Belgium. Forest Ecology and Management. 87, 193–207.

Hillel, D., 1998. Environmental Soil Physics. Academic Press, San Diego, CA.

Lipiec, J., Hajnos, M., Świeboda, R., 2012. Estimating effects of compaction on pore size distribution of soil aggregates by mercury porosimeter. Geoderma. 179–180, 20–27.

Lu, Y., Liu, X., Zhang, M., Heitman, J., Horton, R., Ren, T., 2017. Thermo-time domain reflectometry method: advances in monitoring in situ soil bulk density. Methods Soil Anal. 2.

Luxmoore, R.J., 1981. Micro-, meso- and macroporosity of soil. Soil Sci. Soc. Am. J. 45, 671-672.

Matthews, G.P., Laudone, G.M., Gregory, A.S., Bird, N.R.A., de G. Matthews, A.G., Whalley, W.R., 2010. Measurement and simulation of the effect of compaction on the pore structure and saturated hydraulic conductivity of grassland and arable soil. Water Resour. Res. 46, 1–13.

Medvedev, V.V., Cybulko, W.G., 1995. Soil criteria for assessing the maximum permissible ground pressure of agricultural vehicles on Chernozem soils. Soil Till. Res. 36, 153–164.

Monroy, R., Zdravkovic, L., Ridley, A., 2010. Evolution of microstructure in compacted London Clay during wetting and loading. Géotechnique. 60, 105–119.

Norton, R.L, 2009. Cam design and Manufacturing Handbook. Industrial Press, New York.

Ochsner, T.E., Horton, R., Ren, T., 2001. Simultaneous water content, air-filled porosity, and bulk density measurements with thermo-time domain reflectometry. Soil Sci. Soc. Am. J. 65, 1618–1622.

Özgöz, E., Öztekin, T., Günal, H., 2006. Assessment of wheel traffic effect on soil compaction using a soil core sampler. New Zeal. J. Agric. Res. 49, 299–306.

Pagliai, M., Marsili, A., Servadio, P., Vignozzi, N., Pellegrini, S., 2003. Changes in some physical properties of a clay soil in Central Italy following the passage of rubber tracked and wheeled tractors of medium power. Soil Till. Res. 73, 119–129.

Pytka, J., Dąbrowski, J., 2001. Determination of the stress-strain relationship for sandy soil in field experiments. J. Terramechanics. 38, 185–200.

Quiroga, A.R., Buschiazzo, D.E., Peinemann, N., 1999. Soil compaction is related to management practices in the semi-arid Argentine pampas. Soil Till. Res. 52, 21–28.

Ren, T., Noborio, K., Horton, R., 1999. Measuring soil water content, electrical conductivity, and thermal properties with a thermo-time domain reflectometry probe. Soil Sci. Soc. Am. J. 63, 450–457.

Schäffer, B., Stauber, M., Müller, R., Schulin, R., 2007. Changes in the macro-pore structure of restored soil caused by compaction beneath heavy agricultural machinery: a morphometric study. Eur. J. Soil Sci. 58, 1062–1073.

Servadio, P., Marsili, A., Vignozzi, N., Pellegrini, S., Pagliai, M., 2005. Effects on some soil qualities in central Italy following the passage of four wheel drive tractor fitted with single and dual tires. Soil Till. Res. 84, 87–100.

Silva, S.R., Barros, N.F., Costa, L.M., Leite, F.P., 2008. Soil compaction and eucalyptus growth in response to forwarder traffic intensity and load. R. Bras. Ci. Solo 32, 921–932.

Startsev, A.D., McNabb, D.H., 2001. Skidder traffic effects on water retention, pore-size distribution, and van Genuchten parameters of boreal forest soils. Soil Sci. Soc. Am. J. 65, 224–231.

Tarantino, A., de Col, E., 2008. Compaction behaviour of clay. Géotechnique. 58, 199–213.

Taylor, H.M., 1971. Effects of soil strength on seedling emergence, root growth and crop yield. In: Barnes, K.K., Carleton, W.M., Taylor, H.M., Throckmorton, R.I., van den Berg, G.E. (Eds), Compaction of agricultural soils. Am. Soc. of Agric. Eng. St. Joseph, pp. 292–305.

Thom, R., Sivakumar, R., Sivakumar, V., Murray, E.J., Mackinnon, P., 2007. Pore size distribution of unsaturated compacted kaolin: the initial states and final states following saturation. Géotechnique. 57, 469–474.

Tian, Z., Lu, Y., Ren, T., Horton, R., Heitman, J.L., 2018. Improved thermo-time domain reflectometry method for continuous in-situ determination of soil bulk density. Soil Till. Res. 178, 118–129.

Watson, K.W., Luxmoore, R.J., 1986. Estimating macroporosity in a forest watershed by use of a tension infiltrometer. Soil Sci. Soc. Am. J. 50, 578-582.

White, I., Sully, M.J., Perroux, K.M., 1992. Measurement of surface-soil hydraulic properties: disk permeameters, tension infiltrometers, and other techniques. In: Topp, G.C., Reynolds, W.D., Green, R.E. (Eds.), Advances in Measurement of Soil Physical Properties: Bringing Theory into Practice. Soil Sci. Soc. Am. Spec. Pub. 30. Soil Sci. Soc. of Am, Madison, WI, USA, pp. 69–103.

Williamson, J.R., Neilsen, W.A., 2000. The influence of forest site on rate and extent of soil compaction and profile disturbance of skid trails during ground-based harvesting. Can. J. For. Res. 30, 1196–1205.

Wilson, G.V, Luxmoore, R.J., 1988. Infiltration, macroporosity, and mesoporosity distributions on two forested watersheds. Soil Sci. Soc. Am. J. 52, 329–335.

Zhang, R., 1997. Determination of soil sorptivity and hydraulic conductivity from the disk infiltrometer. Soil Sci. Soc. Am. J. 61, 1024–1030.

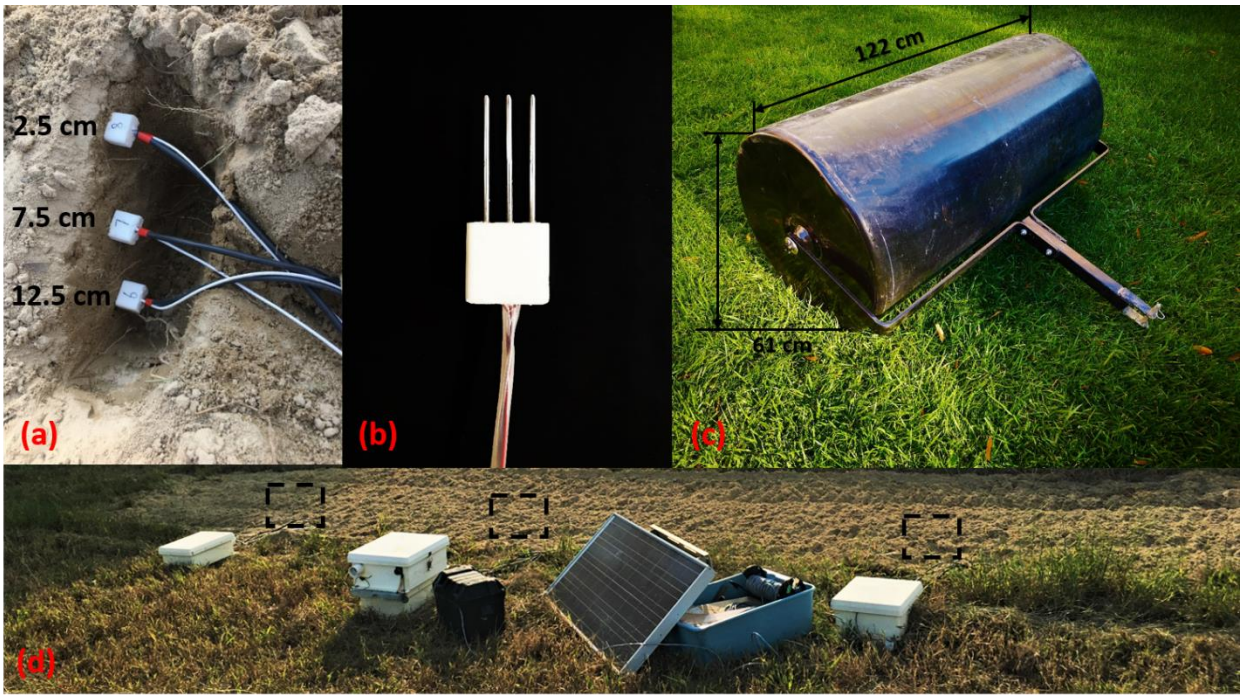

Figure 2.1. Field experiment: (a) thermo-TDR probes installed at three depths; (b) thermo-TDR probe; (c) roller used for compaction; and (d) three data logger boxes connected to probes in each sensor nest with adjacent solar panel. Dashed boxes in panel d indicate the locations where thermo-TDR probes were installed.

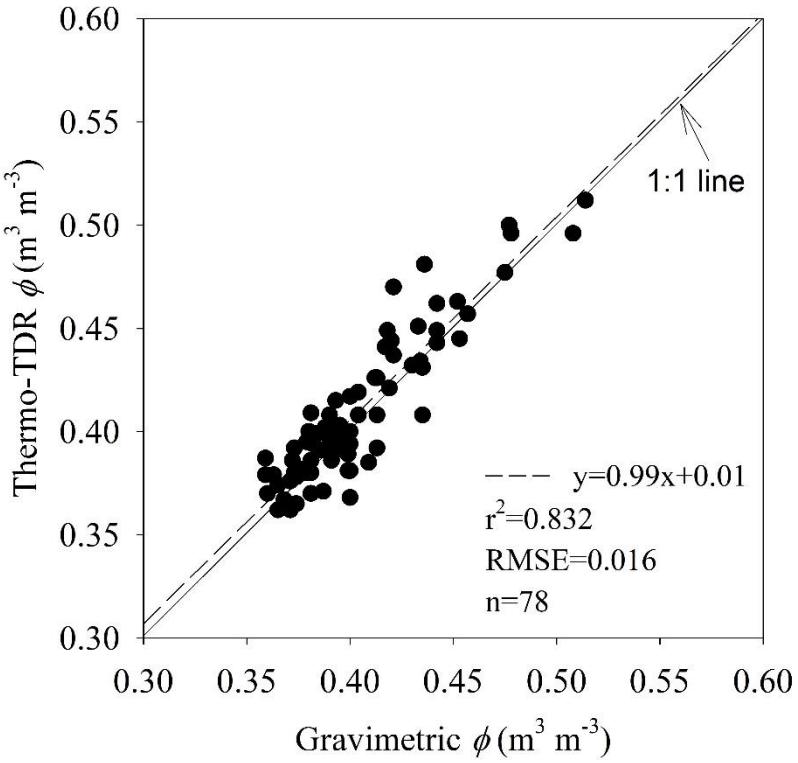

Figure 2.2. Thermo-TDR measured soil porosity (ϕ) compared to ϕ determined by the core (gravimetric) method. The dashed line indicates the fitted linear regression lines.

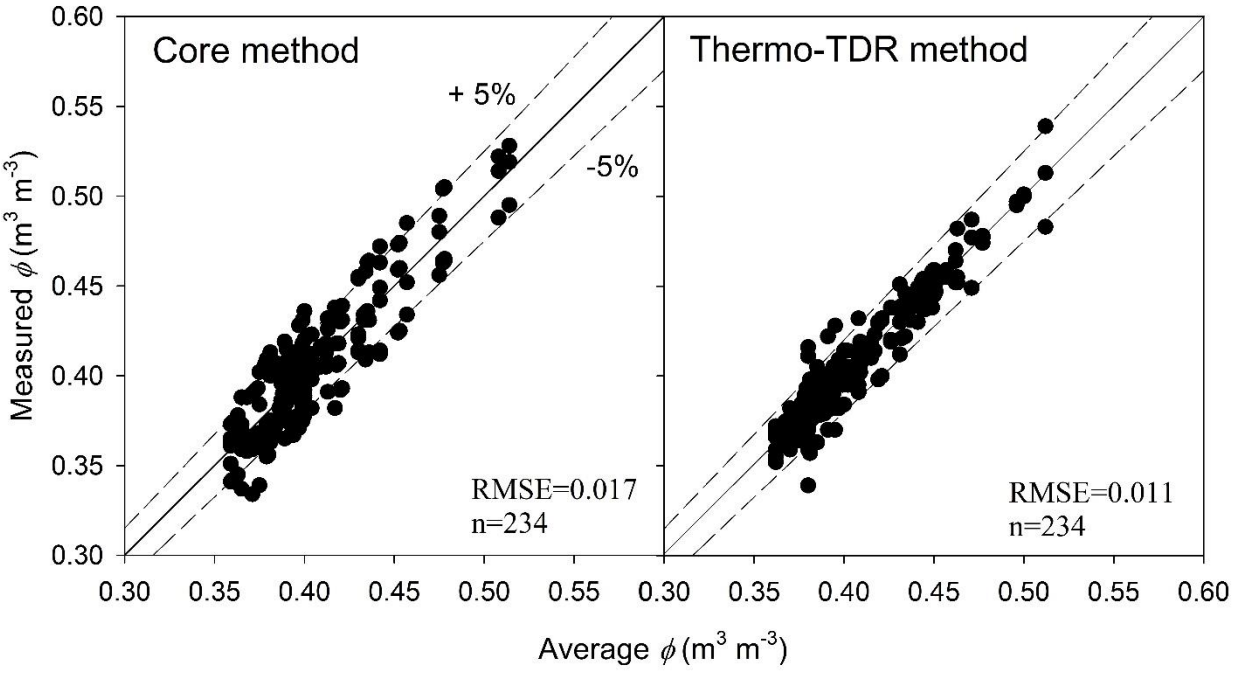

Figure 2.3. Variability of measured soil porosity ϕ by core method and thermo-TDR method for the field soil. Average ϕ is the average of measurement results (three repetitions) while measured ϕ represents individual repetitions. The dashed lines represent the 95% confidence interval.

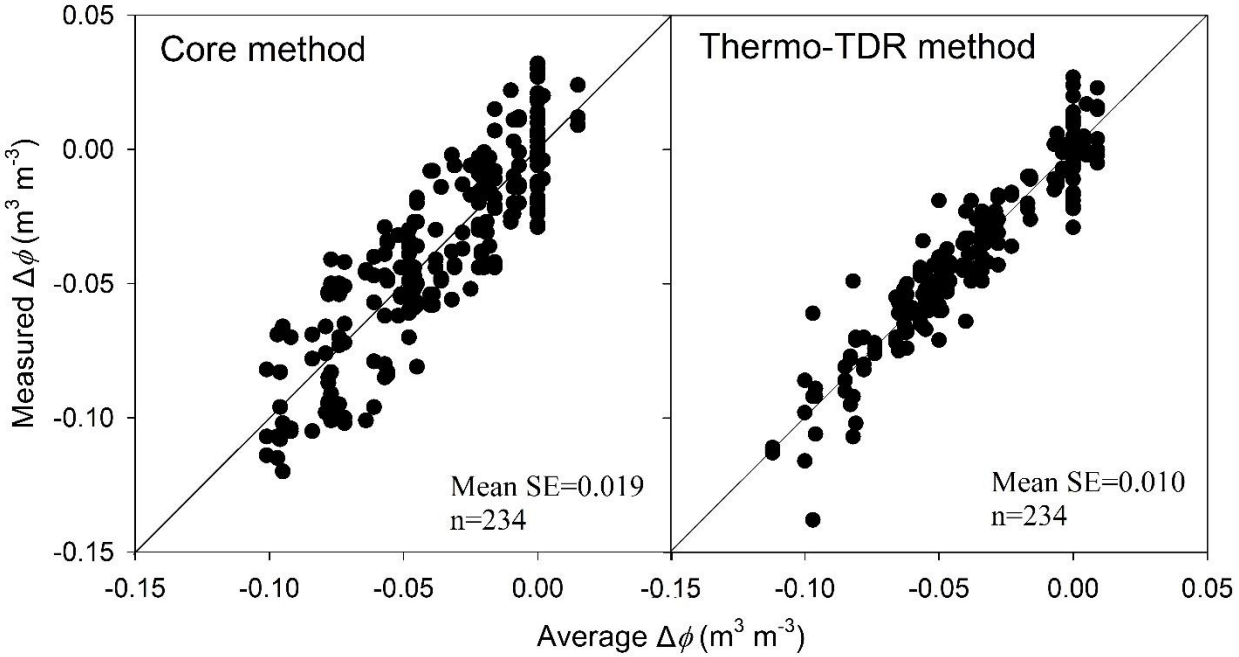

Figure 2.4. Variability of change in soil porosity ($\Delta\phi$) by core method and thermo-TDR method for the field soil. $\Delta\phi$ is equal to the difference between soil porosity measurement values after compaction and initial porosity (before any roller pass). Average $\Delta\phi$ is the average of porosity change results (three repetitions) while measured $\Delta\phi$ represents individual repetition.

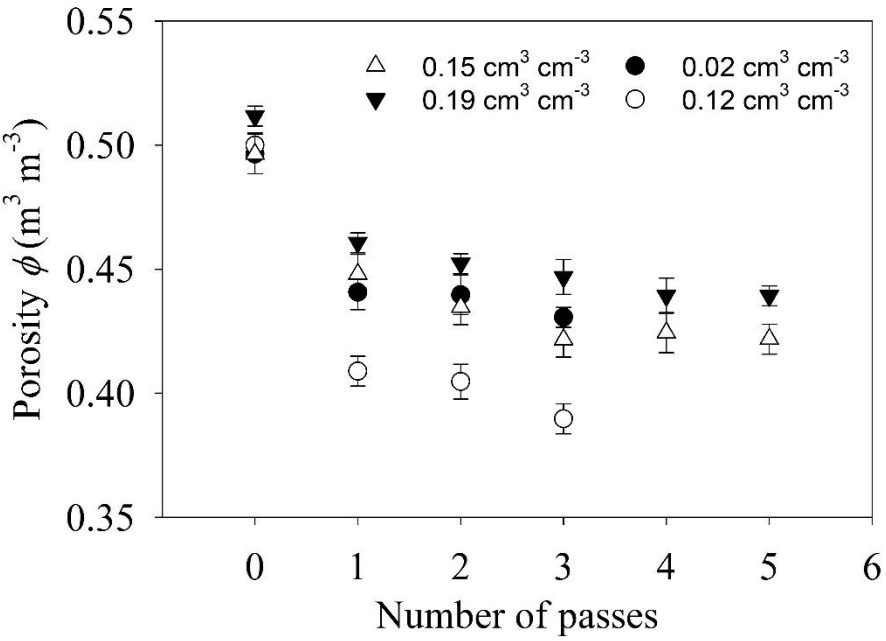

Figure 2.5. Dynamics of soil porosity of the 0-5 cm layer as the number of roller passes (three or five times) increases. The legend values represent initial water contents determined by thermo-TDR at 2.5- cm depth. Number of passes were three at 0.02 and 0.12 cm^3 cm^{-3} and five at 0.15 and 0.19 cm^3 cm^{-3}. Data at 0.21 cm^3 cm^{-3} were excluded due to differences in initial porosity. Error bars represent the standard errors of the measurements.

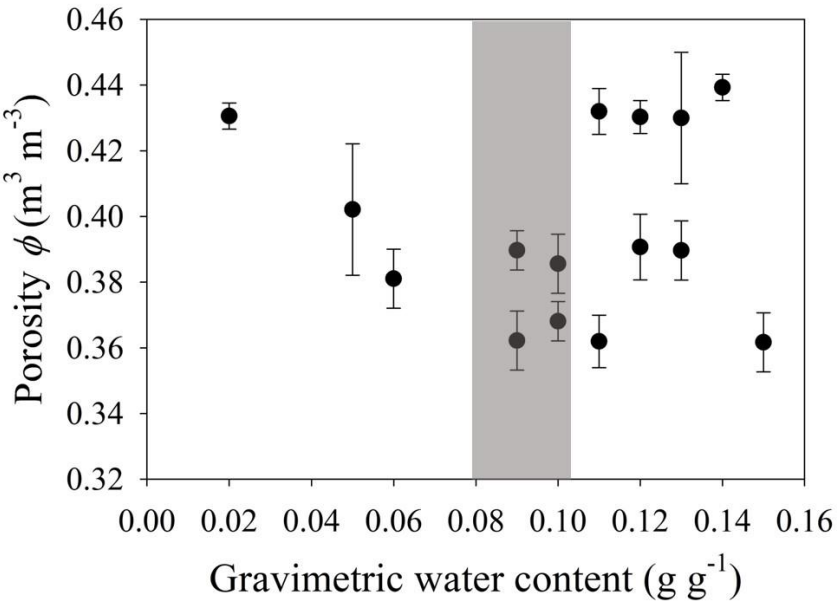

Figure 2.6. Minimum soil porosity following compaction as a function of initial gravimetric water content across all depths. Gray zone indicated the approximate most sensitive water content range at which lowest soil porosity was achieved.

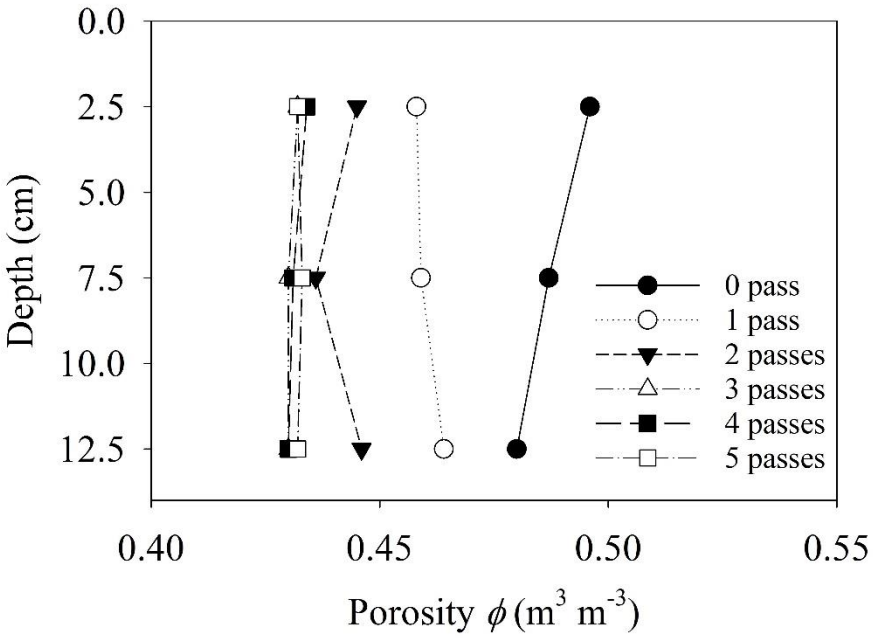

Figure 2.7. Porosity determined by thermo-TDR at 2.5-, 7.5- and 12.5-cm soil depths for water content of 0.15 cm^3 cm^{-3} following compaction. The legend indicates the number of passes during compaction.

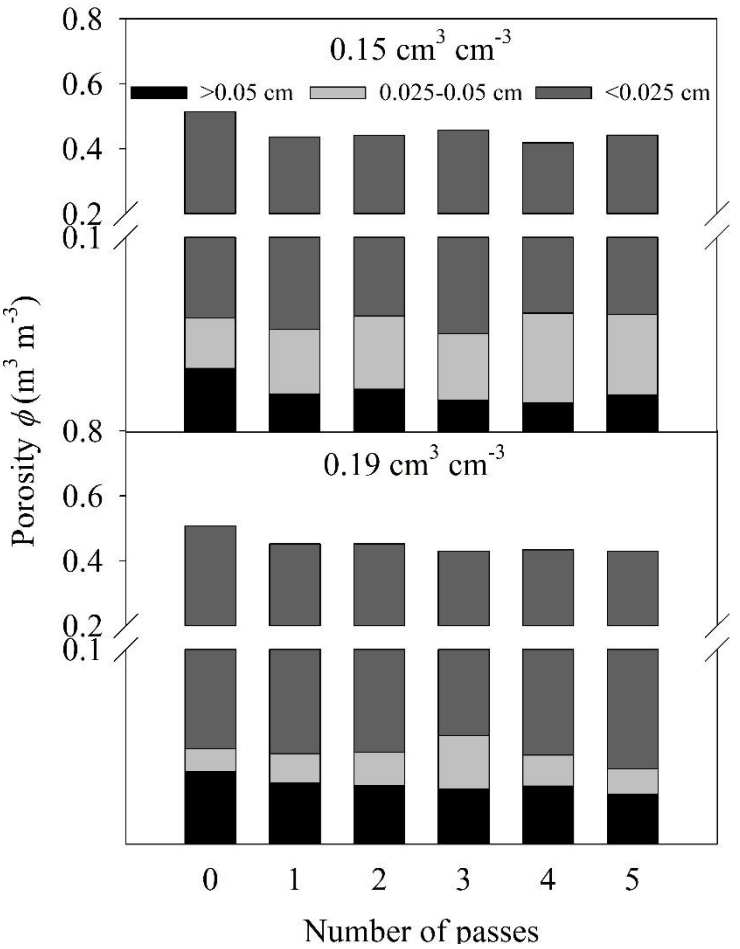

Figure 2.8. Soil pore-size distribution at water contents of 0.15 and 0.19 cm^3 cm^{-3} following compaction. The legend indicates the pore radius size range.

Chapter 3: Estimation of Soil Water Retention Curves from Soil Bulk Electrical Conductivity and Water Content Measurements

Abstract

Measurement of soil water retention curves (SWRCs) is time consuming, and there is no single laboratory device available to measure a SWRC over an entire range of relevant pressures. The van Genuchten (VG) model is commonly used to characterize the shape of the SWRC. Bulk soil electrical conductivity as a function of water content, $\sigma(\theta)$, has been used to estimate hydraulic properties of unsaturated soils, thus making it possible to relate $\sigma(\theta)$ and SWRC. The saturated and residual water content values, θ_s and θ_r, respectively, can be estimated from soil bulk density and particle size distribution. In this study, we present an approach to estimate VG parameters *m* and α from σ measured at saturated and residual soil water contents, as well as $\sigma(\theta)$ values measured at intermediate water contents. A thermo-time domain reflectometry (thermo-TDR) sensor is used to measure σ and θ in the same soil sample volume. SWRCs for three soils with different textures and bulk density values are estimated from $\sigma(\theta)$ measurements and compared with direct SWRC measurements obtained with a tension table and pressure plate extractors. Additional comparisons are made using data obtained from the literature. The proposed method to estimate SWRCs performs well when compared to direct SWRC measurements (with an average RMSE and an average bias of 0.041 and 0.008 $cm^3\ cm^{-3}$, respectively). Results indicate that the new $\sigma(\theta)$ based method accurately estimates SWRCs.

Keywords: electrical conductivity, van Genuchten model, water content, soil water retention curve, matric potential

3.1 Introduction

The soil water retention curve (SWRC), defined as the relationship between soil water content (θ) and soil water matric potential (ψ), is an important soil hydraulic relationship (Wösten and van Genuchten, 1988; Tietje and Tapkenhinrichs, 1993). The SWRC is fundamental for studying water flow processes, solute transport, and for estimating field capacity, permanent wilting point, and unsaturated hydraulic conductivity (Colman, 1947; Rawls et al., 1998; Vogel and Cislerova, 1998; Kirkham, 2005).

SWRC measurements can be time consuming and tedious (Schaap et al., 2001; Mohammadi and Vanclooster, 2011). Generally, it takes several weeks to obtain the full SWRC with laboratory equipment. Many theoretical and empirical approaches have been suggested to estimate the SWRC. Researchers have developed pedotransfer functions that estimate SWRCs from more easily measured soil properties (Campbell and Shiozawa 1994; Assouline et al., 1998; Rajkai et al. 2004; Saxton and Rawls, 2006). Various empirical models have also been developed to describe SWRCs (Gardner, 1958; Brooks and Corey, 1964; Campbell, 1974; Clapp and Hornberger, 1978; van Genuchten, 1980; Russo, 1988; Fredlund and Xing, 1994; Kosugi, 1994). Although the van Genuchten (1980) model does not describe the SWRC at θ values less than the residual water content, it is a widely used model (Cornelis et al., 2005).

In porous media, water flow and electrical current flow through electrolytes are analogous processes, and both are influenced by pore structure, porosity, tortuosity, and connectivity. Because bulk electrical conductivity (σ) is an easily measured soil property, it is possible to use σ measurements to aid the estimation of hydraulic conductivity of unsaturated soils (Urish, 1981; Slater and Lesmes, 2002; Doussan and Ruy, 2009; Niu et al., 2015). Although hydraulic

conductivity can be related to σ and described as a function of ψ and θ, relationships between σ(θ) and the SWRC (i.e., $\psi(\theta)$) are not yet well-developed.

The objective of this study was to develop a new method to estimate SWRC parameters from σ, θ and other easily measured soil properties. The new method was tested with both newly collected data and with published data. In the last section of the paper, some limitations regarding the new method are discussed.

3.2 Model Development

The van Genuchten (1980) model describes the SWRC as

$$S_e = \frac{\theta - \theta_r}{\theta_s - \theta_r} = \left[\frac{1}{1 + \left(\alpha |\psi| \right)^n} \right]^m \quad [1]$$

where S_e is effective saturation, θ is volumetric water content ($cm^3\ cm^{-3}$), θ_s and θ_r are the saturated and residual water contents ($cm^3\ cm^{-3}$), respectively, ψ is the soil water matric potential (hPa), α (> 0, cm^{-1}) is related to the inverse of the air-entry pressure, n (>1) is a pore-size distribution parameter, and $m = 1 - 1/n$ ($0 < m < 1$).

The four parameters θ_s, θ_r, α and n in the van Genuchten (1980) model can be determined by fitting Eq. [1] to SWRC measurements. In this paper, we introduce an approach to determine these parameters from soil particle size distribution, bulk density (ρ_b), and σ(θ) measurements.

When θ_s is assumed to equal the soil porosity, it can be calculated as,

$$\theta_s = 1 - \frac{\rho_b}{\rho_s} \quad [2]$$

where ρ_s is the soil particle density (assumed as 2.65 g cm^{-3}).

Residual water content (θ_r) is assumed to be the water content value below which liquid water is discontinuous and there is no liquid water flow in the soil (i.e., hydraulic conductivity is zero).

The value of θ_r is related to the specific surface of a soil, which is influenced by clay content and mineralogy (Poeplau et al., 2015). Additionally, ρ_b also affects θ_r (Assouline, 2004; Assouline, 2006; Mualem and Assouline, 1989; Tian et al., 2018). Based on data representing 50 soils (Table 3.1), we developed a simple empirical expression describing a relationship between clay fraction (f_{clay}), ρ_b, and θ_r (Fig. 3.1, $R^2 = 0.82$):

$$\theta_r = (0.0033 f_{clay} + 0.007)\rho_b / \rho_w \quad [3]$$

where ρ_w is the density of water, assumed to be 1 g cm^{-3}.

The parameter *m* is a shape factor for the SWRC model of Eq. [1]. Its estimation is somewhat less straightforward from routinely measured soil properties. We combine theory from several previous studies to arrive at an approach for estimating *m* from measurements of $\sigma(\theta)$ in the following analysis.

The bulk σ soil is represented by the summation of two terms (Rhoades et al., 1976; Friedman, 2005):

$$\sigma = \sigma_b + \sigma_s \quad [4]$$

where σ_b is electrical conductivity of the bulk liquid phase and σ_s is electrical conduction occurring at the liquid–solid interface (Waxman and Smits, 1968; Sen et al., 1988; Revil and Glover, 1998). Conductance through the solid-solid pathway is always ignored because this pathway is disrupted by water films surrounding the particles or by void spaces within the matrix that are filled with air (Rhoades et al., 1989).

The σ_b value is affected by three factors: effective water content (θ_{eff}) which accounts for the immobility of ions near the solid particle surface, electrical conductivity of soil solution (σ_w) and the specific geometry of the soil solution (F_g) (Mualem and Friedman, 1991). Thus, σ_b can be estimated as

$$\sigma_b = \sigma_w \theta_{eff} F_g \quad [5]$$

where θ_{eff} can be estimated as

$$\theta_{eff} = \theta\text{-}\theta_{1.5} \approx \theta\text{-}\theta_r \quad [6]$$

where $\theta_{1.5}$ is the water content value associated with a matric potential of -1.5 MPa.

Because F_g cannot be determined directly, we rely on the theoretical model of Mualem and Friedman (1991), which assumes that changes in water saturation have identical effects on σ and hydraulic conductivity. Thus, F_g is derived from the ratio of unsaturated soil hydraulic conductivity (K_{soil}) to that for capillary bundles (K_{cap}) with identical water retention:

$$F_g = \frac{K_{soil}}{K_{cap}} = (\theta\text{-}\theta_r)^{\beta} \frac{\left[\int_0^{S_e} \frac{1}{\psi(x)} dx\right]^2}{\int_0^{S_e} \frac{1}{\psi(x)^2} dx} \quad [7]$$

where β is an empirical pore-tortuosity factor that is commonly fixed as 0.5 (Mualem, 1976). However, many other studies have indicated that β differs among soils (Schuh and Cline, 1990; Yates et al., 1992; Leij et al., 1996). Examining data for 235 soils included in the UNSODA database, Schaap and Leij (2000) found that β was always negative, and they proposed different β values for various soil textures. In this study, we use the β values (-1.28 for sand, -6.97 for loam and clay loam) reported by Schaap and Leij (2000).

By combining Eqs. [1] and [7], the integrals in the numerator and the denominator of Eq. [7] can be rewritten (van Genuchten, 1980). Thus, F_g can be expressed as the following closed-form expression (Heimovaara et al., 1995):

$$F_g = (\theta\text{-}\theta_r)^{\beta} \frac{\left[1-(1-S_e^{1/m})^m\right]^2}{1-(1-S_e^{1/p})^p} \quad [8]$$

where p(q) is analogous to m(n) with $p = 1 - 2/q$.

Therefore, by inserting Eqs. [5], [6] and [8] into Eq. [4], Eq. [4] can be rewritten as:

$$\sigma = \sigma_w \left(\theta\text{-}\theta_r\right)^{\beta+1} \frac{\left[1-(1-S_e^{1/m})^m\right]^2}{1-(1-S_e^{1/p})^p} + \sigma_s \quad [9]$$

At either saturated or residual water contents, the right side of Eq. [9] can be simplified. Thus, we obtain the bulk soil electrical conductivity at saturation (σ_{sat}) and at residual water content (σ_{res}):

$$\sigma_{sat} = \left(\theta_s\text{-}\theta_r\right)^{\beta+1} \sigma_w + \sigma_s \quad [10]$$

$$\sigma_{res} = \sigma_s \quad [11]$$

This leads to the following equation between relative σ and S_e:

$$\frac{\sigma\text{-}\sigma_{res}}{\sigma_{sat}\text{-}\sigma_{res}} = \frac{\left[1-(1-S_e^{1/m})^m\right]^2}{1-(1-S_e^{1/p})^p} S_e^{\beta+1} \quad [12]$$

By fitting Eq. [12] to relative σ and relative θ data, *m* can be obtained from Eq. [12].

After obtaining θ_s, θ_r, and *m* from Eqs. [2], [3], and [12], α is the lone remaining unknown parameter in the van Genuchten SWRC model. It can be estimated from other parameters (θ_s, θ_r, *m*) using the following approach.

As illustrated in Figure 3.2, the following expression can be obtained from a SWRC:

$$A_i = \frac{\theta_s - \theta_i}{\ln|\psi_i| - \ln|\psi_a|} \quad [13]$$

where A_i is the magnitude of the slope at the inflection point (the point where the modulus of slope reaches its maximum), θ_i and ψ_i are the water content and matric potential at the inflection point, respectively. Parameter ψ_a is the air-entry pressure, which has been approximated from the intersection of the tangent line drawn across the inflection point and horizontal line drawn across θ_s (Fredlund and Xing, 1994; Zhai and Rahardjo, 2012). In this study, ψ in natural log (ln| ψ|) rather

than in the common log ($\log|\psi|$) was used to simplify the calculation of the derivative of Eq. [1] at the inflection point from Eqs. [A5]-[A7] in Dexter (2004):

$$A_i = \frac{d(\theta_i)}{d(\ln|\psi_i|)} = \left| -n(\theta_s - \theta_r)\left[1 + \frac{1}{m}\right]^{-(m+1)} \right| \quad [14]$$

$$\theta_i = (\theta_s - \theta_r)\left[1 + \frac{1}{m}\right]^{-m} + \theta_r \quad [15]$$

$$\psi_i = \frac{1}{\alpha}\left(\frac{1}{m}\right)^{\frac{1}{n}} \quad [16]$$

We used α (cm^{-1}) and ψ_a (cm) for 63 soils of different soil textures (Fig. 3.3) from published data and the UNSODA database (Fig. 3.4) and developed the empirical relationship between them as:

$$\psi_a = (0.30/\alpha)^{1.26} \quad [17]$$

Eq. [13] can be rewritten as:

$$\left| -n(\theta_s - \theta_r)\left[1 + \frac{1}{m}\right]^{-(m+1)} \right| = \frac{\theta_s - \left((\theta_s - \theta_r)\left[1 + \frac{1}{m}\right]^{-m} + \theta_r\right)}{\ln\left|\frac{1}{\alpha}\left(\frac{1}{m}\right)^{\frac{1}{n}}\right| - \ln\left|\left(\frac{0.30}{\alpha}\right)^{1.26}\right|} \quad [18]$$

A value for α can thus be obtained from θ_s, θ_r and m (n) using Eq. [18].

3.3 Materials and Methods

3.3.1 Laboratory Experiments

Laboratory measurements of σ(θ) and SWRC were performed on sand (Glassil 530, Unimin Corporation-Marston, NC), silt loam- (Tennessee, USA) and clay loam- (Illinois, USA) textured soil materials packed at various bulk densities. The basic physical properties of these soils are presented in Table 3.2. The soil samples were dried, ground and sieved through a 2-mm screen,

and then repacked into soil columns (50-mm inner diameter and 50-mm long) to selected ρ_b values (Table 3.2). At each ρ_b, three repetitions were used. A tension table (08.01 Sandbox, Eijkelkamp, Zeitz, Germany) was used to measure SWRCs in a matric potential range of 0 to -100 cm. The soil cores were placed on the tension table and slowly saturated with tap water from the bottom. Thermo-TDR sensors were inserted vertically into the samples from the top to determine σ and θ at each selected matric potential value. Details about thermo-TDR sensors can be found in Lu et al. (2017), and approaches for calculating σ and θ from sensor measurements can be found in Heimovaara et al. (1995) and Ren et al. (1999), respectively. Sequential drainage of initially saturated soil samples to equilibrium matric potentials of -5, -10, -20, -30, -40, -50, -60, -80, -100 cm, was achieved on the tension table. The θ value was determined each 4h after changing to a new matric potential until θ was stable. After each hydraulic equilibrium was achieved (i.e., θ was stable), σ and θ were measured three times at each matric potential.

The pressure plate extractor method (Dane and Hopmans, 2002) was used to measure SWRCs at additional matric potential values of -50, -100, -500, -1000 and -1500 kPa (an additional measurement at 30 kPa was also included on the clay loam-textured soils). Samples were pre-saturated with tap water and then desorbed to each corresponding matric potential. To obtain σ(θ) data corresponding to these conditions, we repacked the soil columns at the appropriate θ values corresponding to desired ψ values as indicated by the SWRC. Samples were established by adding the proper amounts of tap water to the soil and mixing thoroughly. The moist soil was then packed into a soil column (50-mm inner diameter and 50-mm long) at selected ρ_b values. Thermo-TDR sensors were again used to determine σ(θ) with three repetitions at each condition.

In addition to making new laboratory observations, we also analyzed data reported by Doussan and Ruy (2009). Their laboratory measurements included a loam (Collias, France) and a sand

(Fontainebleau, France). Electrical conductivity measurements were obtained with a pair of electrodes embedded in soil samples on a tension table or in a pressure chamber for matric potential values ranging from 0 to -1471 kPa (150 m H_2O). SWRCs at ψ values lower than 1471 kPa were reached by air drying the samples.

3.3.2 Statistical Analysis

In this study, we compared SWRCs estimated by the proposed $\sigma(\theta)$ method to the directly measured SWRCs. The estimated SWRCs were evaluated using root mean square error (RMSE) and bias:

$$\text{RMSE}=\sqrt{\frac{\sum\left(\theta_{\text{estimated}}-\theta_{\text{measured}}\right)^2}{N}} \quad [19]$$

$$\text{Bias}=\frac{\sum\left(\theta_{\text{estimated}}-\theta_{\text{measured}}\right)}{N} \quad [20]$$

where N was the number of data pairs, and $\theta_{\text{estimated}}$ and θ_{measured} were the estimated and measured water content values, respectively.

3.4. Results and Discussion

3.4.1 Validation of the Estimated θ_s and θ_r Values

Figure 3.5 compares the θ_s values estimated by Eq. [2] to measured θ_s values. Equation [1] was fitted to the newly obtained θ_s dataset and to θ_s values from Doussan and Ruy (2009). Overall, Eq. [2] agree well with the measured values with a bias of 0.015 $cm^3\ cm^{-3}$ and a RMSE of 0.022 $cm^3\ cm^{-3}$. The slight overestimation is possibly caused by entrapped air in soil pores (van Genuchten et al., 1991; Snehota et al., 2015). Even so, the performance of Eq. [2] is sufficient for subsequent analysis.

Validation results in Figure 3.6 indicate that Eq. [3] estimates θ_r well for most of the soils (with a bias of -0.001 $cm^3\ cm^{-3}$ and RMSE of 0.048 $cm^3\ cm^{-3}$). Although the errors are larger than

those for θ_s estimates, the θ_r estimates are deemed to be acceptable, because for a soil with a wide range of water contents, θ_r is often less important than are the other van Genuchten parameters (*m* and α) in describing the SWRC.

3.4.2 Using σ(θ) to Estimate a SWRC

We used a combination of Eqs. [2], [3], [12] and [18] to estimate the SWRC curve, which is hereafter, denoted as the "σ(θ)-SWRC method". The σ(θ)-SWRC method was tested on five soils. The measured and estimated SWRC data are presented in Figure 3.7. As evident, the fitted curves for the σ(θ)-SWRC method followed the patterns of the measured SWRCs for sand and clay loam soils with various ρ_b values, which indicated that the σ(θ)-SWRC method accurately estimated the SWRC. The exceptions were for the $\ln|\psi|$ range between 3 and 5 for sand and $\ln|\psi|$ larger than 6 for silt loam, where the SWRCs estimated by the σ(θ)-SWRC method were flatter and provided larger θ estimates than the measured values. The performance of the σ(θ)-SWRC method became worse as ρ_b increased (Table 3.3). For example, for clay loam, the RMSEs were 0.024, 0.036 and 0.066 $cm^3\ cm^{-3}$ for ρ_b values of 1.05, 1.1 and 1.2 $g\ cm^{-3}$, respectively. The corresponding biases were -0.015, 0.034 and 0.051 $cm^3\ cm^{-3}$, respectively.

The σ(θ)-SWRC method was also tested with data for two soils reported by Doussan and Ruy (2009). Overall, the approach performed well for Fontainebleau sand and Collias loam (Figure. 3.8). Doussan and Ruy (2009) also reported measured values for a silty clay loam, but we did not analyze those data, because the unimodal VG model (Eq. [1]) did not fit the bimodal SWRC of the silty clay loam soil well.

The performance of the σ(θ)-SWRC method for each of the soils evaluated in this study is presented in Figure 3.9. In general, θ values estimated at selected ψ values via the σ(θ)-SWRC method showed a high degree of agreement to the measured θ values. The slopes of the regression

lines and the coefficients of determination (R^2) for all of the soils were greater than 0.90, indicating that the σ(θ)-SWRC method provided reliable estimates. Error analysis showed that the RMSE was 0.020-0.066 $cm^3\ cm^{-3}$ and the bias was -0.018-0.051 $cm^3\ cm^{-3}$ (Table 3.3). Across the five soils, the σ(θ)-SWRC method gave θ estimates with an average RMSE and an average bias of 0.041 $cm^3\ cm^{-3}$ and 0.008 $cm^3\ cm^{-3}$, respectively. Thus, the general accuracy of the σ(θ)-SWRC method was reasonable.

3.4.3 Model Limitations

There are some limitations to the σ(θ)-SWRC method. Eqs. [9]-[11] treat σ_s as a constant independent of θ for a specific soil. However, Amente et al. (2000) observed that σ_s increases as θ increases (θ must be larger than a certain value similar to θ_r) for sandy soils. Additionally, σ_s is affected by pore geometry (i.e., pore connectivity and tortuosity) at saturation. Waxman and Smits (1968) propose a model for soils containing clay and exhibiting significant surface conduction, which represents σ_s as follows:

$$\sigma_s = \frac{S^{\gamma-1}\sigma_{sur}}{F_{sat}} \qquad [21]$$

where S is degree of saturation ($=\theta/\theta_s$), γ is a cementation exponent, F_{sat} is the electrical formation factor at saturation and σ_{sur} is electrical conductivity of a solid surface associated with counter ions of the electrical double layer. The value for σ_{sur} is related to cation exchange capacity, and thus, in part, it is related to the soil clay content. Therefore, σ_s tends to increase as clay content increases, and thus, larger m estimation error occurs in analysis where we assume σ_s to be a constant in order to eliminate it on the left side of Eq. [12]. Estimation error for m causes inaccurate α estimates, and thus, inaccurate SWRC estimation.

In addition, ρ_b also influences the performance of the σ(θ)-SWRC method for the same reason. As ρ_b increases, S and σ_s increase at the same value of water content, thus causing larger error due

to the assumption that σ_s is constant. As mentioned, the σ(θ)-SWRC method performance worsens as ρ_b values increase for a given soil (Figure 3.7).

The model of Mualem and Friedman (1991) also has some limitations. First, it assumes that water content has an identical effect on the soil electrical conductivity and the hydraulic conductivity. However, this assumption is invalid for fine-textured soils where electrical conduction is dominated by surface conduction (surface area). Surface area affects the two parameters in opposite ways: as surface area increases, σ increases (surface conduction increases) but permeability decreases, thus hydraulic conductivity decreases. Secondly, the Mualem and Friedman (1991) model does not properly describe the σ of soils close to full saturation (Eq. [10]), and the prediction from this model behaves anomalously after exceeding a certain water content (water content corresponding to air-entry value ψ_a) (Weerts et al., 1999). These limitations influence its performance on estimating SWRC parameters from σ(θ).

3.5 Conclusion

In this study, we developed a σ(θ)-SWRC method to estimate the van Genuchten SWRC parameters from σ(θ) measurements. The σ(θ)-SWRC method performed well on five soils of various textures and ρ_b values. Estimation of SWRCs with the σ(θ)-SWRC method should be further evaluated for a wide range of soils.

3.6 Acknowledgements

Thanks to Dr. Doussan for providing electrical conductivity and water content data for additional soils. This research was supported through the China Scholarship Council, US Army Research Laboratory (Grant Number: W911NF-16-1-0287), US National Science Foundation (Grant Number: 1633806), and the USDA-NIFA Multi-State Project 4188.

3.7 References

Abdelkabir, M., Bruno, B., Miche, A., Mbonimpa, M., 2013. Conversion of the modified kovćs model parameters to the Brooks and Corey and van Genuchten model parameters for the water retention curve of sandy and silty soils. J. Irrig. Drain. Eng. 139, 388–398.

Amente, G., Baker, J.M., Reece, C.F., 2000. Estimation of soil solution electrical conductivity from bulk soil electrical conductivity in sandy soils. Soil Sci. Soc. Am. J. 64, 1931–1939.

Assouline, S., Tavares-Filho, J., Tessier, D., 1997. Effect of compaction on soil physical and hydraulic properties: Experimental results and modeling. Soil Sci. Soc. Am. J. 61, 390–398.

Assouline, S., Tessier, D., Bruand, A., 1998. A conceptual model of the soil water retention curve. Water Resour. Res. 34, 223–231.

Assouline, S., 2004. Rainfall-induced soil surface sealing: A critical review of observations, conceptual models, and solutions. Vadose Zo. J. 3, 570–591.

Assouline, S., 2006. Modeling the relationship between soil bulk density and the water retention curve. Vadose Zo. J. 5, 554–563.

Brooks, R.H., Corey, A.T., 1964. Hydraulic properties of porous media. In Hydrology papers. Papers, 3 Colorado State Univ., Fort Collins, CO., p. 27.

Campbell, G.S., 1974. A simple method for determining unsaturated conductivity from moisture retention data. Soil Sci. 117, 311–314.

Campbell, G.S., Shiozawa, S., 1994. Prediction of hydraulic properties of soils using particle-size distribution and bulk density data. Indirect Methods for Estimating the Hydraulic Properties of Unsaturated Soils. University of California, Riverside, CA, pp. 317–328.

Clapp, R.B., Hornberger, G.M., 1978. Empirical equations for some soil hydraulic properties. Water Resour. Res. 14, 601–604.

Colman, E., 1947. A laboratory procedure for determining the field capacity of soils. Soil Sci. 63, 277–284.

Cornelis, W.M., Khlosi, M., Hartmann, R., Van Meirvenne, M., De Vos, B., 2005. Comparison of unimodal analytical expressions for the soil-water retention curve. Soil Sci. Soc. Am. J. 69, 1902–1911.

Dane, J.H., Hopmans, J.W., 2002. Water retention and storage. In: Dane, J.H., Topp, G.C. (Eds.), Methods of Soil Analysis. Part. 4. Physical Methods. SSSA, Madison, WI, pp. 671–796.

Dexter, A.R., 2004. Soil physical quality Part I. Theory, effects of soil texture, density, and organic mailer, and effects on root growth. Geoderma 120, 201–214.

Doussan, C., Ruy, S., 2009. Prediction of unsaturated soil hydraulic conductivity with electrical conductivity. Water Resour. Res. 45, 1–12.

Fredlund, D.G., Xing, A., 1994. Equations for the soil-water characteristic curve. Can. Geotech. J. 31, 521–532.

Friedman, S.P., 2005. Soil properties influencing apparent electrical conductivity: A review. Comput. Electron. Agric. 46, 45–70.

Gardner, W.R., 1958. Some steady-state solutions of the unsaturated moisture flow equation with application to evaporation from a water table. Soil Sci. 85, 228–232.

Heimovaara, T.J., Focke, a. G., Bouten, W., Verstraten, J.M., 1995. Assessing temporal variations in soil water composition with time domain reflectometry. Soil Sci. Soc. Am. J. 59, 689–698.

Rajkai, K., Kabos, S., Van Genuchten, M.T., 2004. Estimating the water retention curve from soil properties: Comparison of linear, nonlinear and concomitant variable methods. Soil Tillage Res. 79, 145–152.

Kirkham, M. B., 2005. Principles of soil and plant water relations, 500 pp., Elsevier Academic Press, Amsterdam, San Diego, California.

Kosugi, K., 1994. Three-parameter lognormal distribution model for the soil water retention. Water Resour. Res. 30, 891–901.

Leij, F. J., Alves, W. J., and van Genuchten, M. T., 1996. The UNSODA unsaturated soil hydraulic database: User's manual, National Risk Management Research Laboratory, Office of Research and Development, US Environmental Protection Agency.

Lu, S., Ren, T., Gong, Y., Horton, R., 2008. Evaluation of three models that describe soil water retention curves from saturation to oven dryness. Soil Sci. Soc. Am. J. 72, 1542–1546.

Lu, Y., Liu, X., Zhang, M., Heitman, J. L., Horton, R., and Ren, T., 2017. Thermo-time domain reflectometry method: Advances in monitoring in situ soil bulk density. Methods of Soil Analysis 2. doi:10.2136/msa2015.0031

Ma, Q., Hook, J.E., Ahuja, L.R., 1999. Influence of three-parameter conversion methods between van Genuchten and Brooks-Corey functions on soil hydraulic properties and water-balance predictions. Water Resour. Res. 35, 2571–2578.

Mohammadi, M.H., Vanclooster, M., 2011. Predicting the soil moisture characteristic curve from particle size distribution with a simple conceptual model. Vadose Zo. J. 10, 594–602.

Moroizumi, T., Horino, H., 2004. Tillage effects on subsurface drainage. Soil Sci. Soc. Am. J. 68, 1138–1144.

Mualem, Y., 1976. A new model for predicting the hydraulic conductivity of unsaturated porous media. Water Resour. Res. 12, 564–566.

Mualem, Y., Assouline, S., 1989. Modeling soil seal as a nonuniform layer. Water Resour. Res. 25, 2101–2108.

Mualem, Y., Friedman, S.P., 1991. Theoretical prediction of electrical conductivity in saturated and unsaturated soil. Water Resour. Res. 27, 2771–2777.

Nemes, A., Schaap, M.G., Leij, F.J., Wösten, J.H.M., 2001. Description of the unsaturated soil hydraulic database UNSODA version 2.0. J. Hydrol. 251, 151–162.

Niu, Q., Fratta, D., Wang, Y.H., 2015. The use of electrical conductivity measurements in the prediction of hydraulic conductivity of unsaturated soils. J. Hydrol. 522, 475–487.

Poeplau, C., Eriksson, J., Kätterer, T., 2015. Estimating residual water content in air-dried soil from organic carbon and clay content. Soil Tillage Res. 145, 181–183.

Rawls, W., Gimenez, D., Grossman, R., W. J. Rawls, D. Gimenez, R. Grossman, Rawls, W., Gimenez, D., Grossman, R., 1998. Use of soil texture, bulk density, and slope of the water retention curve to predict saturated hydraulic conductivity. Trans – ASAE 41, 983–988.

Ren, T., Noborio, K., Horton, R., 1999. Measuring soil water content, electrical conductivity, and thermal properties with a thermo-time domain reflectometry probe. Soil Sci. Soc. Am. J. 63, 450–457.

Revil, A., Glover, P.W.J., 1998. Nature of surface electrical conductivity in natural sands, sandstones, and clays. Geophys. Res. Lett. 25, 691–694.

Rhoades, J.D., Raats, P.A.C., Prather, R.J., 1976. Effects of liquid-phase electrical conductivity, water content, and surface conductivity on bulk soil electrical conductivity. Soil Sci. Soc. Am. J. 40, 651–655.

Rhoades, J.D., Manteghi, N.A., Shouse, P.J., Alves, W.J., 1989. Soil electrical conductivity and soil Salinity: new formulations and calibrations. Soil Sci. Soc. Am. J. 53, 433–439.

Russo, D., 1988. Determining soil hydraulic properties by parameter estimation: On the selection of a model for the hydraulic properties. Water Resour. Res. 24, 453–459.

Saxton, K.E., Rawls, W.J., 2006. Soil water characteristic estimates by texture and organic matter for hydrologic solutions. Soil Sci. Soc. Am. J. 70, 1569–1578.

Schaap, M.G., Leij, F.J., 2000. Improved prediction of unsaturated hydraulic conductivity with the Mualem-van Genuchten model. Soil Sci. Soc. Am. J. 64, 843–851.

Schaap, M.G., Leij, F.J., van Genuchten, M.T., 2001. ROSETTA: a computer program for estimating soil hydraulic parameters with hierarchical pedotransfer functions. J. Hydrol. 251, 163–176.

Schuh, W.M. and Cline, R.L., 1990. Effect on soil properties on unsaturated hydraulic conductivity pore-interaction factors. Soil Sci. Soc. Am. J. 54, 1509–1518.

Scorza Júnior, R.P., da Silva, J.P., 2011. Sensibility analysis of the pearl model for pesticide leaching in the State of Mato Grosso do Sul, Brazil. Eng. Agric. 31, 965–973.

Sen, P.N., Goode, P.A., Sibbit, A., 1988. Electrical conduction in clay bearing sandstones at low and high salinities. J. Appl. Phys. 63, 4832–4840.

Slater, L., Lesmes, D.P., 2002. Electrical-hydraulic relationships observed for unconsolidated sediments. Water Resour. Res. 38, 1–13.

Snehota, M., Jelinkova, V., Sobotkova, M., Sacha, J., Vontobel, P., Hovind, J., 2015. Water and entrapped air redistribution in heterogeneous sand sample: Quantitative neutron imaging of the process. Water Resour. Res. 1359–1371.

Stankovich, J.M., Lockington, D.A., 1995. Brooks-Corey and Van Genuchten soil-water-retention models. J. Irrig. Drain. Eng. 121, 1–7.

Tian, Z., Gao, W., Kool, D., Ren, T., Horton, R., Heitman, J.L., 2018. Approaches for estimating soil water retention curves at various bulk densities with the extended Van Genuchten model. Water Resour. Res. 54, 5584–5601.

Tietje, O., Tapkenhinrichs, M., 1993. Evaluation of pedo-transfer Functions. Soil Sci. Soc. Am. J. 57, 1088–1095.

Urish, D.W., 1981. Electrical resistivity-hydraulic conductivity relationships in glacial outwash aquifers. Water Resour. Res. 17, 1401–1408.

van Genuchten, M.T., 1980. A closed-form equation for predicting the hydraulic conductivity of unsaturated soils. Soil Sci. Soc. Am. J. 44, 892–898.

van Genuchten, M.T., Leij, F.J., Yates, S.R., 1991. The RETC code for quantifying the hydraulic function of unsaturated soils, version 1.0, EPA report 600/2-91/065. US Salinity Laboratory, USDA_ARS, Riverside, California.

Vogel, T., Cislerova, M., 1988. On the reliability of unsaturated hydraulic conductivity calculated from the moisture retention curve. Transp. Porous Media 3, 1–15.

Waxman, M.H., Smits, L.J.M., 1968. Electrical Conductivities in Oil-Bearing Shaly Sands. Soc. Pet. Eng. J. 8, 107–122.

Weerts, A.H., Bouten, W., Verstraten, J.M., 1999. Simultaneous measurement of water retention and electrical conductivity in soils: Testing the Mualem-Friedman tortuosity model. WATER Resour. Res. 35, 1781–1787.

Wösten, J.H.M., Van Genuchten, M.T., 1988. Using texture and other soil properties to predict the unsaturated soil hydraulic functions. Soil Sci. Soc. Am. J. 52, 1762–1770.

Yates, S.R., Van Genuchten, M.T., Warrick, A.W., Leij, F.J., 1992. Analysis of measured, predicted, and estimated hydraulic conductivity using the RETC computer program. Soil Sci. Soc. Am. J. 56, 347–354.

Zhai, Q., Rahardjo, H., 2012. Determination of soil-water characteristic curve variables. Comput. Geotech. 42, 37–43.

Table 3.1 Texture, particle size distribution (PSD) and bulk density (ρ_b) values of soils used to establish a relationship between clay content, ρ_b, and residual water content, Eq. [3] in this study.

Texture	PSD Sand	Silt	Clay	ρ_b	Sources
	----------%----------			g cm^{-3}	
sand	100	0	0	1.52, 1.58, 1.67	New measurements
silt loam	21.5	66.7	11.8	1.05, 1.15, 1.25	
clay loam	23.6	49.2	27.2	1.05, 1.1, 1.2	
loamy sand	85	9	6	1.44, 1.5, 1.55, 1.6, 1.7	Tian et al. (2018)
silt loam	18	56	26	1.09,1.19, 1.29, 1.38	
clay	2	17	81	0.96, 1.27	Assouline et al. (1997)
clay	6	11	83	1.25, 1.6	
sand	93	1	6	1.6	Lu et al. (2008)
sandy loam	67	21	12	1.41	
loam	40	49	11	1.3	
silt loam	27	51	22	1.34	
silty clay loam	19	54	27	1.29	
silt loam	11	70	19	1.33	
silty clay loam	8	60	32	1.32	
silt loam	2	73	25	1.2	
sandy loam	70	21	9	0.68, 0.89	Moroizumi and Horino (2004)
clay	24.5	12.5	63	1.02	Scorza Júnior and da Silva (2011)
clay	22.9	10.8	66.3	1.11	
clay	21.2	9.1	69.7	1.14	
clay	19.5	9.2	71.3	1.11	
clay	19.5	9.2	71.3	1.10	
sandy clay loam	74.3	4.4	21.3	1.42	
sandy clay loam	74.3	2.7	23	1.51	
sandy clay loam	72.6	4.4	23	1.49	
sandy clay loam	71	4.3	24.7	1.46	
sandy clay loam	69.3	4.4	26.3	1.41	
loamy sand	88.8	3.2	8	1.36	
loamy sand	86.9	3.4	9.7	1.55	
loamy sand	85.2	3.7	11.1	1.53	
loamy sand	86.9	3.4	9.7	1.51	
loamy sand	88.8	1.5	9.7	1.47	

Table 3.2 Texture, particle size distribution (PSD) and bulk density (ρ_b) of three newly investigated soils and data obtained from the literature for two soils.

Texture	PSD			ρ_b	Sources
	Sand	Silt	Clay		
	----------%----------			g cm^{-3}	
sand	100	0	0	1.52, 1.58, 1.67	New measurements
silt loam	21.5	66.7	11.8	1.05, 1.15, 1.25	
clay loam	23.6	49.2	27.2	1.05, 1.1, 1.2	
Fontainebleau sand	99.5	0.3	0.2	1.67	Doussan and Ruy (2009)
Collias loam	37.7	48.7	13.6	1.49	

Table 3.3 The root mean square error (RMSE), bias and coefficient of determination (R^2) between σ(θ)-SWRC estimated water content values and measured water content values for soils with various ρ_b values.

Texture	ρ_b g cm^{-3}	RMSE cm^3 cm^{-3}	Bias cm^3 cm^{-3}	R^2
Sand	1.52	0.033	0.005	0.97
	1.58	0.034	0.013	0.97
	1.67	0.035	0.009	0.96
Silt loam	1.05	0.053	0.004	0.95
	1.15	0.048	-0.009	0.95
	1.25	0.049	-0.001	0.93
Clay loam	1.05	0.024	-0.018	0.99
	1.1	0.036	0.034	0.99
	1.2	0.066	0.051	0.91
Fontainebleau sand	1.67	0.033	0.007	0.95
Collias loam	1.49	0.020	-0.001	0.99
Average		**0.041**	**0.008**	**0.95**

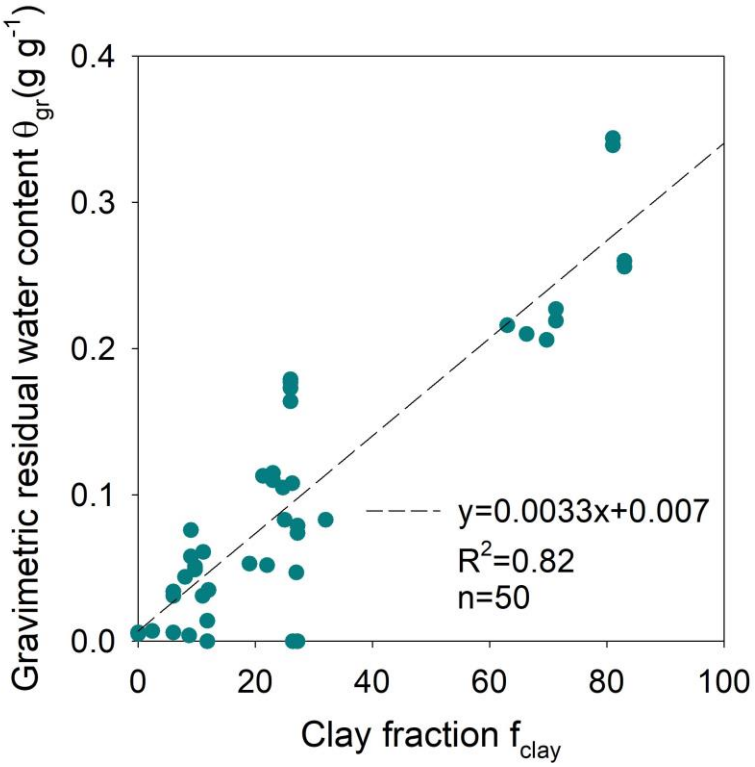

Figure 3.1. Gravimetric residual water content (θ_{gr}) as a function of clay fraction (f_{clay}) for soils in Table 3.1. The dashed line indicates the fitted linear regression line.

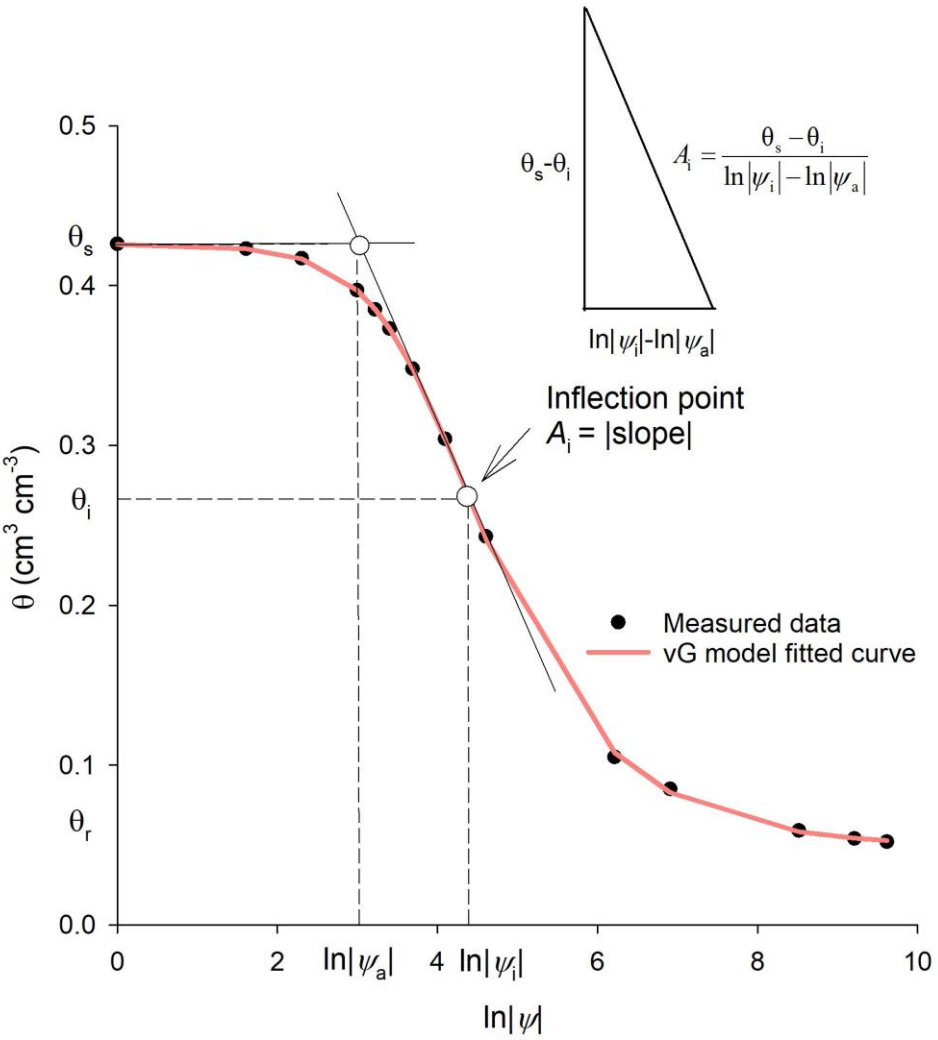

Figure 3.2. Soil water retention curve (SWRC), expressed as volumetric water content, θ (cm^3 cm^{-3}), versus natural log matric potential, ln|ψ|, where the black circle points indicate measured data and the pink solid line (VG fit) indicates the fitted van Genuchten curve (Eq. [1]). The black solid line is drawn across two white circle points with slope -A_i (the left one is the point corresponding to the θ_s and natural log air-entry pressure, ln| ψ_a|; the right point is the inflection point, where the water content and natural log matric potential are θ_i and ln|ψ_i|, respectively).

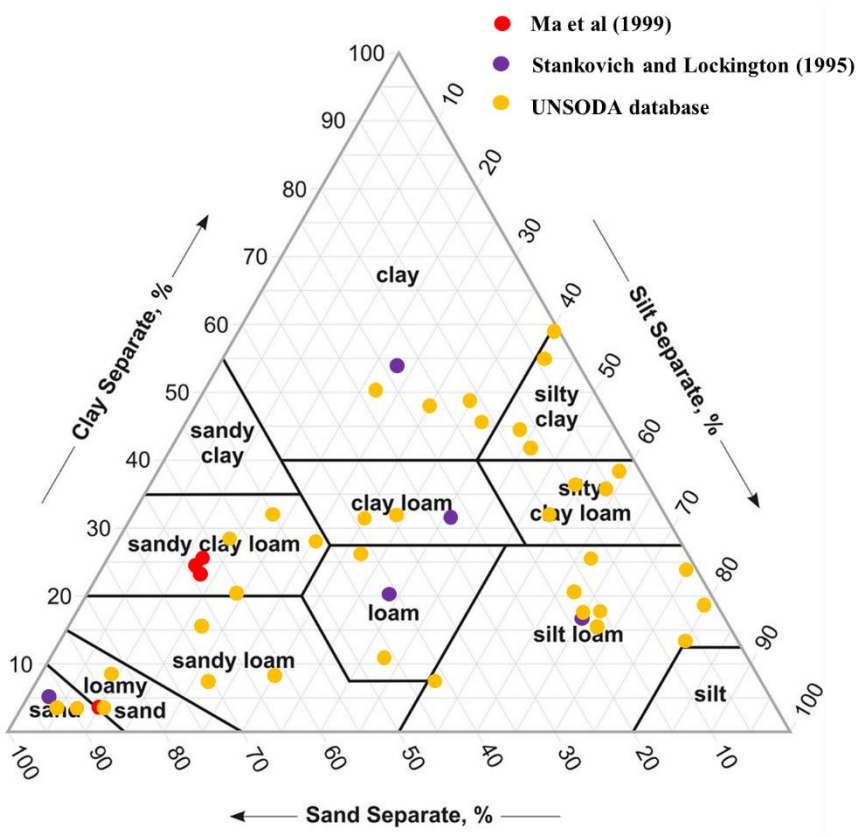

Figure 3.3. Texture classes of the soils used to develop the empirical relationship (Eq. [17]) between van Genuchten parameter α and air-entry pressure (ψ_a). Silty soils from Abdelkabir et al. (2013) were also used, but specific texture data for those soils were not reported, and, thus, not included here. The UNSODA codes of the 39 soils used to develop the relationship are 1091, 1092, 1120, 1122, 1123, 1131, 1164, 1166, 1270, 1280, 1281, 1282, 1290, 1301, 1321, 1340, 1360, 1361, 1362, 1370, 1372, 1380, 1381, 1400, 1480, 2010, 2012, 2100, 2360, 2462, 2570, 2593, 2600, 2620, 2622, 2640, 2710, 2711 and 3033, respectively.

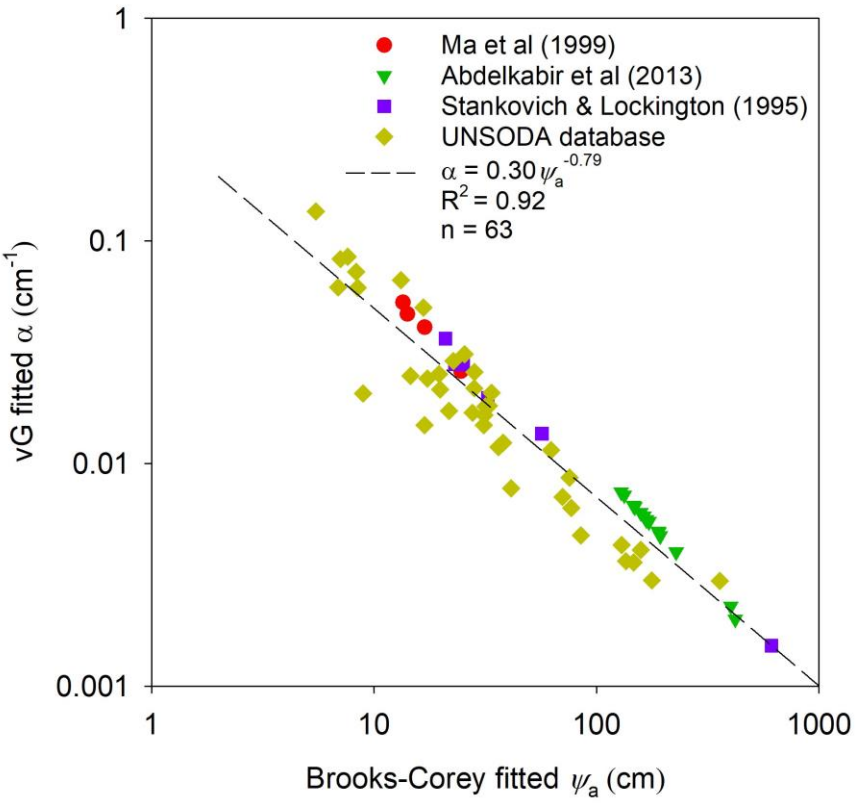

Figure 3.4. The relationship between van Genuchten parameter α and Brooks-Corey model parameter air-entry pressure (ψ_a) for soils from published data and from the UNSODA database (Nemes et al., 2001). The dashed line indicates the fitted linear regression line.

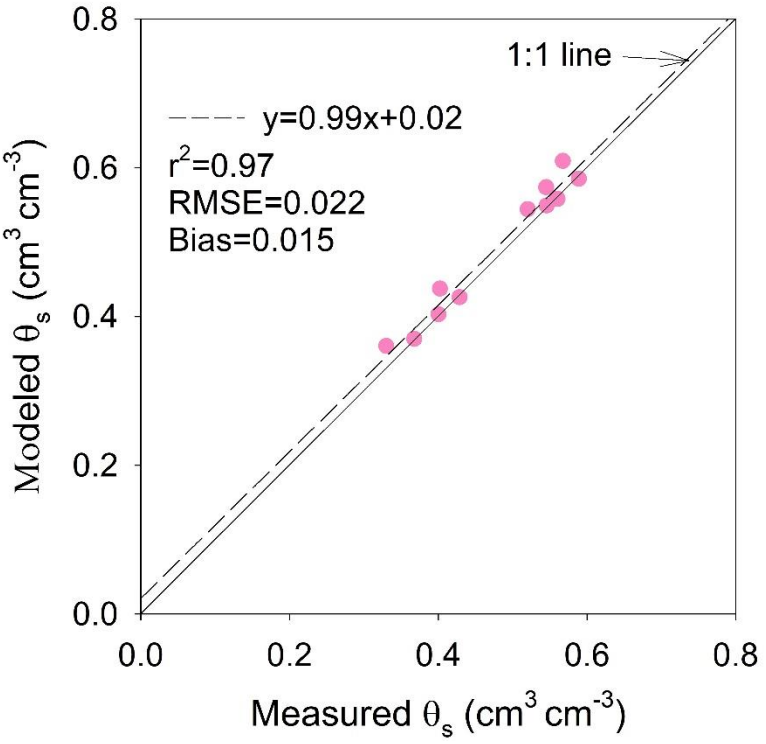

Figure 3.5. Modeled saturated soil water content (θ_s) values obtained with Eq. [2] versus measured θ_s values for soils in Table 3.2.

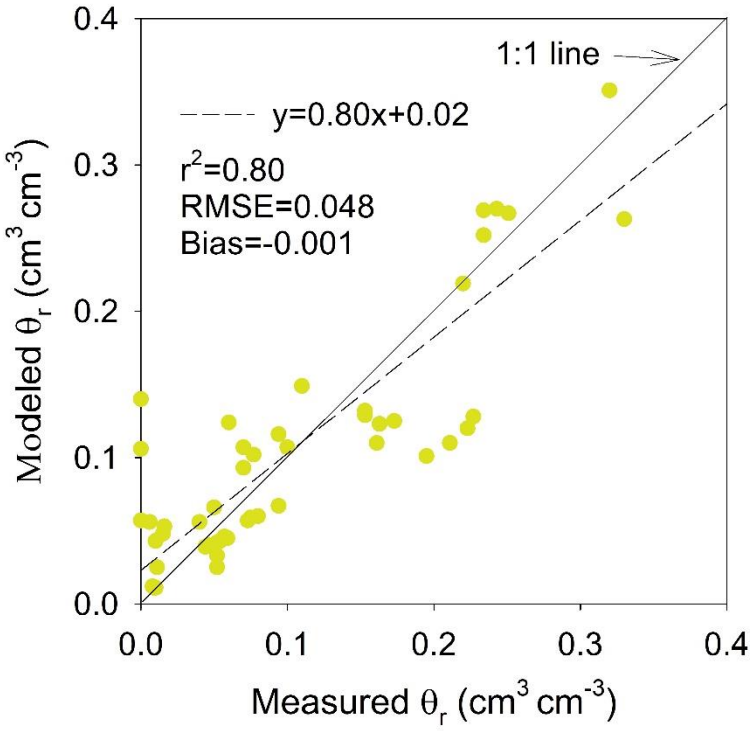

Figure 3.6. Residual water content (θ_r) estimated from clay content and bulk density by Eq. [3] versus measured θ_r values for soils in Table 3.1.

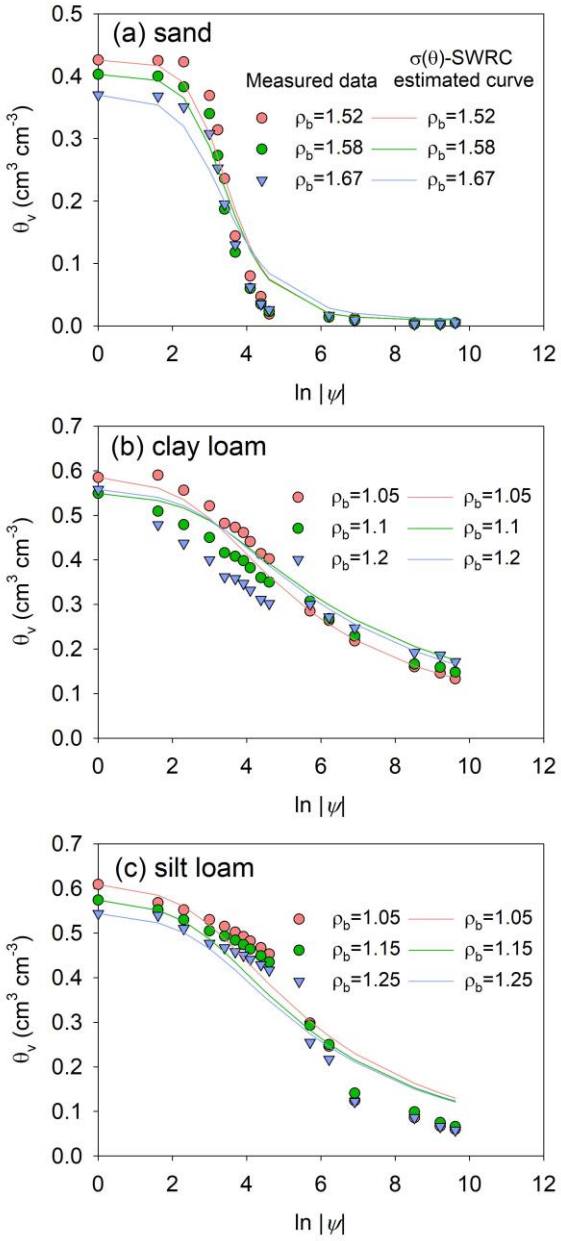

Figure 3.7. Measured and estimated soil water retenion curves (SWRCs) of soils with various bulk density (ρ_b) values, expressed as volumetric water content, θ ($cm^3\ cm^{-3}$), versus natural log matric potential, ln|ψ|, where the circles indicate measured data and the solid line (σ(θ)-SWRC) indicates SWRCs estimated by the σ(θ)-SWRC method (Eqs. [2], [3], [12] and [18]).

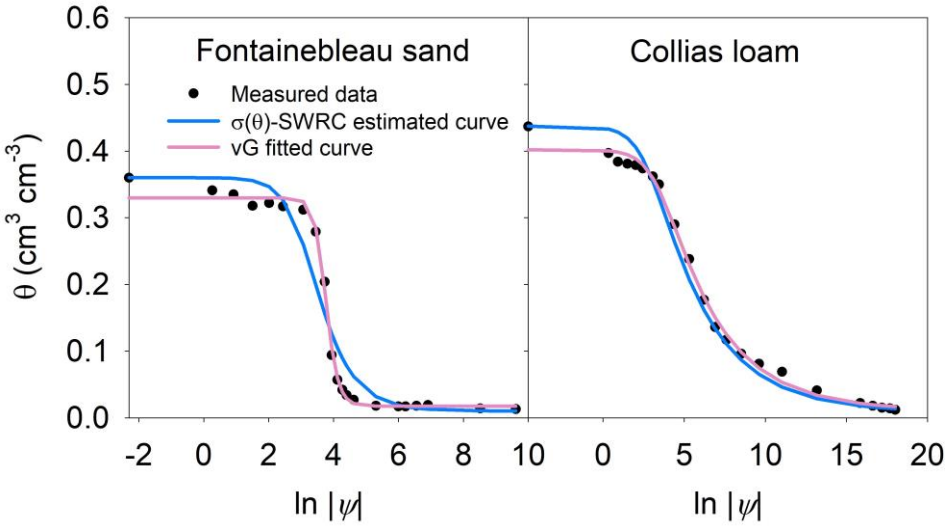

Figure 3.8. Measured, fitted, and estimated soil water retenion curves (SWRCs) of soils from Doussan and Ruy (2009), expressed as volumetric water content, θ (cm^3 cm^{-3}), versus natural log matric potential, ln|ψ|, where the black circle points indicate measured values, the blue and red solid lines indicate SWRCs estimated by the σ(θ)-SWRC method (Eqs. [2], [3], [12] and [18]) proposed in this study and the fitted van Genuchten model (Eq. [1]), respectively.

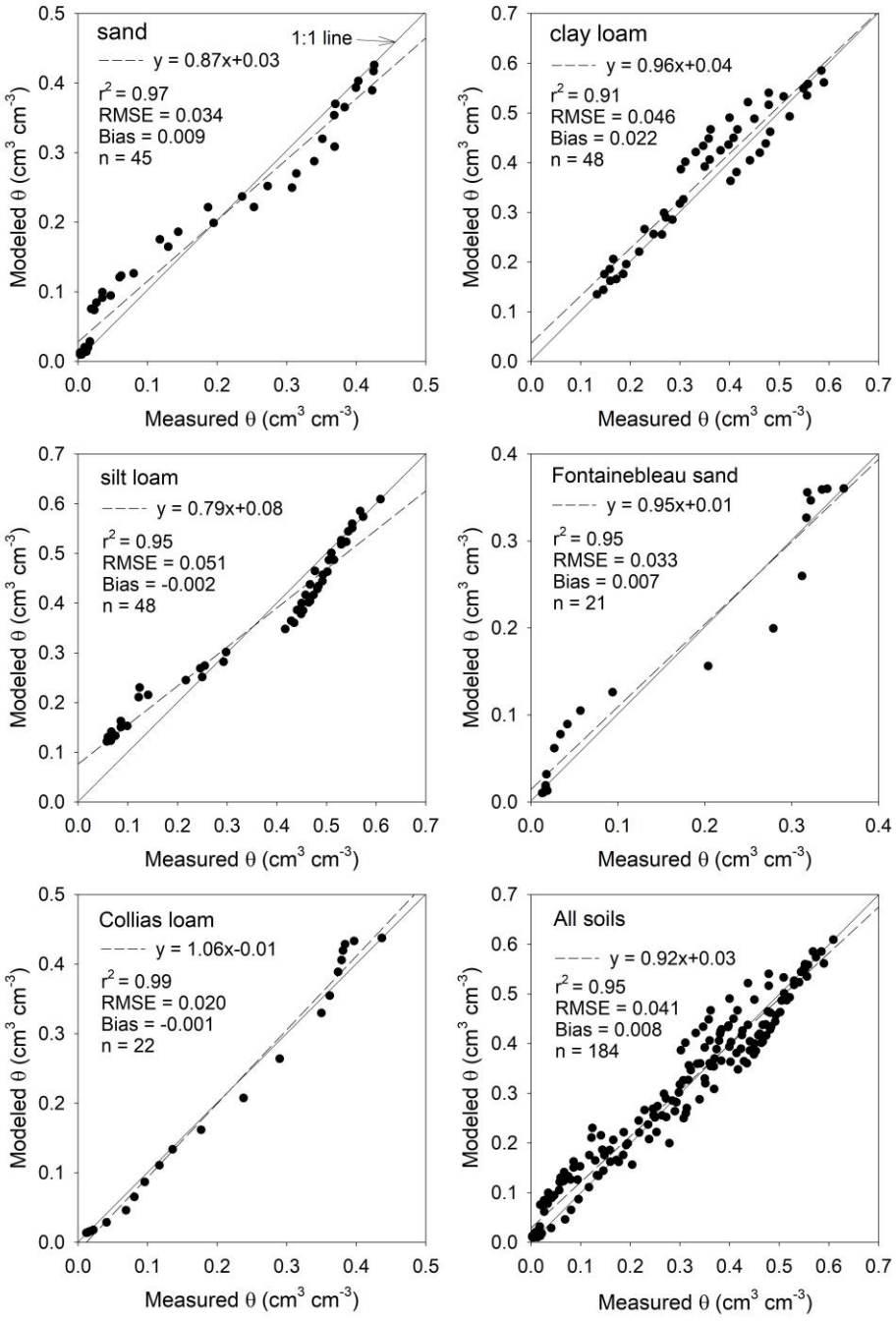

Figure 3.9. θ-values estimated by the σ(θ)-SWRC method versus measured θ-values at the same soil matric potential, ψ, for all soils in this study. "All soils" in the last panel indicates comparison combined results for all soils examined in this study. The dashed lines indicate the fitted linear regression lines.

Chapter 4: Estimation of Soil Water Retention Curve from Thermal Conductivity and Other Soil Properties

Abstract:

Measurement of soil water retention curves (SWRCs) is time consuming and estimation of SWRC parameters remains difficult. The van Genuchten (VG) model is commonly used to characterize the shape of the SWRC. Based on the similarity between SWRCs and thermal conductivity (λ) curves presented as a function of soil water content (θ), Lu and Dong (LD) proposed a unified conceptual $\lambda(\theta)$ model to estimate $\lambda(\theta)$ from SWRCs. Their work makes it possible to relate the shape of $\lambda(\theta)$ and SWRCs. In this study, we present an empirical approach to estimate VG parameter *m* from shape parameter *p* of the LD model. The saturated and residual water content values, θ_s and θ_r, respectively, can be estimated from soil bulk density and particle size distribution. The remaining VG parameter α can be further obtained from θ_s, θ_r and *m* using a geometrical relationship. The SWRCs of three soils from published data were estimated from measured $\lambda(\theta)$ data and soil properties, and then compared with direct SWRC measurements. The proposed method to estimate SWRCs performs well when compared to direct SWRC measurements (with root mean square errors for estimated θ value ranging from 0.017 to 0.054 $m^3\ m^{-3}$ and bias ranging from -0.021 to 0.041 $m^3\ m^{-3}$). Results indicate that the proposed method accurately estimates SWRCs from $\lambda(\theta)$ and soil properties.

Key words: thermal conductivity, van Genuchten model, water content, soil water retention curve, matric potential

4.1 Introduction

Describing and quantifying water flow and chemical transport in the vadose zone requires knowledge of the soil water retention curve (SWRC) which relates soil water matric potential (ψ) and water content (θ) at equilibrium. The SWRC is also a key soil property for estimation of plant water availability, watershed runoff prediction, and environmental quality management (Bescansa et al., 2006; Miyata et al., 2007).

SWRCs vary in space and time due to variations in other soil properties, management, disturbance, and plant growth, among other factors. Consequently, SWRC models have been developed to allow their estimation with limited measurements (Gardner, 1958; Brooks and Corey, 1964; Campbell, 1974; van Genuchten, 1980; Russo, 1988; Fredlund and Xing, 1994; Kosugi, 1994; Dexter et al., 2008; Omuto, 2009). These models typically contain shape parameters, which can be obtained by fitting the SWRC model to experimental data. Unfortunately, estimating the parameters in these models remains difficult and time-consuming. Several studies have consequently been carried out to predict the parameters using pedotransfer functions (Cosby et al., 1984; Saxton et al., 1986; Rawls et al., 2001; Wösten et al., 2001; Vereecken et al., 2010) including neural network analyses (Schaap and Bouten, 1996; Schaap and Leji., 1998). However, the reliability of applying these relationships is uncertain and requires careful validation for regions or conditions beyond those under which they were originally developed.

Generally, there are four regimes, hydration, pendular, funicular, and capillary, defining the SWRC along a path of increasing water content and resulting from two distinct principal forces: adsorption and capillarity (Tuller et al., 1999; Lu and Likos, 2004; Kim et al., 2015). As θ increases, the energy level of pore water increases from hydration through capillary regime, and each of these regimes also has different effects on soil thermal conductivity (λ) variations.

Tarnawski and Gori (2002) divided the thermal conductivity-water content curve ($\lambda(\theta)$) into four similar zones representing residual, transitory meniscus, micro/macroporous capillary, and superfluous water. The range and boundary of each regime depends on the soil and liquid type and micro-structures (i.e., particle geometry, particle/pore size distribution, pore-water arrangement, and interfacial properties), which can be identified as the key governing factors for $\lambda(\theta)$. More importantly, these factors can be characterized by SWRCs. Because of the close correlation between $\lambda(\theta)$ and SWRCs, McCumber and Pielke (1981) established an exponential function between ψ and λ and Lu et al. (2019) further developed a generalized model between them. Recently, Likos (2014) estimated $\lambda(\theta)$ from bimodal water retention curves using measurements of SWRCs for coarse-textured soils. Considering the similarity between the sigmoid shape of SWRCs and corresponding $\lambda(\theta)$ behavior, Lu and Dong (2015) proposed a closed-form $\lambda(\theta)$ model like that of the van Genuchten (1980) SWRC model. The parameters in their model are fitted from measurements of SWRCs in the entire θ range. This work suggests that it may also be possible to consider the inverse in order to estimate SWRCs from $\lambda(\theta)$. Such an approach has some advantages in that λ can be more easily measured than ψ over a range of conditions, particularly in the field (Ochsner and Baker, 2008).

The objective of this study was to develop a new approach to estimate van Genuchten (1980) SWRC parameters from $\lambda(\theta)$ and other easily measured soil properties. The model is established based on 20 soils with different textures. The new approach was evaluated with three additional soils using published data.

4.2 Materials and Methods

4.2.1 Estimating the SWRC from λ(θ)

Numerous empirical parametric models have been proposed with the van Genuchten (1980) equations being the most commonly applied in soil and porous media research. van Genuchten (1980) defined the following SWRC:

$$\frac{\theta-\theta_r}{\theta_s-\theta_r}=\left[1+\left(\alpha|\psi|\right)^{1/(1-m)}\right]^{-m} \quad [1]$$

where θ_s is the saturated water content ($m^3\ m^{-3}$), θ_r is the residual water contents ($m^3\ m^{-3}$), α (> 0, m^{-1}) is related to the inverse of the air-entry pressure, and m ($0 < m < 1$) is a pore-size distribution parameter.

The four parameters θ_s, θ_r, α and m in the van Genuchten (1980) model can be determined by fitting Eq. [1] to SWRC measurements. Chapter 3 presented an approach to estimate θ_s and θ_r from soil properties as follow:

$$\theta_s=1-\rho_b/\rho_s \quad [2]$$

$$\theta_r=(0.0033f_{clay}+0.007)\,\rho_b/\rho_w \quad [3]$$

where ρ_b is soil bulk density ($Mg\ m^{-3}$), ρ_s is soil particle density ($Mg\ m^{-3}$), f_{clay} is clay content, ρ_w is density of water (1 $Mg\ m^{-3}$ at 20 °C).

As illustrated in Figs. 4.1-4.2, both the SWRC ($\theta(\psi)$) and $\lambda(\theta)$ have a sigmoidal shape. Based on observations and the characteristics of the sigmoid function, Lu and Dong (2015) proposed a closed-form equation analogous to the van Genuchten model for estimating $\lambda(\theta)$:

$$\frac{\lambda-\lambda_{dry}}{\lambda_{sat}-\lambda_{dry}}=1-\left[1+\left(\frac{\theta}{\theta_f}\right)^{1/(1-p)}\right]^{-p} \quad [4]$$

where λ_{sat} and λ_{dry} are the thermal conductivity of saturated and dry soils (W m^{-1} K^{-1}), respectively, θ_f is the funicular water content which is the onset of the funicular regime, and p ($0 < p < 1$) is defined as the pore fluid network connectivity parameter for $\lambda(\theta)$. Eq. [4] is hereafter denoted as the LD model. We hypothesized that there may exist some intrinsic relationship between a soil's SWRC and $\lambda(\theta)$, such that a quantitative relationship between p and m for all types of soils can be established.

The parameters λ_{sat} and λ_{dry} can be either directly measured or indirectly fitted from Eq. [4]. However, when $\lambda(\theta)$ datasets are at limited levels of water content, λ_{sat} and λ_{dry} are calculated from independent equations to ensure the accuracy of θ_f and p estimation with LD model. In terms of λ_{sat}, a geometric mean equation has been widely used as given by Johansen (1975):

$$\lambda_{sat} = \left(\lambda_q^{q}\lambda_0^{1-q}\right)^{1-\phi}\lambda_w^{\phi} \quad [5]$$

where q is the quartz content, ϕ is soil porosity, λ_q, λ_0 and λ_w are the thermal conductivity of quartz (7.7 W m^{-1} K^{-1}), other minerals (2.0 W m^{-1} K^{-1} for soils with $q > 0.2$, and 3.0 W m^{-1} K^{-1} for soils with $q \leqslant 0.2$) and water (0.594 W m^{-1} K^{-1} at 20 °C), respectively. To calculate λ_{sat}, we followed the same assumption as Lu et al. (2007) that the quartz content was equal to sand content. In addition, an empirical linear relationship between λ_{dry} and ϕ was proposed by Lu et al. (2007):

$$\lambda_{dry} = -0.56\phi + 0.51 \quad [6]$$

Since θ_s and θ_r could be estimated using Eqs. [2] and [3], once m is obtained from pore fluid network connectivity parameter p, the lone remaining parameter α in the van Genuchten SWRC model can be estimated from the other three parameters (θ_s, θ_r, m) using the following geometrical relationship based on air-entry value and inflection point characteristics (Chapter 3):

$$\left|\left(\frac{\theta_s-\theta_r}{m-1}\right)\left(1+\frac{1}{m}\right)^{-(m+1)}\right| = \frac{\theta_s-\left[\left(\theta_s-\theta_r\right)-\left(1+\frac{1}{m}\right)^{-m}+\theta_r\right]}{\ln\left|\frac{1}{\alpha}\left(\frac{1}{m}\right)^{1-m}\right|-\ln\left|\left(\frac{0.30}{\alpha}\right)^{1.26}\right|} \quad [7]$$

4.2.2 Literature Datasets

Literature SWRC and λ(θ) data for 23 soils with wide ranges of texture were used to calibrate and verify the proposed approach (Fig. 4.3). Table 4.1 presents the basic physical properties and sources of the 23 datasets.

Soils 1-7 and soil 8 were collected from the surface layers (0–30-cm depth) and subsurface, respectively (Lu et al., 2008). In their study, the soil samples were air dried, ground, and sieved through a 2-mm screen, and then repacked into soil columns (50-mm inner diameter and 10-mm high) according to the desired ρ_b. The pressure plate extractor method (Dane and Hopmans, 2002) was used to measure SWRCs for the $|\psi|$ range$\leqslant$1500 kPa, and the dew point potentiometer (WP4T, Decagon Devices, Pullman, WA) was used to determine SWRCs in the $|\psi|$ range > 1500 kPa. Thermo-TDR sensors were used to measure the λ and θ measurements for soils 1-8. Details about thermo-TDR sensors can be found in Lu et al. (2017), and approaches for calculating λ and θ from sensor data measurement can be found in Ren et al. (1999).

For soils 9 and 10 (Jansen et al., 2002), SWRC parameters for both soils were obtained with the ROSETTA program (Schaap, 2002). For the λ measurement, 80% of the sand, 35% of the silt and 5% of the clay were considered as quartz to calculate the λ (de Vries, 1958; Milly and Eagleson, 1980). For soils 11-13 (Tang and Nowamooz, 2019), a thermal response test was used to determine λ and a numerical framework was employed to simulate the SWRCs for the three soils. Details about the thermal response test and numerical framework can be found in Tang and Nowamooz (2018).

For soils 14-20, θ and corresponding λ values were continuously monitored using a soil moisture sensor (ECH_2O EC-5, Decagon Devices, Pullman, WA) and a thermal property analyzer (SH-1, KD-2 Pro, Decagon Devices, Pullman, WA), respectively. SWRCs of soils 14-15 (Smits et al., 2010; Likos, 2014) were measured using a tensiometer. The tensiometer was connected to a differential pressure transducer (Model P55D, Validyne Engineering Corporation, Northridge, CA). The transient water release and imbibition method was used to determine the SWRCs of soils 16-20 (Dong et al., 2015; Lu and Dong, 2015) which has been proven a simple and fast technique to obtain SWRCs for various types of soils (Wayllace and Lu, 2012).

For soils 21-23, SWRC measurements from complete saturation to ψ of -5, -10, -20, -30, -40, -50, -60, -80 and -100 cm were conducted with a tension table (08.01 Sandbox, Eijkelkamp, Zeitz, Germany). The pressure plate extractor method was used to measure θ at additional ψ of -50, -100, -500, -1000 and -1500 kPa (an additional measurement at 30 kPa was also included on the soil 23). To obtain λ and θ data corresponding to these conditions, the soil columns were repacked at different θ corresponding to desired ψ values from the measured SWRC. Thermo-TDR sensors were again used to determine λ and θ at each condition.

4.2.3 Statistical Analysis

In this study, we compared SWRCs estimated from λ(θ) to direct measurement of SWRCs. The estimated SWRCs were evaluated using root mean square error (RMSE) and bias:

$$\mathrm{RMSE}=\sqrt{\frac{\sum\left(\theta_{\mathrm{estimated}}-\theta_{\mathrm{measured}}\right)^2}{N}} \quad [8]$$

$$\mathrm{Bias}=\frac{\sum\left(\theta_{\mathrm{estimated}}-\theta_{\mathrm{measured}}\right)}{N} \quad [9]$$

where N was the number of data pairs, and $\theta_{\mathrm{estimated}}$ and $\theta_{\mathrm{measured}}$ were the estimated and measured water content values, respectively.

4.3. Results and Discussion

4.3.1 Correlation between SWRCs and λ(θ)

The measurement results of λ(θ) from 13 soils (soils 1-13) are presented in Figs. 4.1-4.2. The λ(θ) for the 13 soils were generally sigmoidal in shape, which is in line with the reports of Lu and Dong (2015). SWRCs in this study were expressed as θ versus log|ψ|, which is the common log of ψ (cm). In the residual water domain corresponding to high |ψ| (between dryness and θ_r), a thin water film is formed on soil particle surfaces by adsorption (Tarnawski and Leong, 2000; Revil and Lu, 2013). The film thickness is so thin that heat conduction at this stage is mainly through the solid mineral phase, and λ is relatively constant. This trait (flat tail of λ(θ)) is less clear in coarse-textured soils (soils 1, 2, 9 and 12). The higher the fines content of a soil, the more pronounced is the flat tail of λ at low θ. As |ψ| decreases or θ increases (between θ_r and θ_f), water menisci form near the particle contacts, and when the surfaces of all soil particles are coated, water bridges are formed between solid particles (Ewing and Horton, 2007). This significantly expands the heat transfer paths through the water bridge connecting particles and results in a rapidly increasing trend in λ. θ_f is the inflection point of λ(θ) s at which the rate of change in λ with θ reaches the maximum, and it indicates that menisci are interconnected to each other. Generally, θ_f is related with clay content and fine-textured soils (soils 4, 5, 7, 8, 10 and 13) have higher θ_f than coarse-textured soils (Table 4.2). As θ continues to increase from θ_f, or |ψ| continues to decrease, water retention enters the funicular regime where water bridges grow and begin to merge with adjacent ones. This results in further enhancement of λ, but the rate of change in λ with respect to θ gradually decreases. Eventually, when |ψ| becomes small or θ increases until saturation, λ approaches its maximum value of λ_{sat}. λ changes in this water retention regime are small, as further

changes from replacement of air with water do not effectively change the conductive heat transfer pathways.

4.3.2 Performance of the LD Model

In order to fit reliable *p* values from the LD model for further *m* estimation, the performance and predictability of the LD model (Eqs. [4]-[6]) was investigated using 13 soils covering a wide range of soil textures (with available $\lambda(\theta)$ and SWRC datasets). As evidenced in Figs. 4.1-4.2, the fitted curves for the LD model could capture the flat tail of the $\lambda(\theta)$ and the drastic onset of the pendular regime where the λ increases rapidly as θ increases. This indicated that the LD model accurately estimated the $\lambda(\theta)$. The slopes of the regression lines and the coefficients of determination (R^2) for most of the soils were greater than 0.95, indicating that the LD model provided reliable estimates (Table 4.3). Error analysis showed that the RMSE was 0.019-0.098 W m^{-1} K^{-1} and the bias was within ranges of -0.017 to 0.012 W m^{-1} K^{-1}. Thus, the general accuracy of the LD model was reasonable with an average RMSE of 0.058 W m^{-1} K^{-1}, an average bias of -0.004 W m^{-1} K^{-1}, and an average R^2 of 0.99.

4.3.3 Estimating SWRCs from $\lambda(\theta)$

By fitting Eq. [1] to SWRC measurements and Eqs. [4]-[6] to measured thermal conductivity data, parameters of VG model (θ_s, θ_r, α, *m*) and LD model (λ_{sat}, λ_{dry}, θ_f, *p*) were determined. The best-fit parameters obtained using the least squares method are listed in Table 4.2. Because of the similar shape of SWRCs and $\lambda(\theta)$, there exists a link between shape parameters *m* and *p* of the respective models. Examining data for 20 soils with a wide range of soil textures, an empirical relationship between VG model parameter *m* and LD model parameter *p* was observed (Fig. 4.4, $R^2 = 0.70$):

$$m = 0.059\,p^{-2.89} \qquad [10]$$

The schematic flowchart presented in Fig. 4.5 summarized the general steps to estimate the parameters of SWRC from measured λ(θ) data and other soil properties.

4.3.4 Validation of λ(θ)-SWRC Approach

We introduced an approach to estimate SWRCs from λ(θ), which is hereafter denoted as the "λ(θ)-SWRC" approach (Eqs. [2], [3], [7] and [10]). Figure 4.6 compares estimated SWRCs (solid lines) using the λ(θ)-SWRC approach for soils 21–23 to the corresponding measured data (circles). Overall, the fitted curves for the λ(θ)-SWRC approach followed the patterns of the measured SWRCs for three soils with various ρ_b values, which indicated that the λ(θ)-SWRC approach accurately estimated the SWRCs. For soil 21 at ρ_b of 1.52 Mg m^{-3}, the SWRC estimated by the λ(θ)-SWRC approach was flatter and generated lower θ estimates at low $|\psi|$ range and higher θ estimates at high $|\psi|$ range than the measured values. In addition, compared to the measured data, the λ(θ)-SWRC approach overestimated θ across the whole ψ range for soil 23 at ρ_b of 1.2 Mg m^{-3}. The slope ($d\theta/d|\psi|$) of the SWRC is dominated by parameter *m* (van Genuchten et al., 1980). Therefore, these deviations indicated an underestimation of parameter *m* from Eq. [10] for soil 21 and overestimation of parameter *m* for soil 23. Despite these discrepancies, the λ(θ)-SWRC approach still produced good SWRC estimates for three soils at various ρ_b values.

The performance of the λ(θ)-SWRC approach for the three soils used for validation are presented in Figure 4.7. In general, θ values estimated at selected ψ values via the λ(θ)-SWRC approach showed a high degree of agreement compared to the measured θ values. The coefficients of determination (R^2) for all soils at various ρ_b values were greater than 0.90, indicating that the λ(θ)-SWRC approach provided reliable estimates. The RMSE and bias between the measured and estimated curves ranged from 0.017 to 0.054 m^3 m^{-3} and from -0.021 to 0.041 m^3 m^{-3} (Table 4.4). In general, for all three soils, average RMSE, bias and R^2 of the λ(θ)-SWRC approach were 0.043

m^3 m^{-3}, 0.012 m^3 m^{-3} and 0.95, respectively (Table 4.4). Thus, the λ(θ)-SWRC approach can provide acceptable estimates.

4.3.5 Further Application and Discussion

As shown in Fig. 4.5, the λ(θ)-SWRC approach needs measured λ(θ) data and three soil properties (ρ_b, particle density and texture) as inputs. For a specific soil, soil particle density and texture are generally constants. This means only λ(θ) and ρ_b data are required to estimate the SWRC when using the λ(θ)-SWRC approach in practice. In-situ determination of θ, λ and ρ_b has been achieved in previous studies (Liu et al., 2014; Zhang et al., 2017; Tian et al., 2018; Fu et al., 2019). Thus, this suggests that the λ(θ)-SWRC approach may have potential for monitoring the dynamics of in-situ SWRCs.

Chapter 3 proposed a model to estimate the SWRC from bulk electrical conductivity (σ)-water content measurements. Compared to σ(θ)-SWRC model, the new approach proposed in this study has some advantages. First, λ is less temperature dependent than σ at normal soil temperature ranges (Nouveau et al., 2016). This is especially crucial in field condition where soil temperature shows obvious spatial and temporal variation. Second, both models needs λ (or σ) measurements at dry and saturation conditions. As mentioned above, both λ_{sat} and λ_{dry} are a function of ρ_b and therefore can be monitored continuously. In contrast, there have been no available universal equations to estimate the σ at dry and saturation condition which affects the practical application of the σ(θ)-SWRC model in the field.

4.4. Conclusion

A λ(θ)-SWRC approach was developed to estimate van Genuchten SWRC parameters from λ(θ)) and soil properties (bulk density, particle density and soil texture) based on 20 soils with a wide range of textures from published data. For a given soil, the model is simple and easy to use:

only $\lambda(\theta)$ and ρ_b measurements are needed to estimate the SWRCs. Overall, the $\lambda(\theta)$-SWRC method performed well on three soils of various textures and ρ_b values. The results of this study showed the potential to measure the SWRCs continuously from $\lambda(\theta)$ in the field.

4.5 Acknowledgements

This research was supported through the China Scholarship Council, US Army Research Laboratory (Grant Number: W911NF-16-1-0287), US National Science Foundation (Grant Number: 1633806), and the USDA-NIFA Multi-State Project 4188.

4.6 References

Bescansa, P., Imaz, M.J., Virto, I., Enrique, A., Hoogmoed, W.B., 2006. Soil water retention as affected by tillage and residue management in semiarid Spain. Soil Tillage Res. 87, 19–27.

Brooks, R.H., Corey, A.T., 1964. Hydraulic properties of porous medium. Hydrology Paper Number 3. Colorado State University, USA.

Campbell, G.S., 1974. A simple method for determining unsaturated conductivity from moisture retention data. Soil Science 117, 311–314.

Cosby, B.J., Horn Berger, G.M., Clapp, R.B., Gann, T.R., 1984. A statistical exploration of soil moisture characteristics to the physical properties of soils. Water Resour. Res. 20, 682–690.

Dane, J.H., Hopmans, J.W., 2002. Water retention and storage. In: Dane, J.H., Topp, G.C. (Eds.), Methods of Soil Analysis. Part. 4. Physical Methods. SSSA, Madison, WI, pp. 671–796.

Dexter, A.R., Czyz, E.A., Richard, G., Reszkowska, A., 2008. A user-friendly water retention function that takes account of the textural and structural pore spaces in soil. Geoderma 143, 243–253.

de Vries, D.A., 1958. Simultaneous transfer of heat and moisture in porous media. Trans. Am. Geophys. Union 39, 909–916.

Dong, Y., McCartney, J.S., Lu, N., 2015. Critical Review of Thermal Conductivity Models for Unsaturated Soils. Geotech. Geol. Eng. 33, 207–221.

Ewing, R., Horton, R., 2007. Thermal conductivity of a cubic lattice of spheres with capillary bridges. J. Phys. D. Appl. Phys. 40, 4959–4965.

Fredlund, D.G., Xing, A., 1994. Equations for the soil–water characteristic curve. Canadian Geotechnical Journal 31, 521–532.

Fu, Y., Tian, Z., Amoozegar, A., Heitman, J., 2019. Measuring dynamic changes of soil porosity during compaction. Soil Tillage Res. 193, 114–121.

Gardner,W.R.,1958. Some steady state solutions of the unsaturated moisture flow equation with application to evaporation from a water table. Soil Science 85, 228–232.

Janssen, H., Carmeliet, J., Hens, H., 2002. The Influence of soil moisture in the unsaturated zone on the heat loss from buildings via the ground. J. Therm. Envel. Build. Sci. 250, 275–298.

Johansen, O. 1975. Thermal conductivity of soils. Ph.D. diss. Norwegian Univ. of Science and Technol., Trondheim (CRREL draft transl. 637, 1977).

Kim, D., Kim, G., Baek, H., 2015. Relationship between thermal conductivity and soil-water characteristic curve of pure bentonite-based grout. Int. J. Heat Mass Transf. 84, 1049–1055.

Kosugi, K., 1994. Three-parameter lognormal distribution model for soil water retention. Water Resour. Res. 30, 891–901.

Likos, W.J., 2014. Modeling thermal conductivity dryout curves from soil-water characteristic curves. J. Geotech. Geoenviron. Eng. 140, 04013056.

Liu, X., Lu, S., Horton, R., Ren, T., 2014. In Situ Monitoring of Soil Bulk Density with a Thermo-TDR Sensor. Soil Sci. Soc. Am. J. 78, 400–407.

Lu, N., Likos, J. W., 2004. Unsaturated soil mechanics, Wiley, Hoboken, NJ.

Lu, N., Dong, Y., 2015. Closed-form equation for thermal conductivity of unsaturated soils at room temperature. J. Geotech. Geoenviron. Eng. 141, 04015016.

Lu, S., Ren, T., Gong, Y., Horton, R., 2007. An improved model for predicting soil thermal conductivity from water content at room temperature. Soil Sci. Soc. Am. J. 71, 8–14.

Lu, S., Ren, T., Gong, Y., Horton, R., 2008. Evaluation of Three Models that Describe Soil Water Retention Curves from Saturation to Oven Dryness. Soil Sci. Soc. Am. J. 72, 1542–1546.

Lu, S., Lu, Y., Peng, W., Ju, Z., Ren, T., 2019. A generalized relationship between thermal conductivity and matric suction of soils. Geoderma 337, 491–497.

Lu, Y., Liu, X., Zhang, M., Heitman, J.L., Horton, R., Ren, T., 2017. Thermo-time domain reflectometry method: Advances in monitoring in situ soil bulk density. Methods of Soil Analysis. 2. doi:10.2136/msa2015.0031

McCumber, M.C., Pielke, R.A., 1981. Simulation of the effects of surface fluxes of heat and moisture in a mesoscale numerical model. J. Geophys. Res. 86, 9929–9938.

Milly, P.C.D. and Eagleson, P.S., 1980. A coupled transport of water and heat in a vertical soil column under atmospheric excitation. Rep. 258, Ralph M. Parsons Lab., Dept. of Civil Engineering, Massachusetts Institute of Technology, Cambridge, MA.

Miyata, S., Kosugi, K., Gomi, T., Onda, Y., Mizuyama, T., 2007. Surface runoff as affected by soil water repellency in a Japanese cypress forest. Hydrol. Process. 21, 2365–2376.

Nouveau, M., Grandjean, G., Leroy, P., Philippe, M., Hedri, E., Boukcim, H., 2016. Electrical and thermal behavior of unsaturated soils: Experimental results. J. Appl. Geophys. 128, 115–122.

Ochsner, T.E., Baker, J.M., 2008. In situ monitoring of soil thermal properties and heat flux during freezing and thawing. Soil Sci. Soc. Am. J. 72, 1025–1032.

Omuto, C.T., 2009. Biexponential model for water retention characteristics. Geoderma 149, 235–242.

Rawls, W.J., Pachepsky, Y.A., Shen, M.H., 2001. Testing soil water retention estimation with the MUUF pedotransfer model using data from the southern United States. J. Hydrol. 251, 177–185.

Ren, T., Noborio, K., Horton, R., 1999. Measuring Soil Water Content, Electrical Conductivity, and Thermal Properties with a Thermo-Time Domain Reflectometry Probe. Soil Sci. Soc. Am. J. 63, 450–457.

Revil, A., Lu, N., 2013. Unified water isotherms for clayey porous materials. Water Resour. Res. 49, 5685–5699.

Russo, D., 1988. Determining soil hydraulic properties by parameter estimation: On the selection of a model for the hydraulic properties. Water Resour. Res. 24, 453–459.

Saxton, K.F., Rawls, W.J., Romberger, J.S., Papendick, R.I., 1986. Estimating generalized soil water characteristics from soil texture. Soil Sci. Soc. Am. J. 50, 1031–1036.

Schaap, M.G., and W. Bouten. 1996. Modeling water retention on curves of sandy soils using neural networks. Water Resour. Res. 32, 3033–3040.

Schaap, M.G., and F.J. Leij. 1998. Using neural networks to predict soil water retention and soil hydraulic conductivity. Soil Tillage Res. 47, 37–42.

Schaap, M.G., 2002. Rosetta v1.2: A computer program for estimating soil hydraulic parameters with hierarchical pedotransfer functions. J. Hydrol. 251, 163–176.

Smits, K.M., Sakaki, T., Limsuwat, A., Illangasekare, T.H., 2010. Thermal conductivity of sands under varying moisture and porosity in drainage–wetting Cycles. Vadose Zo. J. 9, 172.

Tang, F., Nowamooz, H., 2018. Long-term performance of a shallow borehole heat exchanger installed in a geothermal field of Alsace region. Renew. Energy 128, 210–222.

Tang, F., Nowamooz, H., 2019. Sensitive analysis on the effective soil thermal conductivity of the thermal response test considering various testing times, field conditions and u-pipe lengths. Renew. Energy 143, 1732–1743.

Tarnawski, V.R., Leong, W.H., 2000. Thermal conductivity of soils at very low moisture content and moderate temperatures. Transp. Porous Media 41, 137–147.

Tarnawski, V.R., Gori, F., 2002. Enhancement of the cubic cell soil thermal conductivity model. Int. J. Energy Res. 26, 143–157.

Tian, Z., Lu, Y., Ren, T., Horton, R., Heitman, J.L., 2018. Improved thermo-time domain reflectometry method for continuous in-situ determination of soil bulk density. Soil Tillage Res. 178, 118–129.

Tuller, M., Dani, O., Dudley, L.M., 1999. Adsorption and capillary condensation in porous media: Liquid retention and interfacial configurations in angular pores. Water Resour. Res. 35, 1949–1964.

van Genuchten, M.T., 1980. A Closed-form Equation for Predicting the Hydraulic Conductivity of Unsaturated Soils1. Soil Sci. Soc. Am. J. 44, 892–898.

Vereecken, H., Weynants, M., Javaux, M., Pachepsky, Y., Schaap, M.G., Genuchten, M.T. Van, 2010. Using pedotransfer functions to estimate the van Genuchten-Mualem soil hydraulic properties: a review. Vadose Zone J. 9, 795–820.

Wayllace, A., Lu, N., 2012. A transient water release and imbibitions method for rapidly measuring wetting and drying soil water retention and hydraulic conductivity functions. Geotech. Test. J. 35, 103–117.

Wösten, J.H.M., Pachepsky, Y.A., Rawls, W.J., 2001. Pedotransfer functions: bridging the gap between available basic soil data and missing soil hydraulic characteristics. J. Hydrol. 251, 123–150.

Zhang, M., Lu, Y., Heitman, J., Horton, R., Ren, T., 2017. Temporal changes of soil water retention behavior as affected by wetting and drying following tillage. Soil Sci. Soc. Am. J. 81, 1288–1295.

Table 4.1 Texture, particle size distribution, bulk density (ρ_b) and sources of investigated soils from literature data in this study.

Soil No.	Texture	Particle size distribution			ρ_b	Sources
		Sand	Silt	Clay		
		----------%		----------	Mg m^{-3}	
1	sand	93	1	6	1.60	Lu et al. (2008)
2	sandy loam	67	21	12	1.39	
3	loam	40	49	11	1.30	
4	silt loam	27	51	22	1.33	
5	silty clay loam	19	54	27	1.30	
6	silt loam	11	70	19	1.31	
7	silty clay loam	8	60	32	1.30	
8	silt loam	2	73	25	1.20	
9	sandy loam	69	15	16	/	Janssen et al. (2002)
10	loam	37	38	25	/	
11	sand	90	/	/	1.64	Tang and Nowamooz (2019)
12	sandy loam	60	/	/	1.64	
13	clay	20	/	/	1.45	
14	sand	100	0	0	1.77	Smits et al. (2010)
15	sand	100	0	0	1.56	Likos (2014)
16	sand	100	0	0	1.67	Dong et al. (2015)
17	silt	/	/	/	1.50	
18	clayey sand	/	/	/	1.59	
19	clay	0	0	100	1.31	Lu and Dong (2015)
20	clay	0	0	100	1.28	
21	sand	100	0	0	1.52, 1.67	Fu et al. (2020)
22	silt loam	21.5	66.7	11.8	1.05, 1.15	
23	clay loam	23.6	49.2	27.2	1.10, 1.20	

Table 4.2 Fitted parameters of LD model (Eqs. [4]-[6]) and VG model (Eq. [1]) for soils 1–20 in this study. λ_{dry} and λ_{sat} of soils 9-10 are fitted by Eq. [4] and all parameters for soils 14–20 are from Lu and Dong (2015).

	LD model				VG model			
	λ_{sat}	λ_{dry}	θ_f	p	θ_s	θ_r	α	m
Soil No.	W m^{-1} K^{-1}	W m^{-1} K^{-1}	m^3 m^{-3}		m^3 m^{-3}	m^3 m^{-3}	m^{-1}	
1	1.867	0.288	0.037	0.45	0.401	0.016	4.33	0.74
2	1.803	0.244	0.055	0.46	0.441	0.036	3.91	0.38
3	1.582	0.225	0.069	0.48	0.471	0.041	0.76	0.60
4	1.521	0.231	0.113	0.58	0.514	0.029	1.46	0.28
5	1.435	0.225	0.133	0.57	0.540	0.000	4.14	0.18
6	1.392	0.227	0.086	0.58	0.515	0.031	1.38	0.28
7	1.364	0.225	0.126	0.62	0.722	0.000	6.79	0.18
8	1.247	0.204	0.123	0.69	0.552	0.000	1.86	0.18
9	2.278	0.628	0.117	0.68	0.385	0.000	6.56	0.18
10	1.841	0.486	0.162	0.74	0.424	0.000	2.69	0.18
11	2.187	0.312	0.034	0.48	0.366	0.025	4.29	0.34
12	2.087	0.298	0.079	0.57	0.392	0.010	2.42	0.15
13	1.546	0.246	0.220	0.77	0.481	0.010	1.90	0.08
14	2.910	0.287	0.008	0.41	/	0.028	5.80	0.94
15	2.500	0.230	0.032	0.48	/	0.010	1.50	0.85
16	3.100	0.290	0.012	0.41	0.370	0.020	7.70	0.75
17	1.280	0.370	0.062	0.62	0.430	0.030	0.88	0.37
18	1.750	0.450	0.104	0.68	0.410	0.060	0.33	0.36
19	1.157	0.432	0.130	0.60	/	0.133	0.71	0.26
20	1.556	0.239	0.087	0.66	/	0.148	0.61	0.21

Table 4.3 The root mean square error (RMSE), bias and coefficient of determination (R^2) between LD model estimates and measured thermal conductivity values for soils 1–13 in this study.

Soil No.	Texture	RMSE	Bias	R^2
1	sand	0.077	-0.009	0.98
2	sandy loam	0.023	0.005	1
3	loam	0.055	0.012	0.98
4	silt loam	0.041	0.005	0.99
5	silty clay loam	0.024	0.007	0.99
6	silt loam	0.060	-0.013	0.97
7	silty clay loam	0.028	-0.008	0.99
8	silt loam	0.019	-0.004	1
9	sandy loam	0.098	-0.015	0.98
10	loam	0.083	-0.017	0.98
11	sand	0.065	-0.012	0.98
12	sandy loam	0.035	-0.003	0.98
13	clay	0.037	-0.005	0.95
Average		0.058	-0.004	0.99

Table 4.4 The root mean square error (RMSE), bias and coefficient of determination (R^2) between measured soil water retention curve and fitted curves for soils 21–23 in this study.

Soil No.	Texture	ρ_b	RMSE	Bias	R2
21	sand	1.52	0.054	0.013	0.93
		1.67	0.039	0.027	0.96
22	silt loam	1.05	0.047	0	0.96
		1.15	0.046	-0.021	0.95
23	clay loam	1.1	0.017	0.012	0.99
		1.2	0.046	0.041	0.97
Average			0.043	0.012	0.95

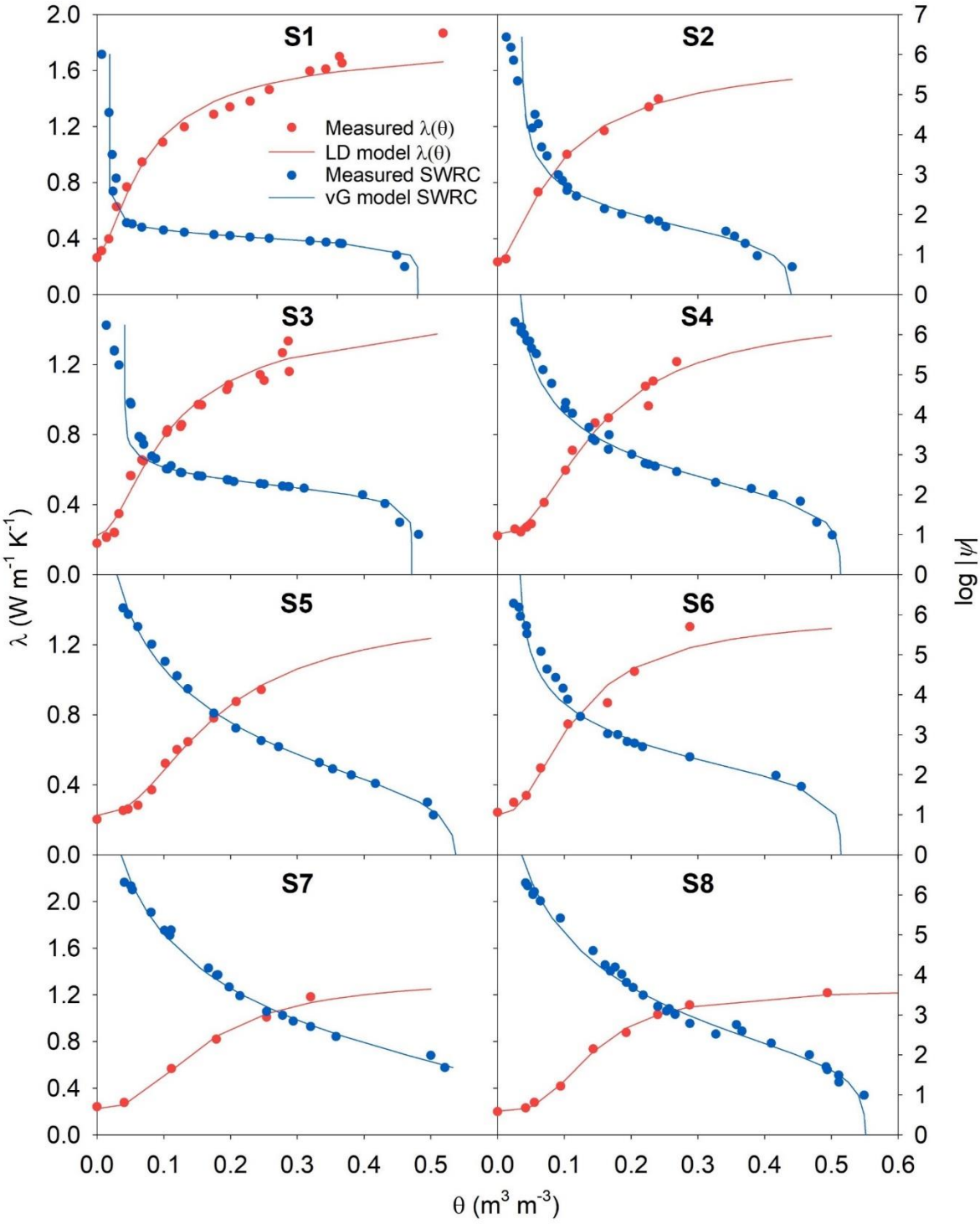

Figure 4.1. Measured and fitted curves for the soil water retention curves (SWRCs) and thermal conductivity curves (λ(θ)) for soils 1–8 in this study.

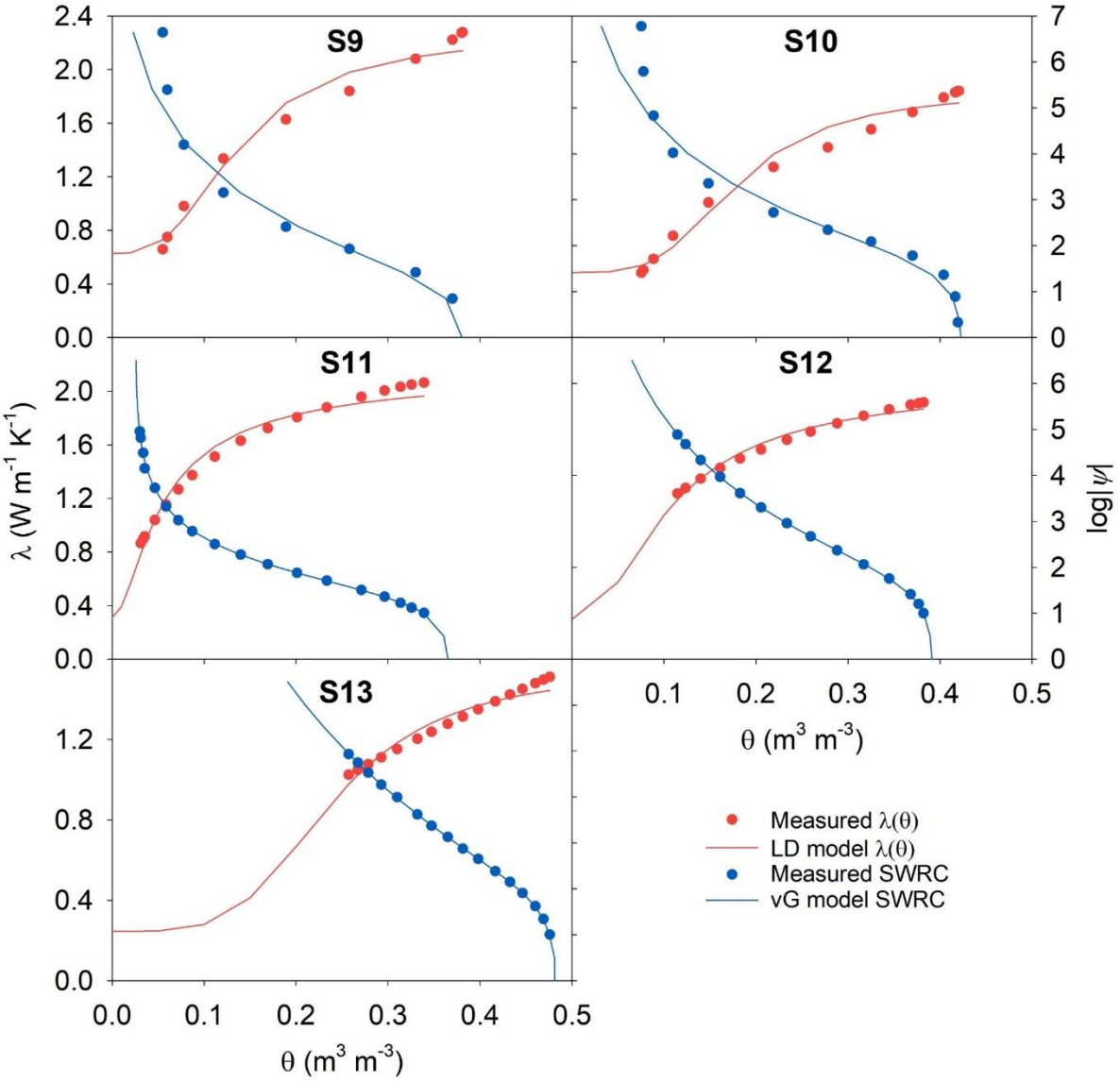

Figure 4.2. Measured and fitted curves for the soil water retention curves (SWRCs) and thermal conductivity curves (λ(θ)) for soils 9–13 in this study.

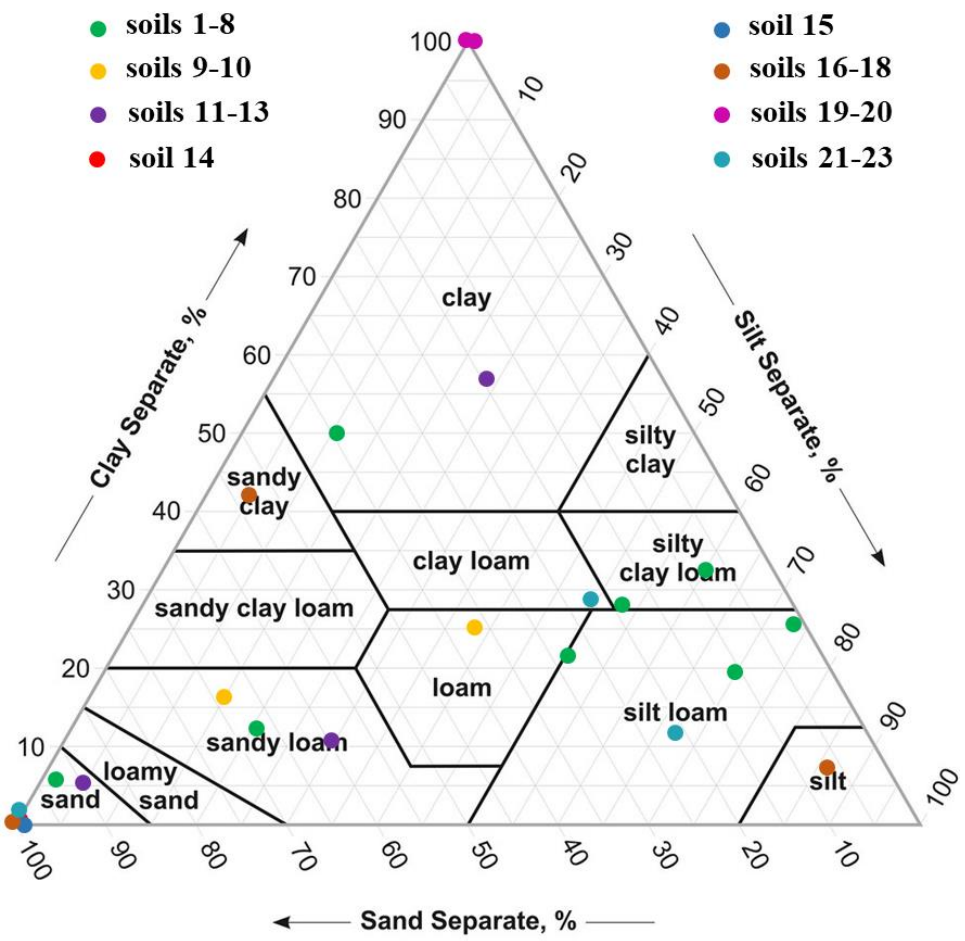

Figure 4.3. Texture classes of the soils used for model calibration (soils 1–20) and validation (soils 21-23). For soils 11-13 and soils 17-18, since no full particle size distribution is available, their texture classes are given at approximate position in Fig. 4.3.

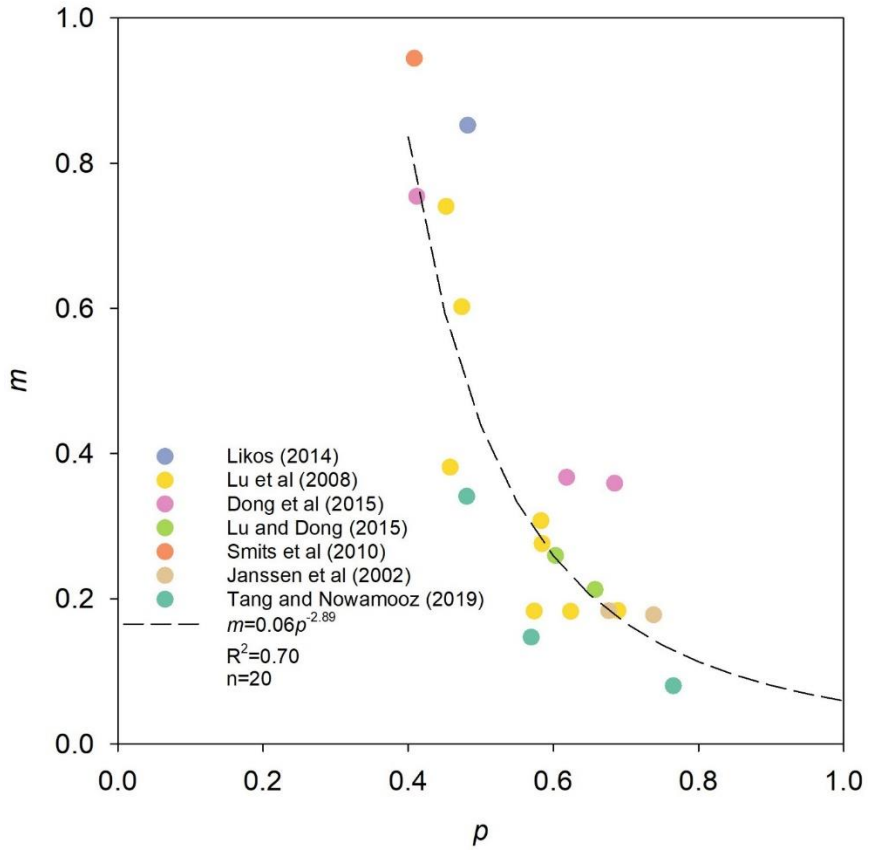

Figure 4.4. The relationship between LD model parameter *p* values and VG model parameter *m* values for soils 1–20. The dash line is the regression with Eq. [10].

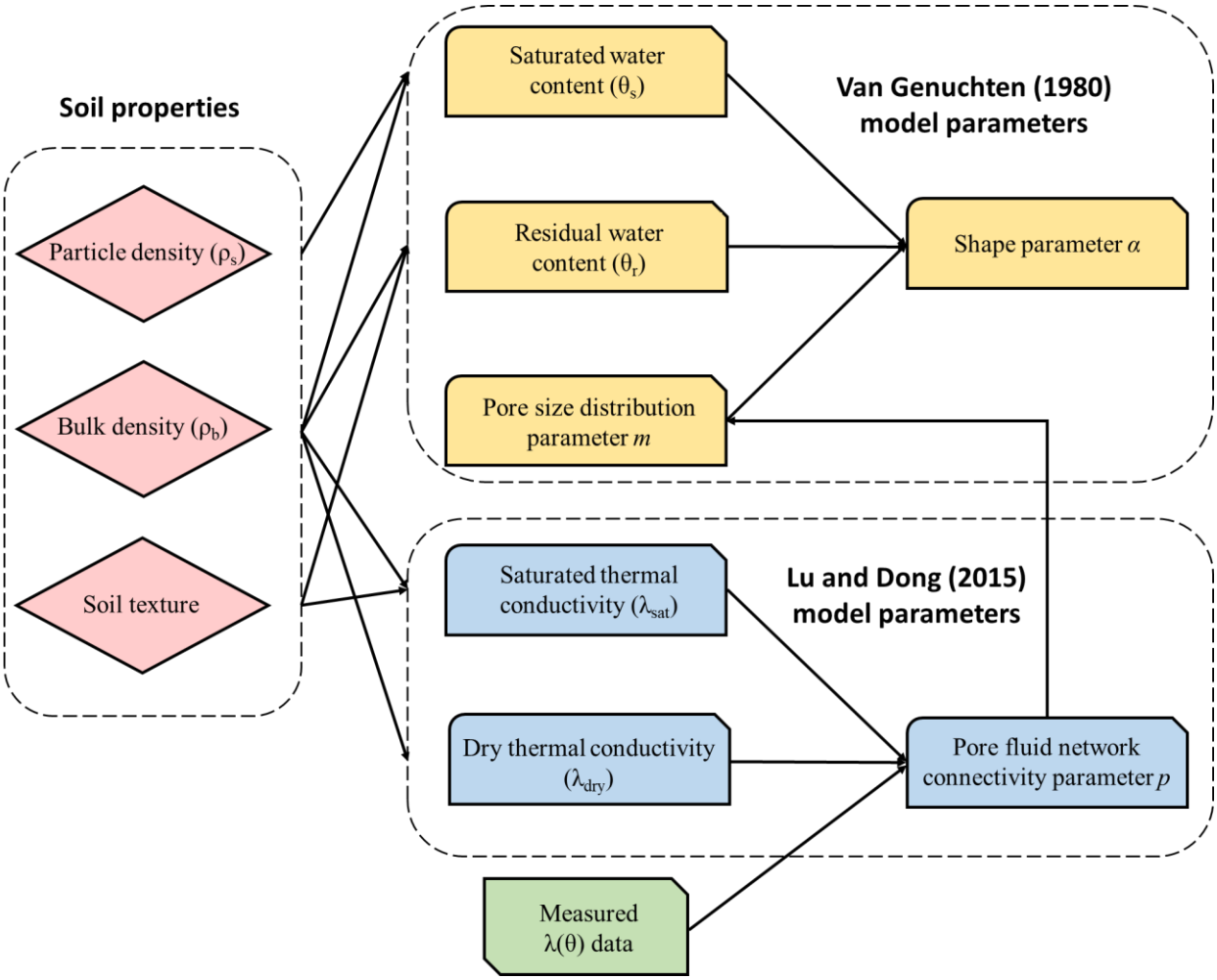

Figure 4.5. Flowchart for estimating soil water retention curve (SWRC) from thermal conductivity curve (λ(θ)) and other soil properties.

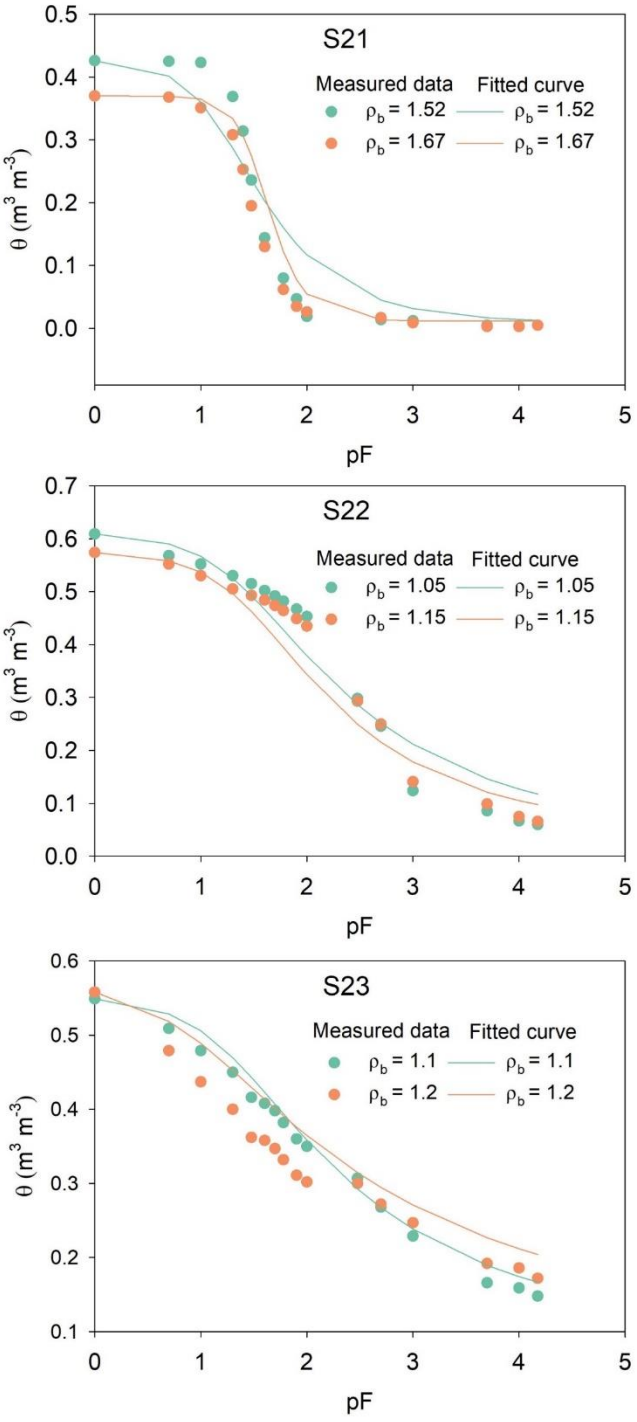

Figure 4.6. Measured and fitted soil water retention curves (SWRCs) of soils 21- 23 with various bulk density (ρ_b) values, where the circles indicate measured data and the solid line indicates SWRCs fitted by the λ(θ)-SWRC method (Eqs. [2], [3], [7] and [10]).

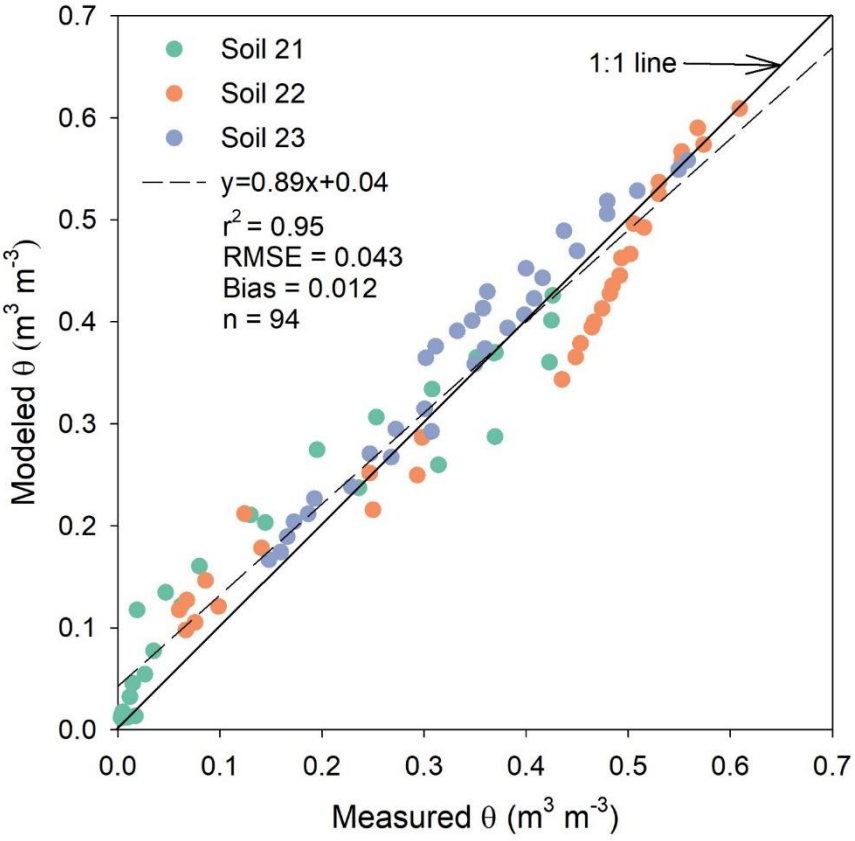

Figure 4.7. Comparison of estimated soil θ by λ (θ)-SWRC approach with measured θ at the same soil matric potential, ψ, for soils 21-23 in this study. The dash lines indicate the fitted linear regression lines for soils 21-23.

Chapter 5: A Generalized Archie's Model for Estimating Soil Bulk Electrical Conductivity from Water Content

Abstract

Electrical conductivity has been used a surrogate to study the spatial and temporal variability of a number of physical soil properties, e.g. porosity, salinity, clay mineral content and soil moisture. In this study, we developed a generalized Archie's model for soil that describes the relationship between electrical conductivity (σ) and volumetric water content (θ). The time domain reflectometry technique, as well as several other approaches (four-electrode and open-ended coaxial line) were used to measure σ and θ for soils for newly-collected and literature data. The performance of the new proposed model was examined and compared with the Rhoades model and the Ewing and Hunt model. A general range for the water phase exponent (w) in the new proposed generalized Archie's model was obtained by fitting σ and θ data from 15 soils in order to suggest a standard value of 2. With our new model, soil σ can be estimated from θ, porosity (ϕ) and particle size distribution with a root mean square error (RMSE) of 0.003-0.749 dS m^{-1} and bias ranging from -0.655 to 0.154 dS m^{-1} for 15 soils when compared to measured σ values.

Keywords: electrical conductivity, phase exponent, water content, Archie's law, porosity

5.1 Introduction

Soil electrical conductivity (σ), the ability of soil to conduct or attenuate electrical current, is a key property in soil science and other related fields like reservoir engineering and petrophysics. Soil electrical conductivity has been widely used in monitoring water deficit, measuring soil salinity, applying electrical resistivity tomography and estimating hydraulic conductivity profiles (Brunet et al., 2010; Moret-Fernández et al., 2012; Vereecken et al., 2014; Xu et al., 2019; Kaleris and Ziogas, 2020). There are many factors that affects σ including porosity (ϕ), water content (θ), soil structure, particle shape and orientation, particle size distribution, cation exchange capacity and temperature (Rhoades et al. 1989; Revil and Glover, 1998; Friedman and Robinson, 2002; Friedman, 2005; Samouelian et al., 2005; Brillante, 2014).

Commonly, the main pathway involved in the current conduction in soils is electrolytic, thus θ is the dominant factor in determining soil σ (Robinson et al., 2008). Archie (1942) developed a power law that describes a relationship between σ and degree of saturation (S). Waxman and Smits (1968) further extended Archie's power law to account for the significant surface conduction in the electrical double layer near clay minerals. Gupta and Hanks (1972) established a linear relationship between σ and θ based on data from two loamy soils. By using the assumption that bulk σ can be contributed from two pathways (electrolytic (water) pathway and interfacial (surface of particles) pathway) in parallel, Rhoades et al. (1976) proposed a parabolic function σ(θ). Rhoades et al. (1989) extended this empirical model to account for mobile, continuous and immobile, and discontinuous aqueous phases; and allowed for different parallel and series solid–liquid conducting pathways. Instead, Glover et al (2000) produced a mixing model with an extended Archie's equation which had two conducting phases (solid and liquid) and each phase had a phase exponent related to its degree of connectedness.

Soil σ values can also be obtained from a "electrical formation factor (F)" introduced by Archie (1942), which represents an approximate representation of the true geometrical configuration of porous rock (Ghanbarian et al., 2014). Nadler (1982) indicated that the relationship between F and θ resembles the shape of the water retention curve. One of the commonly used semi-empirical models for σ is the Mualem and Friedman (1991) model, which is based on the hypothesis that the tortuosity factor for bulk σ is identical to that for hydraulic conductivity. In recent years, the number of theoretical approaches to model electrical conductivity of complex porous media has dramatically increased, particularly as new theories (e.g. percolation theory, critical path analysis, effective medium approximation) have became available (Hunt, 2004; Brovelli and Cassiani, 2010; Sahimi, 2011; Ghanbarian et al., 2014). However, a general σ(θ) model that relies on easily attainable soil parameters has not yet been proposed.

The objective of this study was to develop a new generalized model for estimating the soil bulk σ from θ and other soil basic properties. By fitting the new model to experimental and published data, a value for the phase exponent is proposed. Then a simple σ(θ) relationship is established and tested.

5.2 Model Development

There are three mechanisms that are the dominant forms of electrical conduction in soils: ionic conduction through the pores, electronic conduction, and surface conduction (Knight and Endres, 2005). Ionic conduction is the movement of charged ions in the pores affected by density, charge, and mobility of the ions. Electronic conduction involves the movement of electrons through an interfacial pathway between solid particles. Surface conduction is associated with the ionic migration in the electrical double layer at the fluid-solid interface.

5.2.1 Rhoades Model

For a soil made of nonconductive solid particles, Rhoades et al. (1976) regards soil σ as resulting from two parallel pathways, with one path for conductance via the soil solution and the other path via the fluid-solid interface:

$$\sigma = \sigma_{water}\theta T + \sigma_s \quad [1]$$

where σ_{water} is the electrical conductivity of soil water and σ_s is referred to as bulk surface conductivity, primarily associated with exchangeable cations absorbed on clay minerals. The parameter T is a transmission factor that accounts for the tortuosity of current flow through the water within the void space and any decrease in the mobility of ions near the solid-liquid interface, which can be expressed as,

$$T = a\theta + b \quad [2]$$

where a and b are parameters fitted to experimental data. The empirical parameters a and b varied among different soils.

Thus, the Rhoades model becomes,

$$\sigma = a\sigma_{water}\theta^2 + b\sigma_{water}\theta + \sigma_s \quad [3]$$

5.2.2 Ewing and Hunt Model

Archie (1942) presented two models relating σ and ϕ that are widely used for relating σ and ϕ. The conventional Archie's law is expressed as (Archie, 1942):

$$\sigma = \sigma_{water}\phi^m \quad [4]$$

where m is a shape (cementation) exponent related to the connectivity of the conducting water phase. However, Archie's law is only applicable to the scenario where the solid is nonconductive, and the conducting water saturates the pore space. To apply more broadly and for the unsaturated case, Archie's second law was derived:

$$\sigma = c\sigma_{water} S^{l} \phi^{m} \quad [5]$$

where c is a unitless empirical constant based on experimental data. The saturation exponent l is commonly assumed to be about 2 for both consolidated and unconsolidated sands (Glover, 2017).

By applying continuum percolation theory, Ewing and Hunt (2006) recast the Archie's second law as,

$$\sigma = c\sigma_{water} \left(\theta - \theta_c\right)^{\mu} \quad [6]$$

where θ_c is the critical water content for percolation at which continuous pathways are just connected and μ is an exponent from continuum percolation theory. To adopt the Ewing and Hunt (2006) model at limit condition ($\sigma = \sigma_{water}$ when $\theta = \phi = 1$), Eq. [6] becomes,

$$\sigma = c\sigma_{water} \frac{\left(\theta - \theta_c\right)^{\mu}}{\left(1 - \theta_c\right)^{\mu}} \quad [7]$$

Using the assumption as Rhoades et al (1976) that solid and liquid phases conduct in parallel, σ_s is added to Eq. [7]:

$$\sigma = c\sigma_{water} \frac{\left(\theta - \theta_c\right)^{\mu}}{\left(1 - \theta_c\right)^{\mu}} + \sigma_s \quad [8]$$

5.2.3 The Generalized Archie's Model for Soil

Neither the first nor the second Archie's law account for surface conduction, which can be significant in porous media containing large amounts of clay (Sen et al., 1988; Revil et al., 1998). Even if the effects of surface conduction are included, the Archie's law fails if there are two or more conducting phases in rocks. Glover (2010) presented a modified Archie's law for n conducting phases in rocks,

$$\sigma = \sigma_1 f_1^{m_1} + \sigma_2 f_2^{m_2} + \sigma_3 f_3^{m_3} + \ldots + \sigma_n f_n^{m_n} + g(\sigma_i, \sigma_j, \Theta_{ij}) \quad [9]$$

where σ_i and f_i are the electrical conductivity and volume fraction of the i_{th} phase, respectively; m_i is the exponent of the i_{th} phase, which is related to degree of connectivity of the phase; $g(\sigma_i, \sigma_j, \Theta_{ij})$ is known as the sum of the Stieltjes integrals that represent the interactions between each pair of phases (i_{th} phase and j_{th} phase); and Θ_{ij} represents the resonance density functions dependent on the topology (Glover et al., 2000).

Since soil is a three-phase system including solid, water and air, a generalized Archie's law for soil (based on Eq. [9]) can be expressed in the following form:

$$\sigma = \sigma_{solid}\left(1-\phi\right)^{s} + \sigma_{water}\theta^{w} + \sigma_{air}\left(\phi-\theta\right)^{a} + g(\sigma_i, \sigma_j, \Theta_{ij}) \quad [10]$$

where σ_{solid} and σ_{air} are the electrical conductivity of solid and air, respectively, *s*, *w* and *a* are the phase exponents of solid, water and air, respectively. Since gas is an excellent insulator, the third and fourth terms in Eq. [10] associated with air phase can be eliminated. Thus, Eq. [10] can be rewritten as,

$$\sigma = \sigma_{solid}\left(1-\phi\right)^{s} + \sigma_{water}\theta^{w} + g(\sigma_{solid}, \sigma_{water}, \Theta_{sw}) \quad [11]$$

where $g(\sigma_{solid}, \sigma_w, \Theta_{sw})$ represents the interaction between solid and water phases. It should be noted that in the modified Archie's law proposed by Glover (2000, 2010), the Stieltjes integrals was neglected as a first order simplification. In addition, both the surface conduction and solid conduction have been accounted for in the first term of Eq. [10] as Glover et al. (2000) assumed that the conduction pathways taken for the surface conduction are the same as those through the soil solids. However, this may lead to problems when the generalized Archie's law is applied to clay soils where surface conduction is the dominant conduction mechanism but the geometric distribution of surface of pore space is likely to be different from that of solid phase. Therefore, we kept the Stieltjes integrals in Eq. [10] and used it to represent the surface conduction in soil.

Surface conduction involves the movement of charge in the electrical double layer (i.e. Stern layer and diffuse layer) which forms at the interface between the solid and fluid components. It has been found that the type of clay mineralogy influences the surface conduction contribution (Revil et al., 1998). Not only can there be high clay content in soils, but in soils with fresh water, even with very low clay content, surface conduction can be the dominant form of electrical conduction. Several theoretical or empirical models have been proposed for porous media containing clay and exhibiting significant surface conduction (Sen et al., 1988; Revil et al., 1998; Klein and Santamarina, 2003; Choo and Burns, 2014). Among these previous studies, Waxman and Smits (1968) was most frequently used for the interpretation of σ considering surface conduction:

$$\sigma = \frac{S^{\gamma}}{F}\left(\sigma_{water} + \frac{\sigma_{surface}}{S}\right) \quad [12]$$

where γ is saturation exponent, F is the electrical formation factor and $\sigma_{surface}$ is electrical conductivity of solid surface associated with counter ions in the electrical double layer. It is noteworthy that in the case where the soil is saturated and ionic conduction is dominant over the matrix conduction and surface conduction (very smaller σ_{solid} and $\sigma_{surface}$ compared to σ_{water}), both Eqs. [11] and [12] collapse to Archie's first law (Eq. [4]). Therefore, we assume that F equals to ϕ^{w}. Then by unifying the ionic conduction in Eqs. [11] and [12] (γ is assumed to be equivalent to w) and incorporating the surface conduction from Waxman and Smits model into Eq. [11] yields,

$$\sigma = \sigma_{solid}\left(1-\phi\right)^{s} + \sigma_{water}\theta^{w} + \theta^{w-1}\cdot\phi\cdot\sigma_{surface} \quad [13]$$

At either saturation or dry condition, Eq. [13] can be simplified. Thus, we obtained the σ of soil at saturation (σ_{sat}) and dry condition (σ_{dry}):

$$\sigma_{sat} = \sigma_{solid}\left(1-\phi\right)^{s} + \left(\sigma_{water} + \sigma_{surface}\right)\phi^{w} \quad [14]$$

$$\sigma_{dry} = \sigma_{solid}\left(1-\phi\right)^{s} \quad [15]$$

This leads to the following equation between w, ϕ and σ:

$$\phi^{w} = \frac{\sigma_{sat} - \sigma_{dry}}{\sigma_{water} + \sigma_{surface}} \quad [16]$$

Therefore,

$$\sigma_{water} = \frac{\sigma_{sat} - \sigma_{dry}}{\phi^{w}} - \sigma_{surface} \quad [17]$$

Additionally, $\sigma_{surface}$ is related to cation exchange capacity, and by extension the clay content (Waxman and Smits, 1968; Rhoades et al., 1989). On the basis of 13 soils with a wide range of textures and fluid conductivities, Doussan and Ruy (2009) proposed an empirical equation to estimate the $\sigma_{surface}$ (dS m^{-1}) from particle size distribution,

$$\sigma_{surface} = d\,\frac{f_{clay}}{f_{sand} + f_{silt}} + e \quad [18]$$

where f_{sand}, f_{silt} and f_{clay} are the sand, silt and clay fraction in soil, respectively; and d and e are fitted as 6.539 and 0.183, respectively. Thus, Eq. [13] can be rewritten as,

$$\sigma = \sigma_{dry} + \left(\frac{\sigma_{sat} - \sigma_{dry}}{\phi^{w}} - (d\,\frac{f_{clay}}{f_{sand} + f_{silt}} + e)\right)\theta^{w} + \theta^{w-1}\cdot\phi\cdot(d\,\frac{f_{clay}}{f_{sand} + f_{silt}} + e) \quad [19]$$

5.3. Materials and Methods

5.3.1 Laboratory Experiments

Laboratory measurements of σ and θ were performed on soils 1-6 (sand (Jilin, China), sandy loam (Beijing, China), silt loam (Beijing, China), sand (Glassil 530, Unimin Corporation-Marston, NC), silt loam (Tennessee, USA) and clay loam (Illinois, USA)) for various bulk density (ρ_b) values. The basic physical properties of these soils are presented in Table 5.1. The soil samples

were dried, ground and sieved through a 2-mm screen. All laboratory experiments were conducted at room temperature (25±1°C).

For soils 1-3, various soil water contents were obtained by adding a known amount of water to the samples and mixing thoroughly. The soil water contents of soils 1-3 were 0.00, 0.05, 0.15 and 0.20 cm^3 cm^{-3} ((additional water contents of 0.25 and 0.30 cm^3 cm^{-3} were also included on soils 2 and 3). The moist soil was packed into a column (50.2-mm inner diameter and 50.2 mm high) to a desired bulk density. The packed soil samples were sealed and placed in a constant temperature room for at least 24 h before measurements to ensure thermal equilibration between water and soil. For sandy loam and silty soils, it is difficult to pack the soil samples at high water contents (i.e. 0.25 and 0.30 cm^3 cm^{-3}). We followed the same procedures as Horton et al (1982). The soil samples were initially repacked at 0.10 cm^3 cm^{-3} and bottom of the columns were sealed. Then the top end was covered with gauze and a predetermined amount of water was added to the column until reaching the desired θ. Thermo-time domain reflectometry (thermo-TDR) sensors were used for the σ and θ measurements with the TDR method. Details about thermo-TDR sensors can be found in Lu et al. (2017), and approaches for calculating σ and θ from sensor data measurement can be found in Heimovaara et al. (1995) and Ren et al. (1999), respectively.

For soils 4-6, soil water contents from saturation to dry condition were achieved by desorption from saturation. The soil cores were placed on a tension table (08.01 Sandbox, Eijkelkamp, Zeitz, Germany) and slowly saturated with tap water from the bottom. Thermo-TDR sensors were inserted vertically into the samples from the top to determine σ and θ. Water was drained from the soil samples in steps using the tension table from complete saturation to matric potentials of -5, -10, -20, -30, -40, -50, -60, -80, -100 cm, sequentially. The θ values were determined each 4h after moving to a new matric potential until hydraulic equilibrium was achieved. After hydraulic

equilibrium was achieved (i.e., θ was stable), σ and θ were measured three times at each matric potential. The pressure plate extractor method (Dane and Hopmans, 2002) was used to measure θ at additional matric potentials of -50, -100, -500, -1000 and -1500 kPa (an additional measurement at 30 kPa was also included on the soil 6). Samples were pre-saturated with tap water and then desorbed to each corresponding matric potential. To obtain σ and θ data corresponding to these conditions, we repacked the soil columns at different θ corresponding to target θ values based on pressure plate measurements. Thermo-TDR sensors were again used to determine σ and θ with three repetitions at each condition.

5.3.2 Literature Datasets

In addition to making new laboratory measurements, we also obtained data from the literature. Data for three soils (soils 7-9); Toyoura sand (Japan standard soil), Touryo sandy clay loam (Hokkaido, Japan) and Atsuma sand (Hokkaido, Japan); were obtained from Tokoyo et al. (2016). Electrical conductivity measurements for these soils were collected with the four-electrode technique. Hailemariam et al (2017) investigated three silty soils (soils 10-12) from Thuringia, Germany. In their study, electrical conductivity was measured with an open-ended coaxial line technique. All six soils (soils 7-12) were incrementally wetted from air dry up to saturation by adding a controlled amount of distilled water required for each adjusted θ. In Doussan and Ruy (2009), laboratory data were collected for three soils (soils 13-15): a silty clay loam (Avignon, France), a loam (Collias, France) and a sand (Fontainebleau, France). Electrical conductivity and corresponding water content measurements were obtained with a pair of electrodes embedded in soil samples on a tension table or in a pressure chamber for a range of matric potential value from 0 to -1471 kPa (150 m H_2O).

5.3.3 Statistical Analysis

The performance of the new proposed model was evaluated using the root mean square error (RMSE) and bias:

$$\text{RMSE}=\sqrt{\frac{\sum\left(\sigma_{\text{estimated}}-\sigma_{\text{measured}}\right)}{N}} \quad [20]$$

$$\text{Bias}=\frac{\sum\left(\sigma_{\text{estimated}}-\sigma_{\text{measured}}\right)}{N} \quad [21]$$

where N is the number of data points, and $\sigma_{estimated}$ and $\sigma_{measured}$ were the model estimates and measured values, respectively.

5.4. Results and Fiscussion

5.4.1 Model Evaluation

We first examined the performance of the new model (Eq. [3]), and compared against the Rhoades model (Eq. [8]) and the Ewing and Hunt model (Eq. [19]) using measured σ data on 15 soils (Fig. 1). All models were used to fit the measured soil σ(θ) data for soils 1-15 and parameters of three models were determined. Overall, all three models yielded good fits: slopes and intercepts of regression lines were almost precisely one and near zero, respectively.

Among the three models, the Rhoades model has two parameters (a and b), and three parameters are required for both the Ewing and Hunt model (c, θ_c and μ) and the new model (σ_{dry}, σ_{sat} and w). Since σ_{water} was not given for all soils in this study, it was also obtained via fitting. Based on our fitting results, all parameters of the Rhoades model were dependent on soil type: a and b ranged from -1.2 to 78.1 and -0.1 to 150.6, respectively. Rhoades et al (1976) reported different values of parameters: a = 2.1, b = -0.245 for clay soils and a = 1.3-1.4, b = -0.11 to -0.06 for another three loam soils. After examining 14 soils from published data, Ewing and Hunt (2006) found that c ranged from 1.07 to 2.73 and θ_c varied among different soils (0-0.07). Our analysis of

15 soils in this study showed that c and θ_c had a range of 0.23-3.71 and 0-0.20, respectively. As for exponent μ, it takes a value of 2 for three-dimensional systems but the non-universality of this exponent value has been reported (Feng et al., 1987). This agrees with our fitted values that μ had a wide range between 0.67 and 4.67 for soils 1-15. A conductivity exponent of $\mu = 1.88$ was given for cases where conductivities of solid and liquid phases are similar (Hunt, 2004). Overall, the variability of parameters in the Rhoades model and the Ewing and Hunt model make calibration necessary for each soil when applying them. In contrast, two parameters (σ_{dry} and σ_{sat}) in our new proposed model (Eq. [19]) can be easily determined from measurements. If it is possible to assume w, the lone remaining parameter in the generalized Archie's model, as a constant value, then a simple $\sigma(\theta)$ model can be developed.

5.4.2 Fluid Phase Exponent *w*

In the generalized Archie's model for soil (Eq. [19]), w is the exponent of the water phase and related to the connectedness. If the soil solid is non-conducting, soil is saturated and surface conduction is not considered, the generalized Archie's model for soil turns into a similar form as the classical Archie's law (Eq. [4]) and w is just the same as cementation exponent m in Eq. [4]. Following m in conventional Archie's law, w can take any value from 0 to infinity. A value of $w = 1$ represents a pore system composed of a bundle of capillary tubes that cross the soil pore space in a straight line (Glover, 2010). Sen et al (1981) reported w close to 1.3 for unconsolidated sands packed in the laboratory. Values for w greater than 2.5 and as high as 5 are usually found in carbonates in which the pore space is less well connected (Tiab and Donaldson, 2004). By extension, high values of w represent low water phase connectedness.

By fitting the σ and θ data of soils 1-15 using Eq. [19], the parameter w can be obtained using the least squares method**.** Figure 2 shows the variability of w for soils 1-15. For most of the soils,

w ranged from 1.3 to 2.5. This was consistent with results in Glover et al. (1997) which reported that most porous arenaceous sediments have cementation exponents between 1.5 and 2.5. The only exception was soil 10, which had a *w* value as high as 4.2. This was because soil 15 is an aggregated soil with bimodal pore size distribution (see Fig. 4 in Doussan and Ruy (2009)), which is expected to have large value of cementation exponent because both the intra- and inter-aggregate pores contribute to the bulk σ of a soil (Friedman, 2005). In addition, *w* was also affected by ρ_b. Figure 3 presents the *w* of soils 1-6 with various ρ_b values: as bulk density increased, *w* of most soils (soils 1, 3, 4, 5 and 6) decreased. For soil 2, *w* was insensitive to ρ_b. This was consistent with a detailed examination of mono-sized spheres, where cementation exponent increased systematically from 1.368 to 1.375 as the porosity increased from 0.368 to 0.402 (Wyllie and Gregory, 1955). However, Doyen (1988) reported a contrasting phenomenon, that cementation exponent increased with increasing bulk density.

Since most of the *w* values were concentrated in range between 1.3 and 2.5, we used an average value to represent the general *w*. The average *w* in Fig. 2 was 1.98 or 2.06 when excluding or including the outliers, respectively. To simplify the calculation, we set the *w* as a constant value of 2, then Eq. [18] can be simplified as,

$$\sigma = \sigma_{dry} + \left(\frac{\sigma_{sat} - \sigma_{dry}}{\phi^2} - (0.654 \frac{f_{clay}}{f_{sand} + f_{silt}} + 0.018) \right) \theta^2 + \theta \cdot \phi \cdot (0.654 \frac{f_{clay}}{f_{sand} + f_{silt}} + 0.018) \quad [22]$$

The σ(θ) relationship in Eq. [22] is a second degree polynomial function, comparable to the Rhoades model and Ewing and Hunt model for $u = 2$, although the coefficients of the three models have different meaning. This is no coincidence: this phenomenon may mask a universal dependence of θ on σ. Parameters in Rhoades model are empirical and have no physical meaning. In contrast, *c* gives the medium's tortuosity at saturation, while θ_c is the critical volume for percolation for the Ewing and Hunt model. Parameters in our equation (Eq. [22]) are related to

basic soil properties (e.g. particle size distribution and porosity), and σ values at limits from saturation or dry conditions. The contribution of matrix conductivity to bulk σ was ignored in both Rhoades, and Ewing and Hunt models, and surface conduction (σ_s) was treated as independent of θ in their models. However, the dependency of σ_s on θ has been reported by other studies (Rhoades et al., 1989; Amente et al., 2000).

5.4.3 Performance of the Generalized Archie's Model for Soil

In this study, we proposed the generalized Archie's model (Eq. [22]) for estimating σ from θ, ϕ and particle size distribution. The performance of the new proposed model was examined on 15 soils, 6 from new experimental data (soils 1-6) and 9 from literature data (soils 7-15). Figures 4-5 presents the σ data estimated with the new model and the measured σ results as a function of θ. As evidenced in Figures 4-5, the fitted σ results followed the patterns of the measured σ for most soils with various ρ_b values except for soil 10, which indicated that the new model was able to provide accurate predictions in the entire θ range. In terms of soil 10, compared to measured values, the σ results estimated with the new model were overestimated across the entire θ range. The overestimation of θ occurred because the *w* values for soil 10 was much higher than the assumed value (2). Error analysis showed that the RMSE ranged from 0.003 to 0.749 dS m^{-1} and the corresponding bias was -0.655 to 0.154 dS m^{-1} (Table 5.2). The coefficients of determination (R^2) for all soils except for soil 10 were greater than 0.90.

Figure 6 presents the measured σ versus values estimated from the new model by Eq. [22] for all soils in this study. In general, results from soils 1-15 distributed randomly along 1:1 line: the coefficient of determination (R^2) was as high as 0.95 and error analysis showed that the average RMSE and the corresponding bias were 0.247 dS m^{-1} and -0.062 dS m^{-1}, respectively. Overall, the generalized Archie's model was able to estimate σ accurately for most soils.

5.5 Conclusion

In this study, we developed a generalized Archie's model for estimating σ from easily measured soil properties. We used σ(θ) values from 15 soils to fit the phase exponent *w* for each soil. Then the average *w* value (*w* = 2) was assigned in the generalized Archie's model for estimating σ from easily measured soil properties. Compared with other existing σ(θ) models, our new model is simple and easy to use: σ_{sat} and σ_{dry} can be easily determined and *w* is assumed as a constant value. Model evaluation using new measurements and literature data revealed the new simple σ(θ) model provides accurate predictions of soil electrical conductivity for the 15 investigated soils with different bulk densities and textures. Further studies are required to test the performance of the new model on soils with a wide range of fluid conductivities.

5.6 Acknowledgements

This research was supported through the China Scholarship Council, US Army Research Laboratory (Grant Number: W911NF-16-1-0287), US National Science Foundation (Grant Number: 1633806), and the USDA-NIFA Multi-State Project 4188.

5.7 References

Amente, G., Baker, J.M., Reece, C.F., 2000. Estimation of soil solution electrical conductivity from bulk soil electrical conductivity in sandy soils. Soil Sci. Soc. Am. J. 64, 1931–1939.

Brillante, L., et al., 2014. Monitoring soil volume wetness in heterogeneous soils by electrical resistivity. A field-based pedotransfer function. J. Hydrol. 516, 56–66.

Brovelli, A., Cassiani, G., Dalla, E., Bergamini, F., Pitea, D., Binley, A.M., 2005. Electrical properties of partially saturated sandstones: Novel computational approach with hydrogeophysical applications. Water Resour. Res. 41, 1–12.

Brunet, P., Clément, R., Bouvier, C., 2010. Monitoring soil water content and deficit using Electrical Resistivity Tomography (ERT) - A case study in the Cevennes area, France. J. Hydrol. 380, 146–153.

Archie, G.E., 1942. The electrical resistivity log as an aid in determining some reservoir characteristics. Trans. AIME 146, 54–62.

Choo, H., Burns, S.E., 2014. Review of Archie's equation through theoretical derivation and experimental study on uncoated and hematite coated soils. J. Appl. Geophys. 105, 225–234.

Dane, J.H., Hopmans, J.W., 2002. *Water retention and storage*. In: Dane, J.H., Topp, G.C. (Eds.), *Methods of Soil Analysis. Part. 4. Physical Methods*. SSSA, Madison, WI, pp. 671–796.

Doussan, C., Ruy, S., 2009. Prediction of unsaturated soil hydraulic conductivity with electrical conductivity. Water Resour. Res. 45, 1–12.

Doyen, P.M., 1988. Permeability, conductivity, and pore geometry of sandstones. J. Geophys. Res. 93, 7729–7740.

Ewing, R.P., Hunt, A.G., 2006. Dependence of the electrical conductivity on saturation in real porous media. Vadose Zo. J. 5, 731.

Feng, S., Halperin, B.I., Sen, P.N., 1987. Transport properties of continuum systems near the percolation threshold. Phys. Rev. B 35, 197–214.

Friedman, S.P., Robinson, D.A., 2002. Particle shape characterization using angle of repose measurements for predicting the effective permittivity and electrical conductivity of saturated granular media. Water Resour. Res. 38, 18-1-18–11.

Friedman, S.P., 2005. Soil properties influencing apparent electrical conductivity: A review. Comput. Electron. Agric. 46, 45–70.

Ghanbarian, B., Hunt, A.G., Ewing, R.P., Skinner, T.E., 2014. Universal scaling of the formation factor in porous media derived by combining percolation and effective medium theories. Geophys. Res. Lett. 41, 3884–3890.

Glover, P.W.J., Gómez, J.B., Meredith, P.G., 1997. Damage of saturated rocks undergoing triaxial deformation using complex electrical conductivity measurements: Mechanical modelling. Phys. Chem. Earth 22, 63–68.

Glover, P.W.J., Hole, M.J., Pous, J., 2000. A modified Archie's law for two conducting phases. Earth Planet. Sci. Lett. 180, 369–383.

Glover, P.W.J., 2010. A generalized Archie's law for n phases. Geophysics 75, E247–E265.

Glover, P.W.J., 2017. A new theoretical interpretation of Archie's saturation exponent. Solid Earth 8, 805–816.

Gupta, S.C., Hanks, R.J., 1972. Influence of water content on electrical conductivity of the Soil. Soil Sci. Soc. Am. J. 36, 855–857.

Hailemariam, H., Shrestha, D., Wuttke, F., Wagner, N., 2017. Thermal and dielectric behaviour of fine-grained soils. Environ. Geotech. 4, 79–93.

Heimovaara, T.J., Focke, a. G., Bouten, W., Verstraten, J.M., 1995. Assessing temporal variations in soil water composition with time domain reflectometry. Soil Sci. Soc. Am. J. 59, 689–698.

Horton, R., Wierenga, P.J., Nielsen, D.R., 1982. A rapid technique for obtaining uniform water content distributions in unsaturated soil columns. Soil Sci. 133. 397-399.

Hunt, A.G., 2004. Continuum percolation theory and Archie's Law. Geophys. Res. Lett. 31, 10–13.

Kaleris, V.K., Ziogas, A.I., 2020. Using electrical resistivity logs and short duration pumping tests to estimate hydraulic conductivity profiles. J. Hydrol. 590, 125277.

Klein, K.A., Santamarina, J.C., 2003. Electrical conductivity in soils: underlying phenomena. J. Environ. Eng. Geophys 8, 263–273.

Knight, R.J., Endres, A.L., 2005. 3. An introduction to rock physics principles for near-surface geophysics. Near-Surface Geophys. 31–70.

Lu, Y., Liu, X., Zhang, M., Heitman, J.L., Horton, R., Ren, T., 2017. Thermo-time domain reflectometry method: Advances in monitoring in situ soil bulk density. Methods of Soil Analysis. 2. doi:10.2136/msa2015.0031

Moret-Fernández, D., Vicente, J., Aragüés, R., Peña, C., López, M. V., 2012. A new TDR probe for measurements of soil solution electrical conductivity. J. Hydrol. 448–449, 73–79.

Mualem, Y., Friedman, S.P., 1991. Theoretical prediction of electrical conductivity in saturated and unsaturated soil. Water Resour. Res. 27, 2771–2777.

Nadler, A., 1982. Estimating the soil water dependence of the electrical conductivity soil solution / electrical conductivity bulk soil ration. Soil Sci. Soc. Am. J. 46, 722–726.

Sahimi, M., 2011. Flow and Transport in Porous Media and Fractured Rock: From Classical Methods to Modern Approaches, 2nd ed. John Wiley & Sons, Weinheim.

Ren, T., Noborio, K., Horton, R., 1999. Measuring soil water content, electrical conductivity, and thermal properties with a thermo-time domain reflectometry probe. Soil Sci. Soc. Am. J. 63, 450–457.

Revil, A., Cathles, L.M., Losh, S., Nunn, J.A., 1998. Electrical conductivity in shaly sands with geophysical applications. J. Geophys. Res. Solid Earth 103, 23925–23936.

Revil, A., Glover, P.W.J., 1998. Nature of surface electrical conductivity in natural sands, sandstones, and clays. Geophys. Res. Lett. 25, 691–694.

Rhoades, J.D., Raats, P.A.C., Prather, R.J., 1976. Effects of liquid-phase electrical conductivity, water content, and surface conductivity on bulk soil electrical conductivity. Soil Sci. Soc. Am. J. 40, 651–655.

Rhoades, J.D., Manteghi, N.A., Shouse, P.J., Alves, W.J., 1989. Soil electrical conductivity and soil salinity: new formulations and calibrations. Soil Sci. Soc. Am. J. 53, 433–439.

Robinson, D.A., Campbell, S.C., Hopmans, J.W., Hornbuckle, B.K., Jones, S.B., Knight, R., Odgen, F., Selker, J., Wendroth, O., 2008. Soil moisture measurement for ecological and hydrological watershed-scale observatories: a review. Vadose Zone J. 7, 359–389.

Samouelian, A., Cousin, I., Tabbagh, A., Bruand, A., Richard, G., 2005. Electrical resistivity survey in soil science: a review. Soil Till. Res. 83, 173–193.

Sen, P.N., Scala, C., Cohen, M.H., 1981. A self-similar model for sedimentary-rocks with application to the dielectric-constant of fused glass-beads. Geophysics 46, 781–795.

Sen, P.N., Goode, P.A., Sibbit, A., 1988. Electrical conduction in clay bearing sandstones at low and high salinities. J. Appl. Phys. 63, 4832–4840.

Tiab, D., and E. C. Donaldson, 2004, Petrophysics: theory and practice of measuring reservoir rock and fluid transport properties: Gulf Publishing Company.

Tokoro, T., Ishikawa, T., Shirai, S., Nakamura, T., 2016. Estimation methods for thermal conductivity of sandy soil with electrical characteristics. Soils Found. 56, 927–936.

Vereecken, H., Huisman, J.A., Pachepsky, Y., Montzka, C., van der Kruk, J., Bogena, H., Weihermüller, L., Herbst, M., Martinez, G., Vanderborght, J., 2014. On the spatio-temporal dynamics of soil moisture at the field scale. J. Hydrol. 516, 76–96.

Waxman, M.H., Smits, L.J.M., 1968. Electrical conductivities in oil-bearing shaly sands. Soc. Pet. Eng. J. 243, 107–122.

Wyllie, M.R.J., Gregory, A.R., 1955. Fluid flow through unconsolidated porous aggregates: effect of porosity and particle shape on Kozeny–Carman constants. Ind. Eng. Chem. 47, 1379–1388.

Xu, D., Sun, R., Yeh, T.C.J., Wang, Y.L., Momayez, M., Hao, Y., Lee, C.H., Hu, X., 2019. Mapping soil layers using electrical resistivity tomography and validation: Sandbox experiments. J. Hydrol. 575, 523–536.

Table 5.1 Texture, particle size distribution and bulk density (ρ_b) of soils in this study.

Soil No.	Texture	Particle size distribution			ρ_b	Sources
		Sand	Silt	Clay	g cm^{-3}	
1	sand	0.91	0.03	0.06	1.4, 1.5, 1.6	New measurements
2	sandy loam	0.52	0.36	0.12	1.25, 1.35, 1.45	
3	silt loam	0.34	0.53	0.13	1.15, 1.25, 1.35	
4	sand	1	0	0	1.52, 1.58, 1.67	
5	silt loam	0.215	0.667	0.118	1.05, 1.15, 1.25	
6	clay loam	0.236	0.492	0.272	1.05, 1.1, 1.2	
7	sand	1	0	0	1.59	Tokoro et al. (2016)
8	sandy clay loam	0.53	0.22	0.25	1.28	
9	sand	1	0	0	1.83	
10	silty clay loam	0.157	0.51	0.333	1.64	Doussan and Ruy (2009)
11	loam	0.377	0.487	0.136	1.49	
12	sand	0.995	0.003	0.002	1.67	
13	silt loam	0.249	0.582	0.168	1.49	Hailemariam et al. (2017)
14	silt loam	0.271	0.525	0.202	1.43	
15	silt loam	0.099	0.654	0.246	1.38	

Table 5.2 The root mean square error (RMSE), bias and coefficient of determination (R^2) between σ estimated by the generalized Archie's law for soil (Eq. [22]) and measured σ values of soils 1-15 in this study.

Soil No.	ρ_b g cm^{-3}	RMSE dS m^{-1}	Bias dS m^{-1}	R^2
1	1.4	0.006	0.003	0.98
	1.5	0.007	0.003	0.98
	1.6	0.009	0.002	0.98
2	1.25	0.064	0.050	0.98
	1.35	0.053	0.039	0.98
	1.45	0.058	0.041	0.97
3	1.15	0.080	0.062	0.97
	1.25	0.052	0.040	0.99
	1.35	0.028	0.022	1
4	1.52	0.004	0.002	0.99
	1.58	0.003	0.000	0.99
	1.67	0.004	0.001	0.99
5	1.05	0.031	0.016	0.99
	1.15	0.065	-0.044	0.97
	1.25	0.128	0.024	0.91
6	1.05	0.243	0.074	0.98
	1.1	0.398	-0.321	0.99
	1.2	0.749	-0.655	0.91
7	1.59	0.034	-0.023	0.98
8	1.28	0.147	0.020	0.95
9	1.83	0.026	0.007	0.99
10	1.64	0.188	0.154	0.79
11	1.49	0.022	-0.003	0.99
12	1.67	0.021	-0.011	0.99
13	1.49	0.406	-0.309	0.90
14	1.43	0.493	-0.417	0.91
15	1.38	0.377	-0.277	0.91
Average		0.247	-0.062	0.95

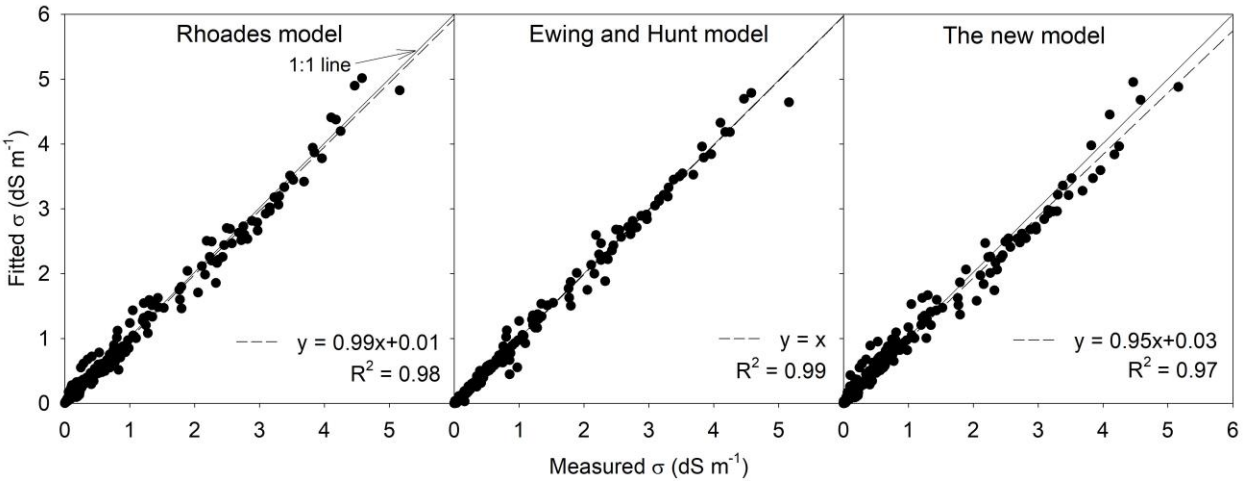

Figure 5.1. Comparison of soil electrical conductivity (σ) fitted with Rhoades model (Eq. [3]), Ewing and Hunt model (Eq. [8]) and the new model (Eq. [19]) versus measured values of σ for all soils in this study. The solid lines are the 1:1 lines, and the dashed lines are the regression lines.

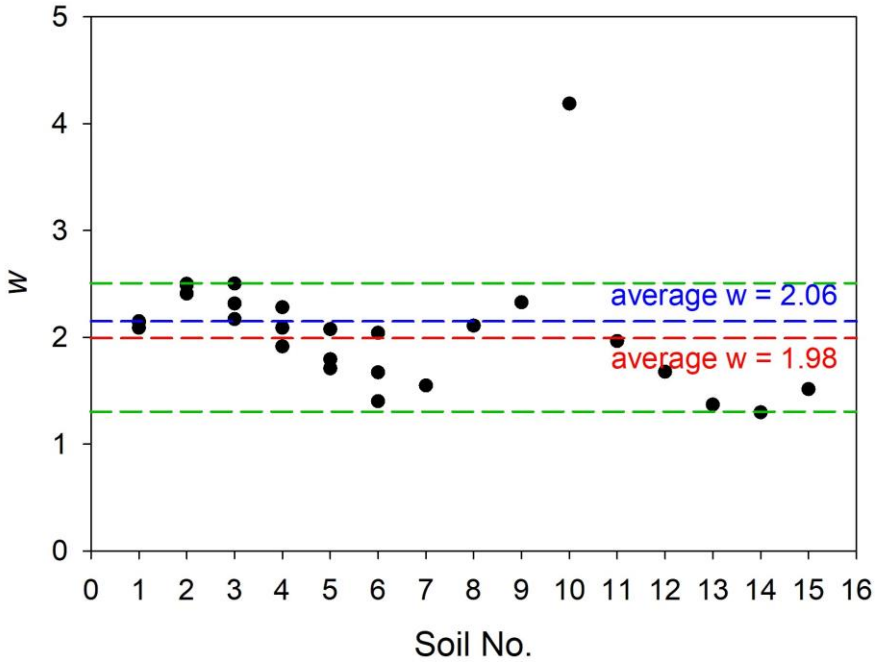

Figure 5.2. The phase exponent *w* as a function of Soil No. The blue and red dash lines represents the average *w* including or excluding the outlier, respectively. Two light green dash line indicates the upper and lower limit of *w* range except for the outlier.

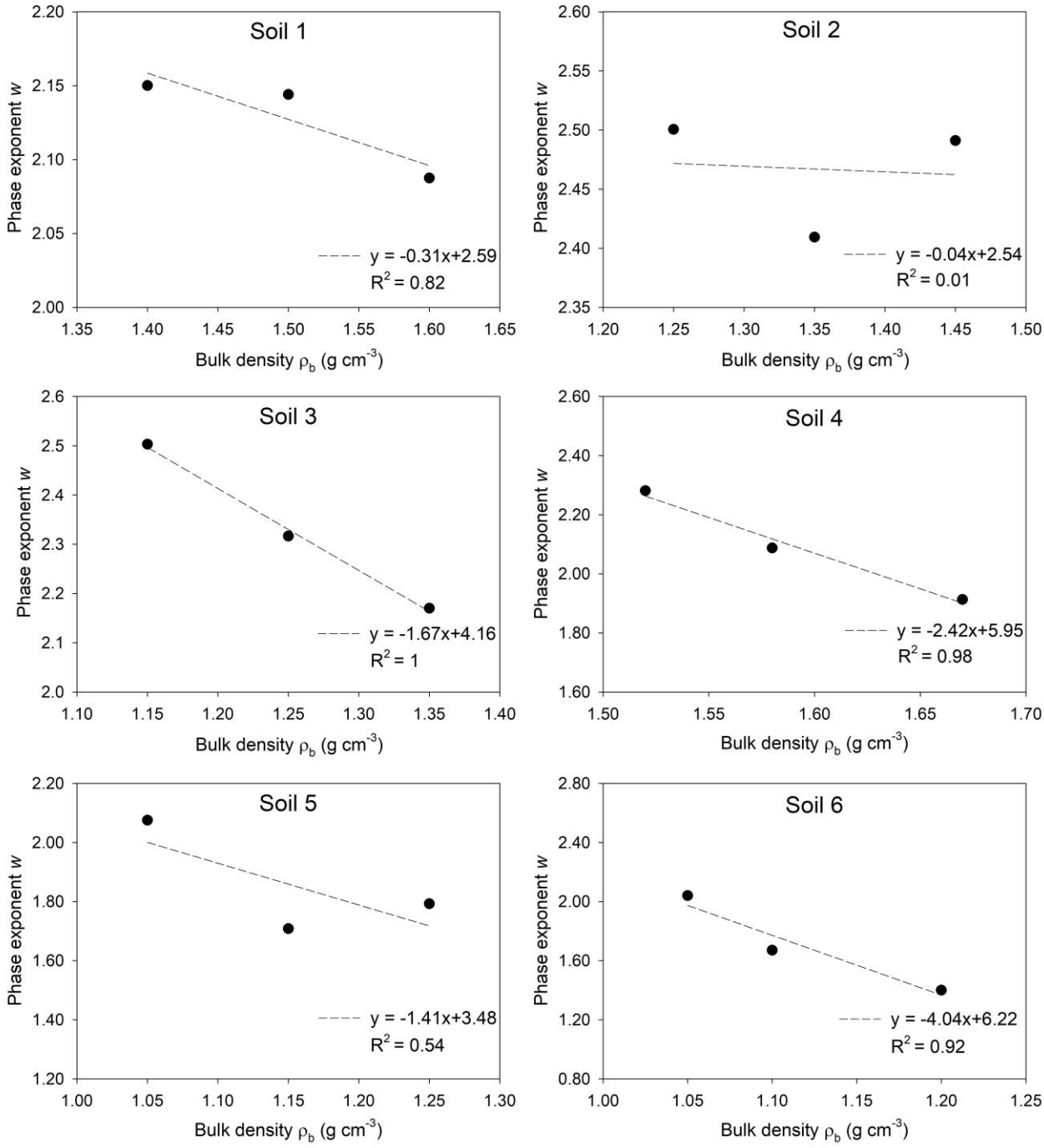

Figure 5.3. The phase exponent *w* of soils 1-6 as a function of bulk density (ρ_b). The dash lines are the regression lines.

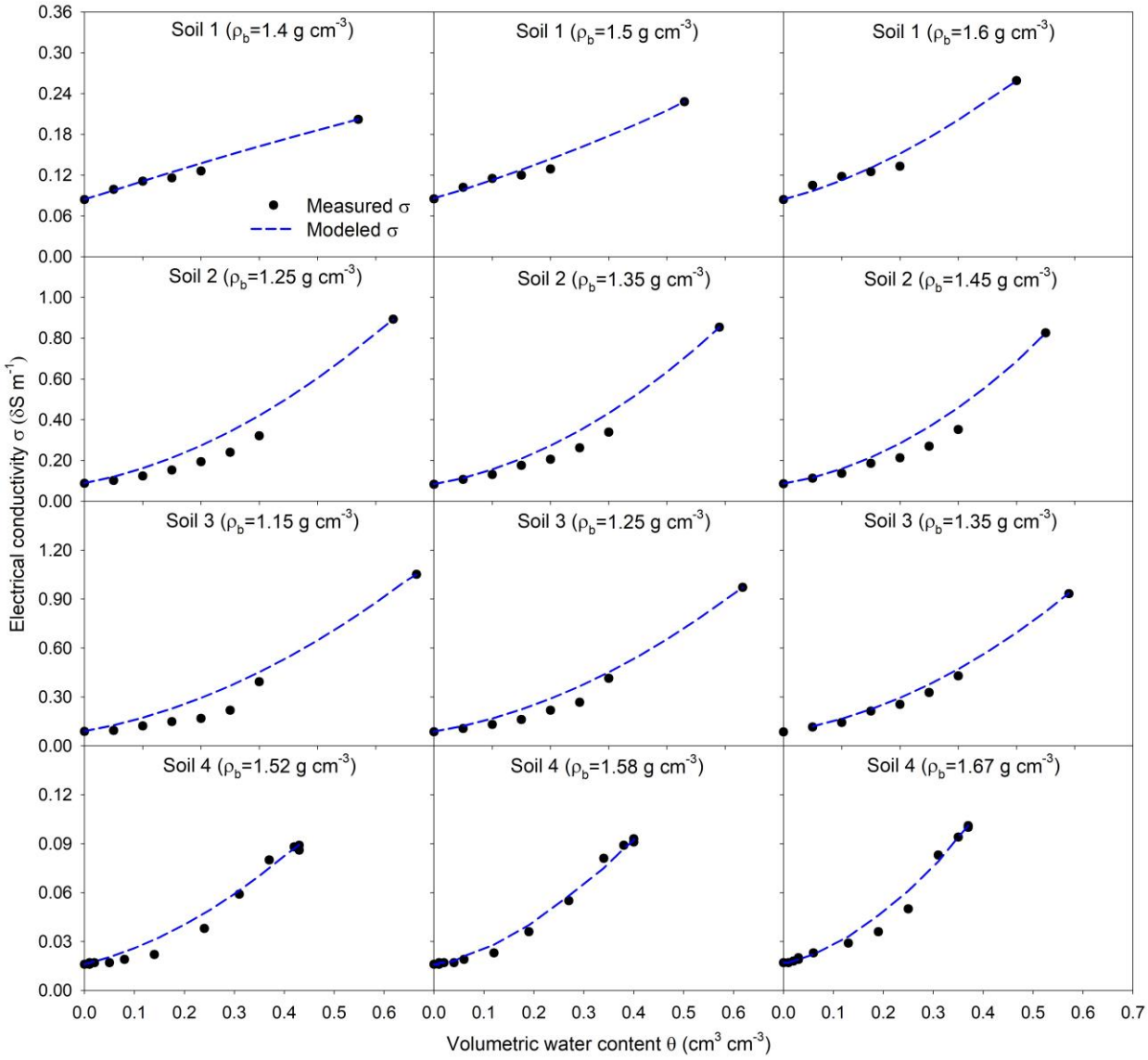

Figure 5.4. Comparison of measured (circles) and estimated (dash lines) electrical conductivity (σ) versus water content (θ) for soils 1-4. The curves were fitted with the generalized Archie's model for soil (Eq. [22]).

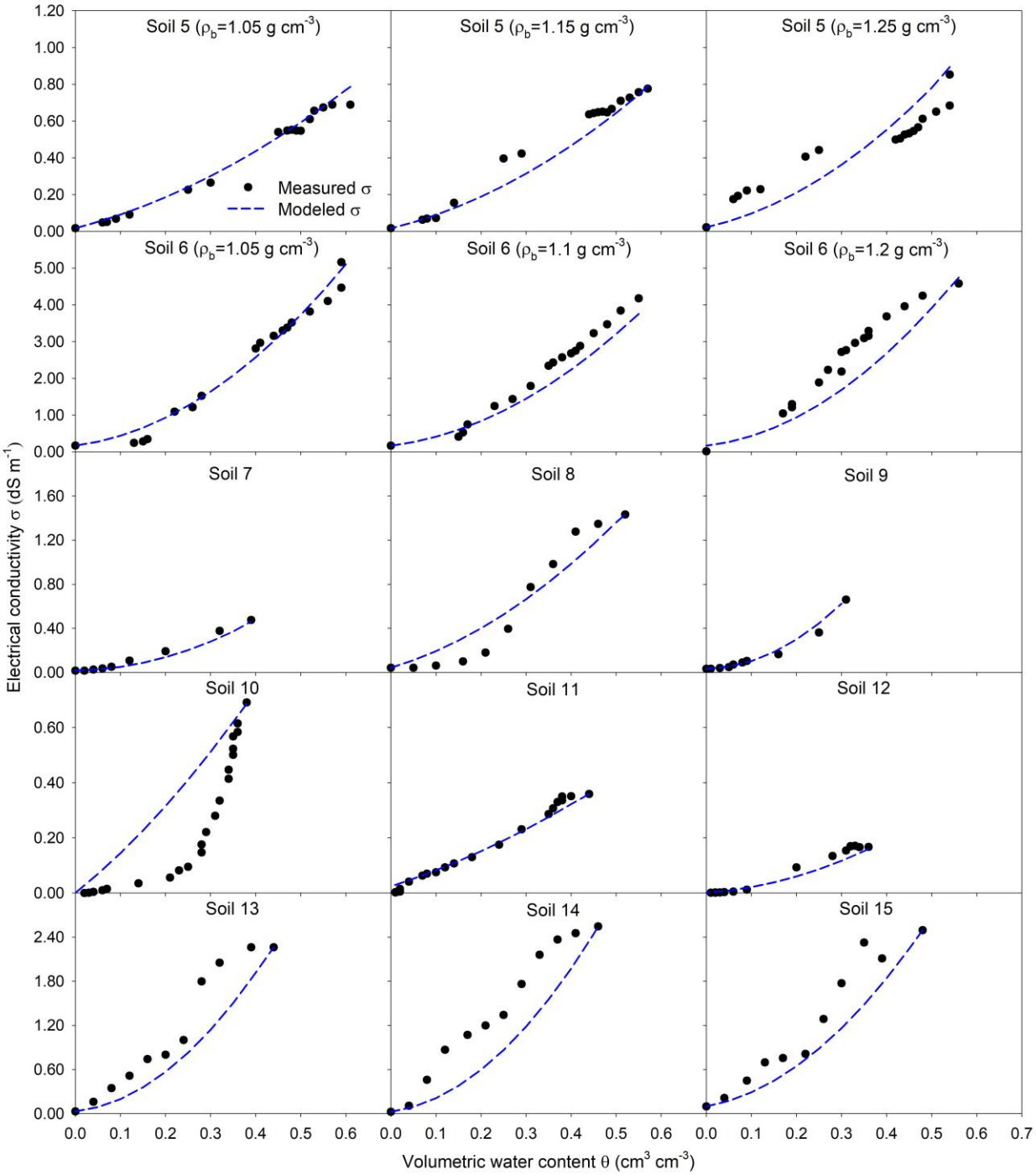

Figure 5.5. Comparison of measured (circles) and estimated (dash lines) electrical conductivity (σ) versus water content (θ) for soils 5-15. The curves were fitted with the generalized Archie's model for soil (Eq. [22]).

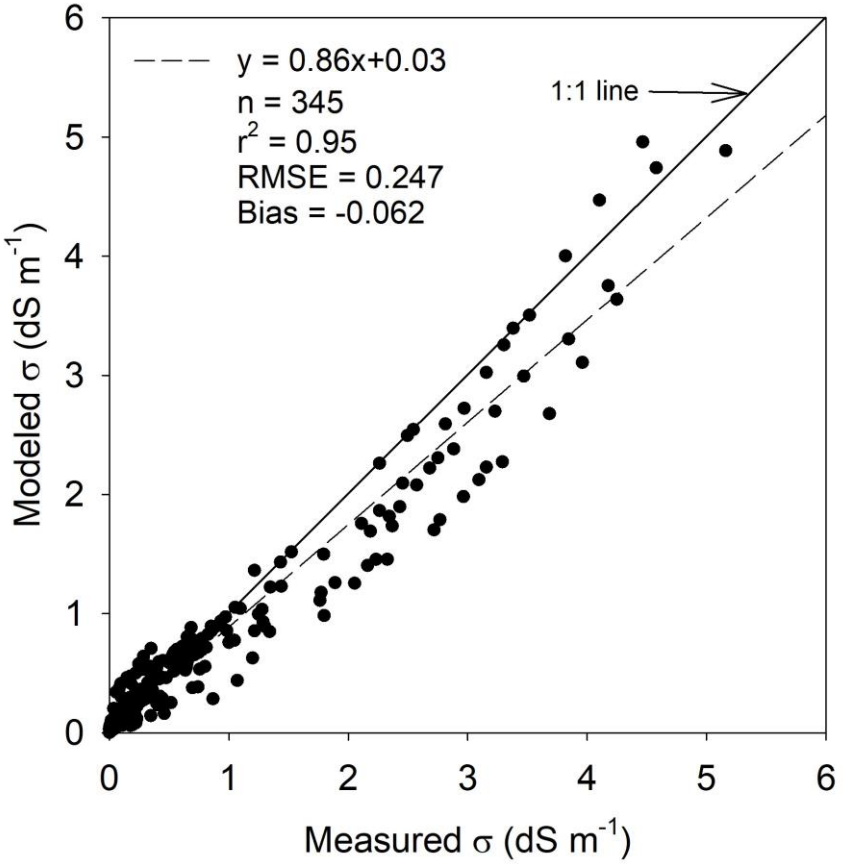

Figure 5.6. Comparison of modeled σ estimated with the generalized Archie's model for soil (Eq. [22]) with measured σ values for all soils in this study. The solid line is 1:1 line. The dash line indicate the fitted linear regression line.

Chapter 6: Summary and Future work

6.1 Summary

We first conducted a field experiment on a sandy soil. The thermo-TDR technique was used to measure the change of in-situ ϕ during compaction. In order to expand this approach to also determine the pore size distribution, a σ(θ)-SWRC approach to estimate the VG parameters from σ and θ measurements was proposed and validated. Based on observations and characteristics of sigmoid functions of λ(θ) and SWRC, we also introduced an empirical relationship to estimate the shape parameter *m* of VG model from *p* of λ(θ) model. Other parameters of the VG model were further obtained from soil properties or using a geometrical relationship. In addition, a simple generalized Archie's model for estimating σ from θ was developed. By fitting measured data to the generalized Archie's model, fluid phase exponent *w* of different soils were obtained and a standard value of *w* was assigned.

Main findings are:

1. The thermo-TDR probes monitored of the dynamics of soil ϕ accurately during compaction. Compared to the core method, the thermo-TDR technique effectively reduced the variability of measurement results. Pores of different size were not proportionally compacted as soil ϕ decreased during compaction.

2. We presented an σ(θ)-SWRC approach to estimate VG parameters. θ_s and θ_r can be estimated from easily measured soil properties (bulk density and particle size distribution). On the basis of the theoretical model of Mualem and Friedman (1991), VG shape parameter *m* can be estimated from σ measured at saturated and residual soil water contents, as well as σ(θ) values measured at intermediate water contents. The remaining VG parameter α can be obtained using a geometric

relationship. The σ(θ)-SWRC model performed well on five soils from newly collected and literature data.

3. We proposed an empirical relationship to estimate the VG parameter *m* from shape parameter *p* of a conceptual λ(θ) model by Lu and Dong (2015). Other VG parameters were obtained using the same way as σ(θ)-SWRC approach. Validation results on three soils from published data indicated that new proposed model can provide accurate estimates compared with direct measurements.

4. A generalized Archie's model for estimating σ from easily measured soil properties was developed. The new model has three parameters: σ_{sat}, σ_{dry} and *w*. σ_{sat} and σ_{dry} can be directly determined and *w* is assumed as a constant value of 2. Model evaluation results revealed that the new simple σ(θ) model could provide accurate predictions of soil σ values for the 15 investigated soils with different bulk densities and textures.

This study is the first time that the thermo-TDR technique was used to measure the change of in-situ ϕ during compaction. Our analysis showed that the thermo-TDR technique has the potential to be applied in the long-term management of traffic-induced soil compaction. With the investigation of relationship between soil transport properties (thermal, electrical and hydraulic properties), we expanded the application of thermal and electrical sensors to determine the pore size distribution. Our work revealed the potential to determine the pore size distribution in the field.

6.2 Future work

There are some new opportunities that need be explored in future work. Here I highlight a few of these opportunities.

1. Hydraulic conductivity (K) is a key property for estimating many processes in the vadose zone. However, it is also one of the least predictable parameter [Revil and Cathles, 1999]. In this study, we developed two approaches for estimating VG parameters from σ (or λ)-θ measurements and other easily measured soil properties. The Mualem-van Genuchten model has been widely used for estimating soil hydraulic conductivity from saturated hydraulic conductivity and VG parameters. This makes further estimation of K from σ (or λ)-θ measurements possible using approaches developed herein.

2. The theoretical basis of σ(θ)-SWRC approach is the model of Mualem and Friedman (1991) which hypothesized that pore geometry controls hydraulic flow and electrical flow in the same way. However, this hypothesis has not been directly tested. In a porous medium consisted of an insulating matrix and an interconnected pore volume, only the volume fraction of the conducting phase and the tortuous paths affects electrical flow. However, the situation is complex for hydraulic flow. The permeability (k) has units of length squared (m^2) and thus depends not only on the porosity and tortuosity but also on the absolute length scales of the pores that govern fluid transport (Banavar and Johnson, 1987). This difference questions the hypothesis: whether the hydraulic and electrical percolation are identical? Thus, the universality of this hypothesis need be tested and further a better relationship between electrical and hydraulic conductivity can be established.

3. In this study, we developed two indirect approaches to determine the indicators of soil structure (ϕ and PSD) from some transport properties (σ and λ). However, they were only evaluated on

repacked soils. Detailed analysis and comparison on intact soils. Influence of soil structure on thermal properties and electrical conductivity has been reported (Horn et al., 1994; Vogel et al., 1997), thus additional validation of the new proposed approaches on intact soils are warranted. This also raises question about the effect of soil aggregation on performance of σ(θ)-SWRC and λ(θ)-SWRC approaches. The examination of σ(θ)-SWRC and λ(θ)-SWRC approaches need be conducted on non-aggregated and aggregated soils of different aggregate sizes.

4. In previous studies, the ability of thermo-TDR to determine the in-situ soil ϕ has been demonstrated (Liu et al., 2014; Tian et al., 2018). However, very few studies have been dedicated to in-situ determination of PSD using sensors. Since σ, λ and θ can be determined automatically, repeatedly and continuously in the field, work in this study revealed the possibility of in-situ determination of SWRCs for the first time. Further validation of this work need be conducted in the field experiment.

6.3 References

Banavar, J.R., Johnson, D.L., 1987. Characteristic pore sizes and transport in porous media. Phys. Rev. B 35, 7283–7286.

Horn, R., Taubner, H., Wuttke, M., Baumgartl, T., 1994. Soil physical properties related to soil structure. Soil Tillage Res. 30, 187–216.

Liu, X., Lu, S., Horton, R., Ren, T., 2014. In Situ Monitoring of Soil Bulk Density with a Thermo-TDR Sensor. Soil Sci. Soc. Am. J. 78, 400.

Mualem, Y., Friedman, S.P., 1991. Theoretical prediction of electrical conductivity in saturated and unsaturated soil. Water Resour. Res. 27, 2771–2777.

Revil, A., Cathles, L.M., 1999. Permeability of shaly sands. Water Resour. Res. 35, 651–662.

Tian, Z., Lu, Y., Ren, T., Horton, R., Heitman, J.L., 2018. Improved thermo-time domain reflectometry method for continuous in-situ determination of soil bulk density. Soil Tillage Res. 178, 118–129.

Vogeler, I., Clothier, B.E., Green, S.R., 1997. TDR estimation of the resident concentration of electrolyte in the soil solution. Aust. J. Soil Res. 35, 515–526.